THE UNIVERSITY OF MICHIGAN

COLLEGE OF ENGINEERING
Department of Mechanical Engineering
Heat Transfer and Thermodynamics Laboratory

Sixth, Seventh, and Eighth Quarterly Progress Reports
for the Period October 1, 1962, to July 1, 1963

LOW HEAT-FLUX BOILING

John A. Clark
Edward R. Lady

ORA Project 04653

under contract with:

U. S. ATOMIC ENERGY COMMISSION
SAVANNAH RIVER OPERATIONS OFFICE
CONTRACT NO. AT(38-1)-260
AIKEN, SOUTH CAROLINA

administered through:

OFFICE OF RESEARCH ADMINISTRATION ANN ARBOR

August 1963

This report was also a dissertation submitted in partial fulfillment of the requirements for the degree of Doctor of Philosophy in The University of Michigan, 1963.

TABLE OF CONTENTS

TABLE OF CONTENTS (Continued)

TABLE OF CONTENTS (Concluded)

LIST OF TABLES

LIST OF FIGURES

LIST OF FIGURES (Concluded)

NOMENCLATURE

Other nomenclature is defined locally as necessary.

A	heat transfer area, ft^2
a	thermal diffusivity = $k/\rho c$; ft^2/hr
c	specific heat, Btu/lbm-°F
D	characteristic diameter, ft
g	gravitational acceleration, ft/sec^2
g_c	mass-force conversion constant = 4.17×10^8 lbm-ft/lbf-hr^2
h	heat transfer coefficient, Btu/hr-ft^2-°F
h_{fg}	latent heat of vaporization, Btu/lbm
i	electrical current per unit area, amp/ft^2
I	total current, amp
J	mechanical heat equivalent, 778.26 ft-lbf/Btu
k	thermal conductivity, Btu/hr-ft-°F
N	number of bubbles
Nu	Nusselt number
p	pressure, lbf/ft^2 or $lbf/in.^2$, as specified
Δp	pressure difference corresponding to superheat (T_w-T_{sat})
Pr	Prandtl number
q	rate of heat transfer, Btu/hr
Re	Reynolds number
r	tube radius, ft
T	temperature, °F

ΔT	temperature difference, °F
μ	viscosity, lbm/hr-ft
ρ	density, lbm/ft^3
ρ_e	electrical resistivity, ohm-cm or ohm-ft, as specified
σ	surface tension, lbf/ft

Subscripts

b	boiling
c	convection
f	liquid phase
i	inside
ℓ	liquid phase
o	outside
sat	saturation
v	vapor phase
w	wall = heating surface

ABSTRACT

This investigation presents experimental data from tests of boiling saturated distilled water from the outer surface of a horizontal tube at low values of heat flux, 5,000-100,000 Btu/hr-ft^2, and elevated pressures, 535-1550 psia. Both natural convection (pool boiling) and water velocities up to 4.7 ft/sec normal to the axis of the tube are studied.

The design of a system to carry out the boiling studies at pressures up to 2000 psia and temperatures up to 635°F is discussed in detail. The entire system is fabricated from 347 stainless steel. It has a circulation rate of 150 gal/min and has means of pressure control and water purification. The heat transfer surface is a 3/4 in. O.D. Monel tube, heated electrically by direct current passing through the tube. The inside wall temperature is measured by four thermocouples. Details of thermocouple calibration are included. The temperature of the outer surface of the tube is determined by subtracting the wall temperature drop from the measured inside temperature.

The results are presented in a series of figures which show the heat flux as a function of wall superheat, (T_w-T_{sat}), for pressures of 535, 1015, and 1550 psia and velocities of 1.3 and 4.7 ft/sec, as well as pool boiling. A pronounced hysteresis effect is noted, with a higher wall superheat required at a given flux for increasing heat flux. The curve for decreasing heat flux is more stable and reproducible. An empirical equation which fits the pool boiling data in the range of 535-1550 psia, for the decreasing heat flux condition, is

$$(q/A) = 13{,}700\ (p^*)^{1.72}(T_w-T_{sat})^{f(p^*)}$$

where $f(p^*) = 1.56\ (p^*)^{-1/6}$ and (q/A) is heat flux, Btu/hr-ft^2, p^* is the reduced pressure, p/p_{crit}, and (T_w-T_{sat}) is the wall superheat, °F. The effect of a velocity normal to the tube is to reduce the wall superheat at a given heat flux.

It is concluded that the heat flux in nucleate boiling of water is proportional to the wall superheat raised to a power between 1.7 and 2.1. The effect of increasing the system pressure in the range studied is to decrease the wall superheat at a given flux. The effect of heat flux history is significant for tests of up to several hours. The temperature difference appears to approach an asymptotic value for prolonged boiling at constant heat flux, regardless of the prior heat flux from the surface.

I. INTRODUCTION

A. PURPOSE

With the advent of the nuclear power plant employing pressurized water as a coolant, a great interest has been focused on heat transfer processes to boiling fluids at all levels of heat flux. The primary emphasis of previous research has been in regions of high heat flux for the obvious reason that operation in these regions results in equipment of minimum size and cost. In the cooling of the pressurized water from a reactor, a heat exchanger may be employed to generate steam by boiling of a second stream of water at a lower pressure. For maximum economy of the overall nuclear power plant cycle, it is necessary to know accurately the heat transfer characteristics of boiling at low heat flux so that the pressurized water circulation rate may be optimized with respect to the size of the heat exchanger which generates the useful steam. Because of the non-exponential behavior of low heat flux boiling, extrapolation of data from regions previously investigated is not satisfactory.

The purpose of this investigation is the study of boiling heat transfer to saturated, pressurized water in the regime of low heat flux. The pressure range covered is 535 to 1550 psia. The regime of low heat flux is defined as that of 5,000 to 100,000 Btu/hr-ft^2. The boiling takes place on the outside surface of a horizontal Monel tube

which is immersed in a pool of water and may be subject to velocities normal to the tube and upward, ranging from 0 to 5 ft/sec.

B. THE BOILING PHENOMENON

The transfer of heat from a hot surface to a saturated liquid is characterized by surface phenomena which differ markedly in physical appearance. These regions are best considered by reference to a curve in which heat flux ($Btu/hr\text{-}ft^2$) is plotted against the temperature difference between the hot wall and the saturation temperature of the liquid. Figure 1 shows a typical boiling characteristic curve.

The region from A to B represents heat transfer without boiling. Inasmuch as the liquid is considered to be saturated, heat transfer to the liquid increases the temperature above the saturation temperature and results in superheated liquid. The warmer, less dense liquid rises from the hot surface to the liquid-vapor interface where evaporation takes place. In a pure fluid no bubbles ever appear in the region.

The appearance of bubbles marks the second major region of the boiling characteristic curve. This is shown as the portion of the curve from B to E. This may be subdivided into three sections which are labeled B-C, C-D, and D-E. The region from B to C is distinguished by small bubbles on the hot surface, which grow from discrete sites or nuclei and then collapse as heat is transferred from them to the bulk of the liquid. As the temperature of the hot surface is increased, the bubbles are detached from the heated surface and rise to the liquid-

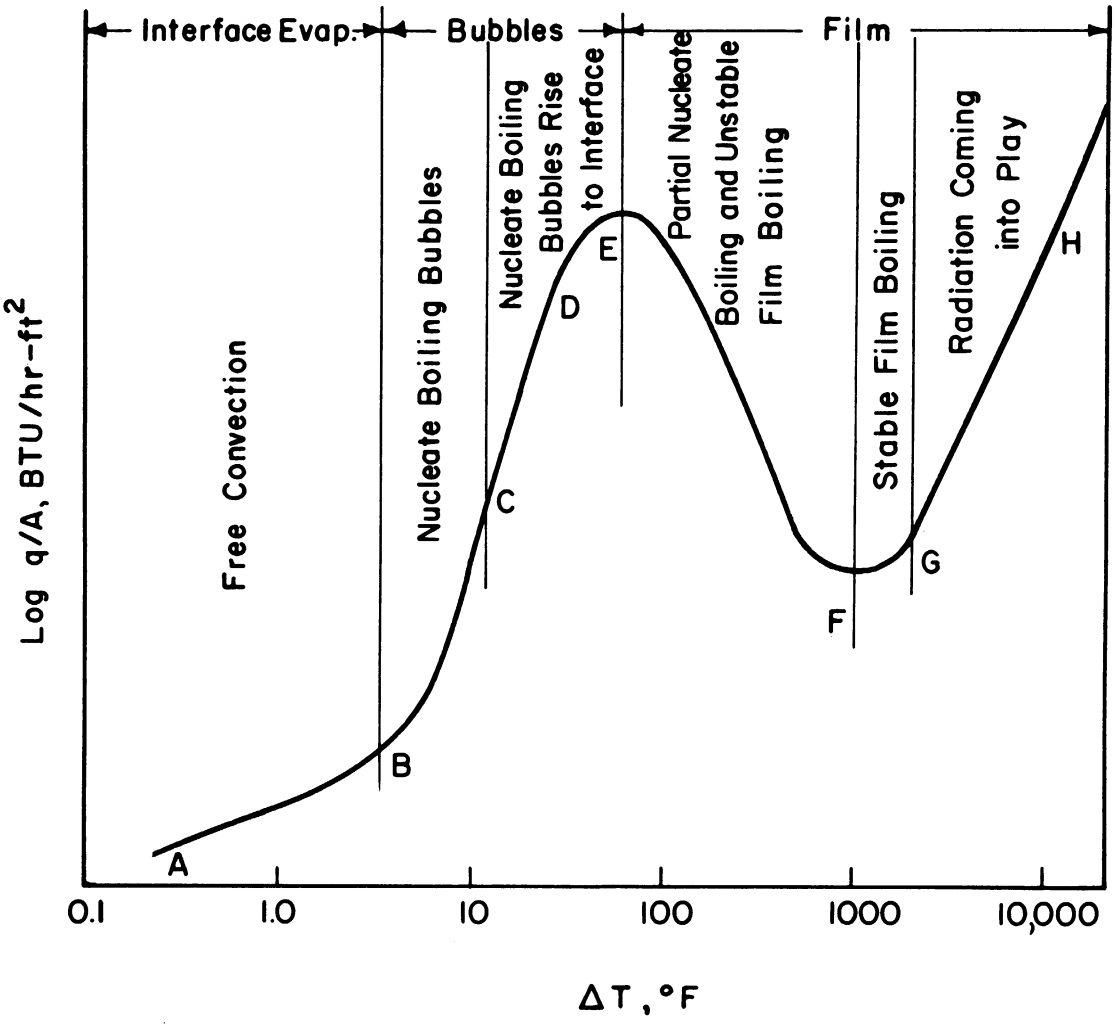

Fig. 1. Typical boiling-characteristic curve.

vapor interface. With increasing temperature difference more and more nucleation sites are activated, resulting in a very rapid increase in the heat flux. This portion of the curve is nearly a straight line and is labeled C-D. Point D is sometimes referred to as the departure from nucleate boiling (DNB). As the temperature difference increases beyond this point the heat flux increases less steeply, as shown by the portion of the curve from D to E. This change in slope may be due to interference of the bubbles with each other. This interference increases until the peak heat flux in nucleate boiling, point E, is reached. This is known as the "burnout point" because any additional heat flux from an electrically heated surface causes a step change in the temperature difference (from E to H) which will probably cause the melting of the electrical resistance heater.

At temperature differences greater than that of the burnout point, the physical appearance again changes. From E to F part of the surface is covered by a film of vapor. The vapor film impedes the flow of heat from the hot surface to the liquid. This results in a negative slope of the curve as seen from E to F. This is inherently an unstable region. At point F the entire heated surface is blanketed by a film of vapor and once more a positive slope occurs. Heat is transferred from the hot surface by conduction through the vapor film to the liquid As the hot surface is increased in temperature, a greater fraction of the heat is transferred by radiation directly from the hot surface to the liquid. This results in a steeper slope, as shown by the portion

of the curve from G to H.

The region of interest in this study concerns the transition from convection without boiling to nucleate boiling, or the portion of Fig. 1 from A to D. It is evident that very small temperature differences between the hot surface and the liquid will exist. It also appears that precise theoretical treatment of a region influenced by two distinct mechanisms is not feasible until experimental data are available to help define the relative importance of each mechanism.

C. LITERATURE REVIEW

The subject of boiling heat transfer has received extensive treatment in the literature. Almost all widely used references and texts devote at least one chapter to the subject.[1-4] A literature survey was made covering the field up until March, 1962, as a part of the overall project under which the present work was conducted. This survey was reported by Clark et al.,[5,6] and is subdivided into the following areas:

1. Nucleation theory.
2. Population of bubble producing sites.
3. Frequency of bubble formation.
4. Bubble dynamics.
5. Mechanism of nucleate boiling.
6. Correlations for pool and forced convection boiling.
7. Effect of type of liquid on boiling heat transfer.
8. Effect of heating surface on nucleate boiling.
9. Effect of pressure on nucleate boiling.

10. Effect of gravity on boiling heat transfer.

11. Effect of vapor quality.

12. Heat transfer and pressure drop in two-phase flow.

These areas will be considered as they apply to the present work.

1. Nucleation Theory

Ebullition is the phenomenon of a superheated liquid forming vapor bubbles at discrete sites, or nuclei, at essentially constant pressure. It differs from cavitation in that the latter is largely isothermal as well as at constant pressure. In both cases nucleation is greatly facilitated if solid surfaces or dissolved and volatile gases are present. A wide diversity of opinion exists concerning the conditions necessary for bubble nucleation from solid surfaces.

Corty and Foust,[7] found that a superheat of up to 50°F was necessary to initiate nucleate boiling of ether, n-pentane, or F-113 from surfaces which had been polished to a mean roughness of from 2 to 20 μin. (rms). Once nucleation was initiated at some apparently random location, the phenomenon spread and covered large areas of the surface. This resulted in a decrease in the superheat temperature (wall temperature minus liquid saturation temperature). A hysteresis effect was noted as shown in Fig. 2. Curve abdc represents the normal nucleate boiling curve, or that curve which was obtained by vigorous boiling at high flux for at least 30 min and then decreasing the heat flux in steps. A plot of heat flux versus temperature difference would have the same general charac-

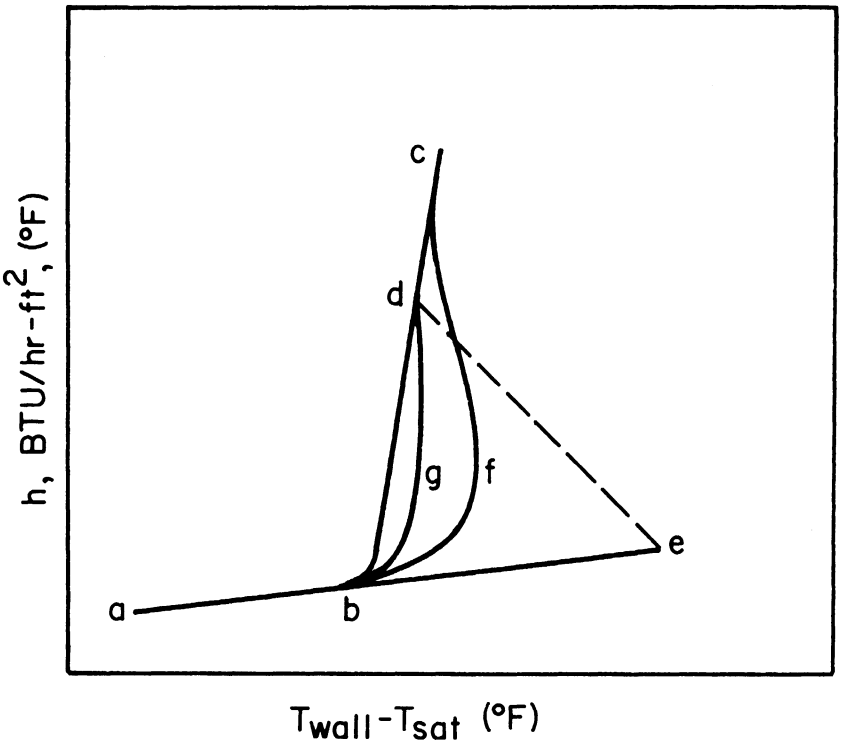

Fig. 2. Hysteresis effect in nucleate boiling.

teristic shape, although with steeper slopes, since the nucleate boiling heat transfer coefficient for pool boiling is defined as

$$h_b = \frac{(q/A)_b}{T_{wall}-T_{sat}} \qquad (1)$$

Again referring to Fig. 2, curve abed shows the results of gradually increasing the heat flux. No nuclei are present initially and no bubbles are formed until point e is reached. Then vigorous boiling takes place and many nuclei are activated rapidly. This results in a decrease in temperature difference to point d. Curve bfc is a curve of increasing heat flux with the condition of some nuclei being active at b, due to previous high heat flux boiling. Curve bgd is also one of increasing heat flux but with more sites active at b than the curve bfc. Corty and Foust observed individual nucleation sites and found them to be pits or scratches. It was also found that a site which only recently ceased to be an active center may be easily reactivated with increased heat flux. From these observations they postulated that nucleation occurs at the surface where minute quantities of vapor or gas are trapped by the cavities on the solid.

Ellion,[8] also supports the vapor trapping postulate and concludes that gas-vapor nuclei stabilized on solid particles are present even though the liquid is not saturated by gas. He states that the excess pressure necessary to form a bubble from a nucleus which has been forced out of the stabilizing particle varies with surface tension, partial pressure of the gas within the nucleus and the nucleus size. He

concludes that nucleation occurs at the heated surface with smaller wall superheats if the wall is not wetted but has gas-vapor nuclei stabilized on it.

Bankoff,[9] extends previous nucleation theory to the superheating of liquids in contact with various solid boundaries. Nucleation in the bulk phase, at flat surfaces, at sharp projections, or in wetted cavities can be dismissed from consideration as possible explanations for experimentally observed superheats. Unwetted cavities, on the other hand, are preferred nucleation sites, but it is difficult to fill these completely with liquid. Therefore it is possible that nucleation almost always occurs at a pre-existing gaseous phase.

2. Population of Bubble Producing Sites

Nucleate boiling is characterized by the presence of unique active sites on the hot surface which have the ability to initiate and support the formation of vapor bubbles. The nucleate boiling process is determined by (i) the density of bubble producing sites, (ii) the rate of vapor production at each site, and (iii) the rate and frequency of growth of the bubbles. As the temperature of the surface is increased above the liquid saturation temperature, the number of nuclei increases and is accompanied by a simultaneous increase in both the heat transfer rate and the heat transfer coefficient.

Jakob,[10] cites earlier works showing that steam bubbles originate only on a few points on the heating surface and that the number of these sites is roughly proportional to the heat flux. From these tests with water at atmospheric pressure and fluxes up to 18,400 Btu/hr-ft^2, he concluded that a linear relation existed between the heat flux and the number of active sites on a horizontal surface, with each site effecting the transfer of 59 Btu/hr in the form of a column of steam bubbles.

Corty and Foust,[7] counted up to 60 active sites per square inch for pentane boiling on nickel at a heat flux of 25,000 Btu/hr-ft^2. Nishikawa et al.,[11] found that for water boiling on a smooth horizontal brass surface, $h \sim (N/A)^{1/3}$. It was found that this relationship is not affected by surface contamination, surface-active agents, dissolved salts, or the degree of surface macroroughness. These results were based on heat fluxes up to 13,600 Btu/hr-ft^2 and a maximum population count of 8/sq in. This work was verified by Kurihara and Myers.[12]

Gaertner and Westwater,[13] by plating a thin layer of nickel on a copper surface during boiling tests, and subsequently counting the number of pin holes in the plate, obtained counts from 0 to a maximum of 1,130/sq in. at 317,000 Btu/hr-ft^2. This was done boiling an aqueous solution of nickel salts containing 20% solids at atmospheric pressure. The geometrical distribution of active sites (pin holes) was found to be random. The heat flux was proportional approximately to the square root of the number of sites

$$q/A = 1400\ (N/A)^{0.47} \qquad (2)$$

The heat flux associated with each site varied from 141 Btu/hr for the first site to 1.95 Btu/hr at the maximum heat flux used of 317,000 Btu/hr-ft^2.

Gaertner,[14] disputes the patch-by-patch growth concept of Corty and Foust.[7] He analyzed the geometrical distribution of nuclei and found it to be entirely random. He further concluded that the bubble population depends on the temperature according to the relation

$$\overline{N} = N_o \exp[-K/T_w^3] \qquad (3)$$

where $\overline{N}$ is the average population of active sites per square foot, N_o and K are constants, and T_w is the absolute temperature of the heated surface, °R.

Clark et al.,[15] used photography with magnifications up to 25,000 to show that pits with diameters between .0003 and .003 in. are very active sites, whereas no bubbles formed at grain boundaries or on the various crystal faces of zinc, an anisotropic material. The photographs were made of ether and pentane boiling at atmospheric pressure.

Hsu,[16] makes a theoretical analysis using previous experimental data for checking the predictions. He assumes a bubble nucleus exists in the mouth of a cavity and considers the effect of the thermal boundary layer thickness and turbulence. He concludes that there is a maximum and minimum size for a site to be active at a given amount of

superheat. He also states that there is an activation of additional sites with increasing heat flux.

3. Frequency of Bubble Formation

Jakob,[1] reports that the frequency of bubble formation depends on the size of the bubbles at the moment of breaking off. For water and carbon tetrachloride the product of the average bubble diameter and the mean frequency varies from 75 to 120 mm/sec, as the bubble size increases from 1 to 5 mm. The bubble diameter is related to the contact angle, surface tension, and liquid-vapor density difference. The frequency of bubble formation is affected by heat flux, surface material, surface condition, flow velocity, etc. Even with all such conditions held constant and at a specified active site, the frequency varies considerably.[17,18]

4. Bubble Dynamics

The physical model, generally postulated, consists of a spherical bubble of vapor surrounded by liquid. The rate of bubble growth is a function of the heat flow which causes evaporation. The entire history of the bubble growth may be divided into the initial, intermediate, and asymptotic stages.

In the initial stage, the growth of a bubble in a liquid is controlled primarily by the surface tension and vapor pressure. It has been shown that because of surface tension effects,[1,19] a minimum amount of superheat in the liquid is necessary for a bubble nucleus

of finite dimensions to form and grow.

After the bubble growth has been initiated, there is a rapid rise in the velocity dR/dt so that inertia effects become important. As the liquid surrounding the bubble cools, the growth rate decreases. Hydrodynamic effects are considered by Plesset and Zwick[20] and Forster and Zuber.[21,22]

In the asymptotic stage, the effects of viscosity and surface tension become vanishingly small. Finally inertia and buoyant forces cause the bubble to be detached from the surface. It should be noted that bubbles may be ejected from the under side of a heated surface, probably due to inertia forces of the liquid set up in the intermediate growth stage.[8]

5. Mechanism of Nucleate Boiling

Three basic mechanisms have been proposed to account for the transfer of heat in nucleate boiling: (a) microconvection heat transfer, (b) latent heat transport, and (c) vapor-liquid exchange.

a. Microconvection Heat Transfer.—The rapid growth of the bubble at a nucleus accelerates the adjacent liquid to a high velocity away from the nucleation site. Upon collapse or bubble departure the reverse occurs. This pulsating action at each site creates currents in the normally laminar boundary layer near the heat transfer surface. With the aid of photographic results, Jakob,[1] and later Rohsenow and Clark,[23] and Gunther and Kreith[24] concluded that only microconvection could ac-

count for the majority of the heat transfer during nucleate boiling.

b. Latent Heat Transport.—This mechanism involves the transfer of latent heat by simultaneous vaporization near the base of the bubble and condensation near the top. Bankoff[45,46] presents and analyzes experimental evidence to support the view that this mechanism becomes dominant at high fluxes.

c. Vapor-Liquid Exchange.—This mechanism considers the growing, collapsing and departing vapor bubbles to act as liquid pumps, by first pushing superheated liquid into the liquid bulk and then allowing the cooler bulk liquid to replace the void left by the collapsed or departed vapor bubble. Forster and Greif,[32] claim that the liquid-vapor exchange mechanism is sufficient to account for the heat flux of nucleate boiling and that microconvection of the superheated sub-layer alone is not compatible with experimental findings.

Zuber,[25] and Chang,[26] have proposed mechanisms which include more than one of the above modes. Chang and Snyder,[27] also consider combined effects and conclude that the high heat flux in nucleate boiling is due principally to the agitation caused by the bubble growing instead of detaching. They also state that the peak heat flux occurs at the condition of maximum number of bubbles from the maximum number of sites. In a later paper Chang,[28] considers the burnout point as being the condition of the maximum rate of bubble generation from a unit area of the heating surface. He also reports that meager experimental data are available for saturated, forced convection boiling. This present

study presents some such data.

6. Correlations

There are many semi-empirical equations proposed for correlating experimental data in nucleate boiling heat transfer. Generally, analysis has been made using dimensionless parameters, determining the various empirical constants by the use of experimental data.

a. Pool Boiling.—Because the major portion of the heat is transferred by microconvection, or turbulence in the boundary caused by vapor-liquid exchange, it may be expected that a relation similar to one which applies to turbulent flow will apply. This is of the type

$$Nu = \phi(Re)\psi(Pr) \tag{4}$$

where the Reynolds number is based on the bubble diameter and mass flow rate. Using this as a starting point and examining experimental data of Addoms,[29] and others, Rohsenow,[30] proposed the following

$$\frac{C_\ell(T_w-T_{sat})}{h_{fg}} = C_{sf}\left[\frac{(q/A)_b}{\mu_\ell h_{fg}}\sqrt{\frac{g_c\sigma}{g(\rho_\ell-\rho_v)}}\right]^{1/3} Pr_\ell^{1.7} \tag{5}$$

The constant C_{sf} depends on the nature of the heating surface-fluid combination, to be obtained from experimental data. Several such constants are given by Rohsenow and Choi.[4] For boiling of a given fluid at a given pressure, this reduces to

$$(q/A)_b = C(T_w-T_{sat})^3 \tag{6}$$

Gilmour,[31] reports that the following equation represents the data of several experimental investigations

$$\frac{(q/A)_b}{(T_w-T_{sat})C_\ell G_\ell} = 0.001\left(\frac{DG_\ell}{\mu_\ell}\right)^{-0.3}\left(\frac{C_\ell\mu_\ell}{k_\ell}\right)^{-0.6}\left(\frac{p^2}{\sigma\rho_\ell}\right)^{0.425} \tag{7}$$

where p is the absolute pressure and $G_\ell = (q/A)_b\rho_\ell/\rho_v h_{fg}$. Again, for a given liquid boiling at a fixed pressure, this reduces to

$$(q/A)_b = C(T_w-T_{sat})^{3.33} \tag{8}$$

Forster and Greif,[32] found that for a single liquid the following expression may be used

$$(q/A)_b = K\left(\frac{k}{2\sigma}\right)\Delta p(T_w-T_{sat})\left(\frac{\rho_\ell B^2}{\mu}\right)^{0.2}(Pr_\ell)^{0.33} \tag{9}$$

where

$$B = \frac{C\rho_\ell\, T_{sat}\sqrt{\pi a}}{(h_{fg}\rho_v)^2 J}\,\Delta p$$

Thus, the heat flux is proportional to $(T_w-T_{sat})\Delta p^{1.4}$. Since, from the Clausius-Clapeyron equation, Δp is proportional to ΔT or (T_w-T_{sat}), this reduces to

$$(q/A)_b \sim (T_w-T_{sat})^{2.4} \tag{10}$$

From a more generalized correlation by the same authors, the simplified relationship is

$$(q/A)_b \sim (T_w-T_{sat})^2 \tag{11}$$

It is evident from the above that various correlations exist, generally expressing the heat flux as a function of the temperature difference between the wall and the saturation temperature of the fluid raised to a power between 2 and 3.33. Experimental data are available in which the exponent varies from 2 to 4.

b. Forced Convection Boiling.—From the above discussion, it is seen that very high heat transfer rates are achieved with pool boiling alone. When the bulk liquid has a velocity past the heated surface it is intuitive that the heat transfer rate would increase for a given temperature difference. Rohsenow,[33] showed how these two effects may be superimposed

$$q/A = (q/A)_c + (q/A)_b \qquad (12)$$

In this case the term $(q/A)_c$ is the heat transfer due to convection without boiling and $(q/A)_b$ is the heat transfer associated with bubble motion alone.

Forster and Greif,[32] examined experimental data which showed virtually no difference in the heat transfer rate under nucleate boiling conditions, regardless of bulk velocity. They conclude that once nucleate boiling occurs at the surface, this mechanism dominates the overall process and the convective term may be neglected. The present work presents data which indicate that this cannot be neglected.

Much work is concerned with very high heat flux and the burnout point.[34] This is not of direct interest in this work but mention must

be made of the work of Vliet and Leppert,[35] who conducted tests with water at atmospheric pressure flowing upward and normal to electrically heated wires and tubes. Pictures show the size and distribution of the vapor bubbles being carried away by the bulk flow which was varied over a velocity range of 1.2 to 9.5 ft/sec. The empirical equation which fits the experiment data is

$$(q/A) = 378 \ (T_w - T_{sat})^{2.0} \qquad (13)$$

In another paper, Vliet and Leppert,[36] state the hydrodynamic boiling pattern with subcooled boiling of water at atmospheric pressure is similar to saturated boiling up to a subcooling of 20 to 30°F.

7. Effects of Liquid, Heating Surface, Pressure, Gravity, and Vapor Quality on Nucleate Boiling

Although the type of liquid, the heating surface, the pressure of the system, the body forces of high or low accelerations, and the vapor quality all have an effect on nucleate boiling, the principal concern here is that of pressure. For a large number of liquids boiling in pools an increase in pressure causes an increase in heat flux for a given temperature difference. This has been demonstrated to be the case for water by the experimental data of Addoms,[29] for pressures from 14.7 to 2465 psia, and Kazakova,[37] for water under a similar pressure range.

Jakob,[1] proposed an equation which expresses the influence of pressure by introducing the ratios of the kinematic viscosity, liquid density, and surface tension at the elevated pressure to their values at

atmospheric pressure. These values are also dependent upon the temperature which increases with the pressure. The various correlations cited above all include the effect of pressure in the various terms. The correlation of Gilmour,[31] includes pressure directly, raised to the 0.85 power, as well as other pressure dependent terms.

II. EXPERIMENTAL APPARATUS AND INSTRUMENTATION

A. SUMMARY

A system was designed to study the boiling of distilled and degassified water external to round tubes. For maximum future use, the system was designed to operate at conditions beyond those attained in the present study. The design conditions are:

Heat flux:	0-400,000 Btu/hr-ft^2
Pressure:	500-2,000 psia
Saturation Temperature:	467-635°F
Velocity:	pool boiling to 5 ft/sec
Subcooling:	1°F maximum
Tube Orientation:	horizontal and vertical

The system was designed sufficiently large to accomodate small bundles of tubes, up to 5 in. in overall diameter. This size is adequate for a tube bundle of 13 tubes, 3/4 in. O.D. on a normal triangular pitch of 1.5 times the outside diameter.

In this study the following ranges of independent variables are investigated:

Heat flux:	2,000 to 216,000 Btu/hr-ft^2
Pressure:	535-1550 psia
Velocity:	pool boiling to 4.7 ft/sec
Subcooling:	0-1°F
Tube Orientation:	horizontal
Tube Material:	Monel
Tube Diameter:	3/4 in. O.D.

The experimental apparatus consists of a stainless steel pressure vessel, 12-3/4 in. O.D. by 36 in. long in which a Monel tube is placed

in a horizontal plane. The Monel tube is heated by the passage of direct current from one end to the other. The vessel is partially filled with distilled water so that the Monel tube is immersed to a depth of approximately 18 in. Means of heating the water, controlling the pressure, creating and measuring the flow of water upward and normal to the axis of the tube, deionizing and degassing the fluid are provided. These are discussed in detail in following sections.

The experimental apparatus is located in the Heat Transfer and Thermodynamics Laboratory of the Department of Mechanical Engineering of The University of Michigan. Facilities supplied by the laboratory include the following:

(1) 12 volt, 3,000 ampere direct current

(2) 25 volt, 2,000 ampere direct current

(3) 460 volt, 3-phase, 60-cycle power—50 kw

(4) 110 volt, 1-phase, 60-cycle power—2 kw

(5) compressed air, 90 psig, 100 std cfm

(6) cooling water, 50 psig, 10 gal/min

A photograph of the experimental apparatus is shown in Fig. 3. This photograph was taken before thermal insulation was applied to the vessel and pipes which have elevated temperatures during operation.

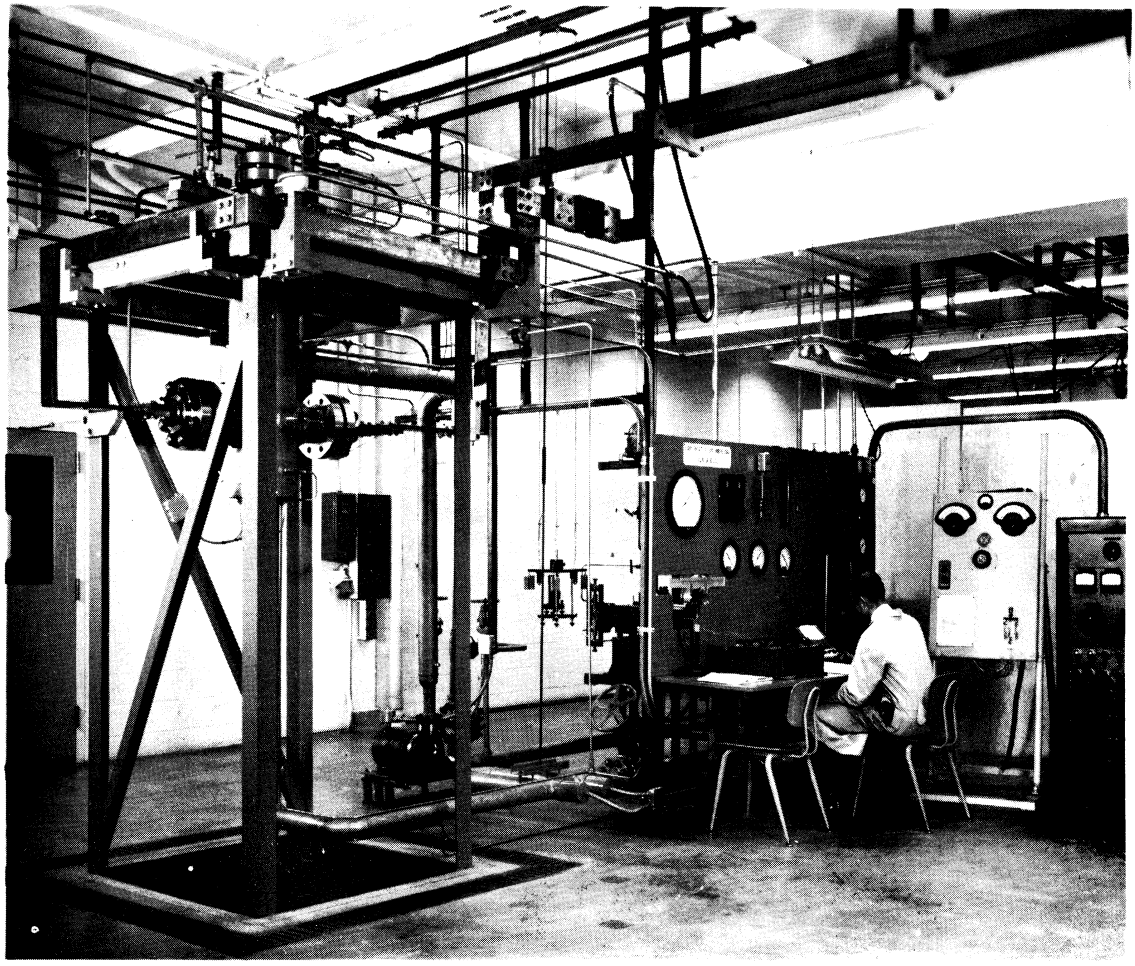

Fig. 3. Low heat flux boiling experimental apparatus.

B. TEST SECTION

The test section is a 7 in. long Monel tube, nominally 3/4 in. O.D. by .049 in. wall, silver soldered to copper electrodes which protrude through flanges of the stainless steel pressure vessel. The Monel tube was supplied by the Wolverine Tube Division, Calumet and Hecla, Inc. as seamless, cold drawn, bright annealed, and in accordance to the specification A.S.T.M. B-163. The chemical analysis provided by the supplier is as follows:

Copper	33.0 %
Iron	1.44%
Nickel	64.2 %
Manganese	1.12%
Silicon	.07%

The mechanical properties provided by the supplier are:

Tensile strength	81,000 psi
Elongation, 2 in.	48%
Yield strength	47,400 psi
Hardness, Rockwell B	74/75

The piece of tubing used in these tests has an average outside diameter of 0.7512 in., based on four measurements at two axial positions and two perpendicular readings at each position. The average tube wall thickness is 0.0526 in., based on eight measurements, four at each end of the tube. The maximum wall thickness is .0540 in. and the minimum is .0510 in. The readings were made with a point micrometer, calibrated with gage blocks.

The outside surface roughness of the Monel tube was measured just prior to insertion into the vessel. A Type Q Profilometer Amplimeter, Model 1, manufactured by the Micrometrical Manufacturing Company, Ann Arbor, was used. Eight traces with the Type MA stylus in the axial direction yielded readings of 5-10 μin. (rms) with a single peak of 15 μin. In the circumferential direction the readings were also 5-10 μin., with a single scratch giving a reading of 13 μin.

A cross section view of the test section is shown in Fig. 4. Temperature measurements of the inside adiabatic wall are made by 12 chromel-constantan thermocouples, 30 gauge, with glass and high temperature varnish insulation. In the drawing only six thermocouples are shown. At each of the positions shown there are four thermocouples, oriented at 0°, 90°, 180°, and 270°. This provides a measure of the variations in temperature in the circumferential direction. A sheet of mica of 0.003 in. thickness is inserted in the tube before the thermocouple assembly is installed. This provides electrical insulation of the thermocouples from the Monel test section, thereby eliminating the problem of direct current pickup in the thermocouple emf measurement. The resistance between the thermocouple and the Monel tube exceeds one megohm. Each thermocouple junction is silver soldered and held in position by a ceramic bead fastened by cement to an Inconel spring. This spring pushes each thermo-

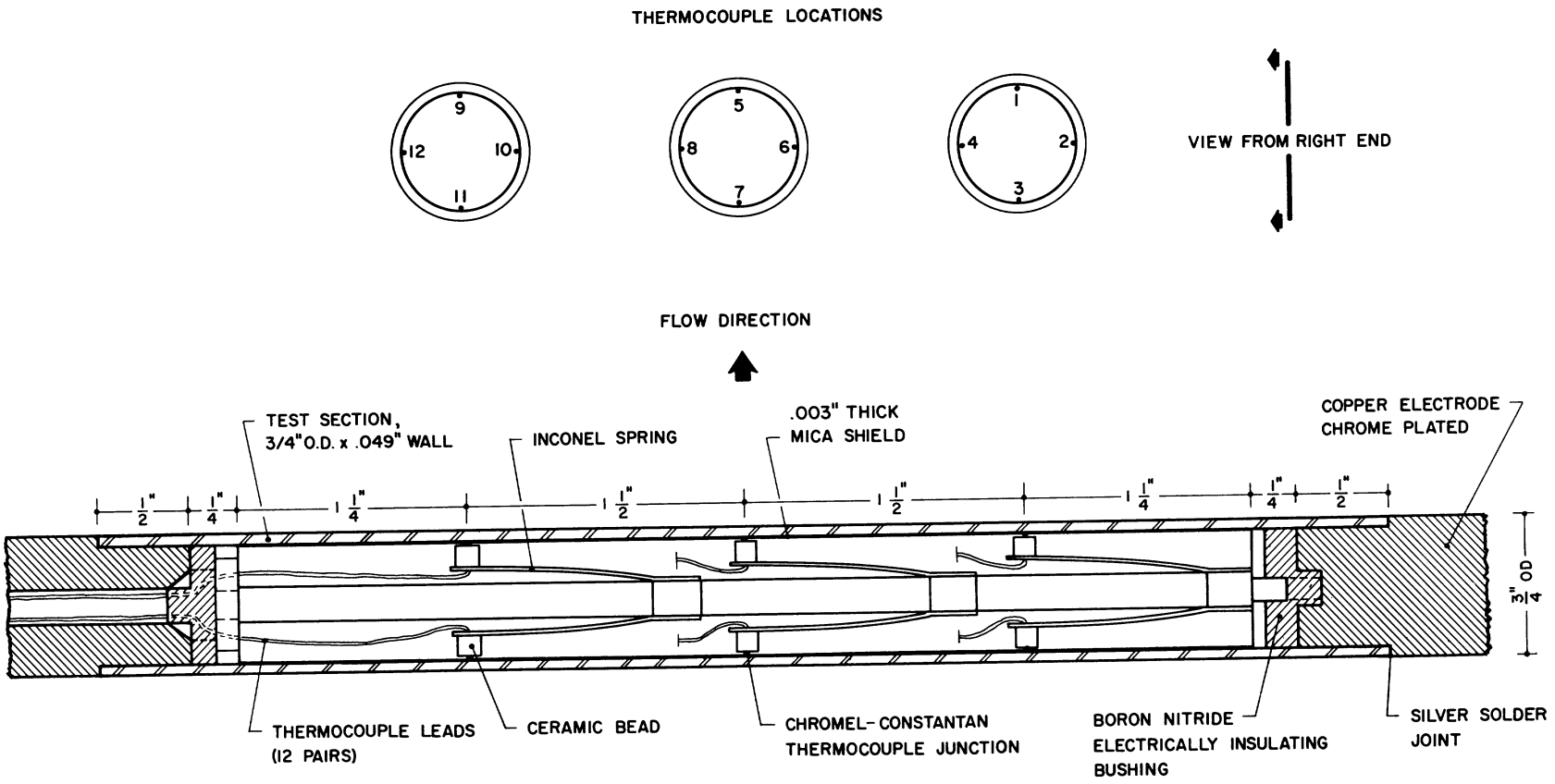

Fig. 4. Test section.

couple junction against the mica sheet with a force of about 1 lb. The 12 pairs of thermocouple leads pass from the test section through an axial hole, 1/4 in. diam, in one end of the copper electrode.

The test section is silver soldered to a nickel and chrome plated copper electrode of 3/4 in. diam. The overall length of the electrode is 55 in. The electrode diameter is increased to 1 in. where it passes through the vessel flange in order to minimize the current density and resultant Joulean heating of the copper.

The electrode must be electrically insulated from the test vessel at the gland through the flange. A special stuffing box was designed to utilize high temperature steam packing which is electrically non-conducting. The packing arrangement consists of alternate layers of Garlock 900 asbestos sheet packing and John Crane Superseal 4-J braided asbestos, mica lubricated packing. The sheet packing is machined into the solid rings 1-5/8 in. O.D. by 1 in. I.D. by 1/4 in. thick. These rings center the electrode in the gland and resist extrusion of the softer braided packing. The braided packing is supplied in a continuous roll, 5/16 in. square in cross section. Single rings with overlapping beveled ends are formed and placed between the layers of sheet packing. The softer braided packing makes the seal pressure tight. A stainless steel gland is used to tighten the packing initially and while in service. The gland has a larger than normal inside diameter in order to avoid accidental short circuiting of

the electrode. The gland is tightened by a follower plate which is pulled by three studs fastened to the vessel flange. The electrical resistance between the electrode and the vessel is over 100,000 ohms without water in the vessel. The resistance is approximately 100 ohms when the vessel is filled with water to the normal operating level. Since the vessel is grounded and the voltage on the electrode is about 10 volts above ground, the current leakage to ground is 0.1 ampere. This is negligibly small compared to the electrode current of 200 to 2500 amperes.

C. TEST VESSEL

The boiling studies are carried out in a test vessel, designed and fabricated in accordance with the ASME Pressure Vessel Code, Section VIII. The maximum working conditions are 2,000 psig and 650°F. The shell consists of 1 in. thick, type 347 stainless steel, ASME Specification A 312 T 347. Its length is 38 in. and the outside diameter is 12-3/4 in. The heads are flat T 347 forgings, 4 in. thick. The vessel is oriented with its axis vertical and is supported approximately 8 ft above the floor by two lugs bolted to a structural steel framework.

A cross sectional view of the test vessel and its assembled components is shown in Fig 5. The horizontal test section is held in the center of the vessel by the electrodes, which in turn are held rigidly in place by the electrically insulated packing gland. All

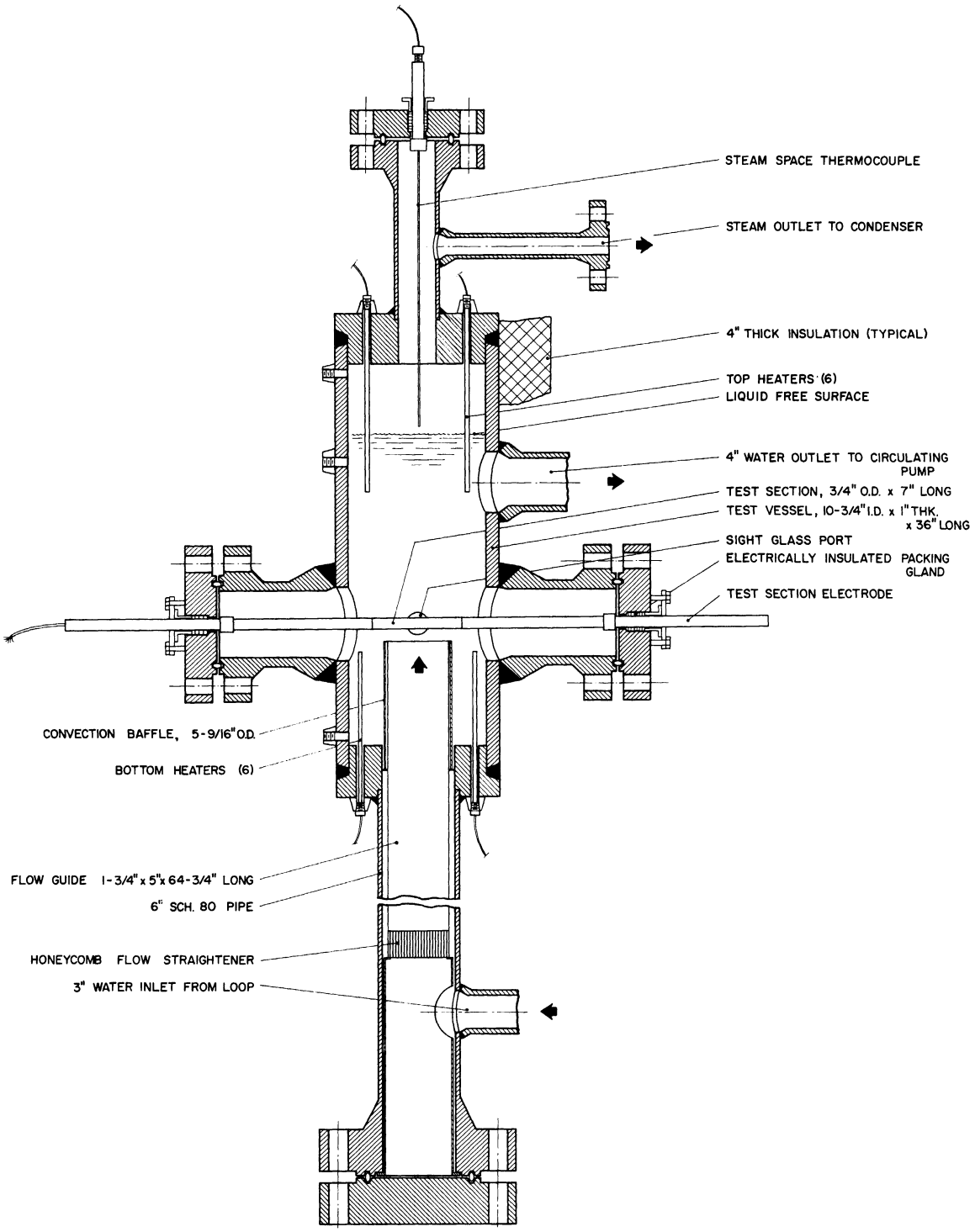

Fig. 5. Test vessel assembly.

flanges are type 347 stainless steel, 1500 lb ring joint type, with a welding neck connection.

The free surface of the water, about 18 in. above the test section, is shown in the figure. Above the free surface is a steam space. All air is vented from the steam space by vigorous boiling of the water for 2 hr prior to each series of runs. During this time the pressure is held to less than 30 psig and a continuous venting of steam and air is permitted. Steam passes out of the test vessel to the condenser and the condensate is returned by gravity flow countercurrent to the steam. The steam space temperature is measured by a calibrated chromel-constantan thermocouple encased in a 1/8 in. diam stainless steel sheath.

Forced convection of water upward and normal to the test section is caused by a circulating pump which is mounted in the main flow loop external to the test vessel. Water from the vessel is conducted to the pump suction by a 4 in. schedule 80 outlet pipe. The water is returned through a 3 in. schedule 80 pipe and enters a 6 in. schedule 80 pipe 8 in. above floor level. Inside the 6 in. pipe is a stainless steel flow guide 64-3/4 in. long. The floor guide is rectangular in cross-section, approximately 1-3/4 in by 5 in. Baffles prevent water from flowing upward between the inside wall of the 6 in. pipe and the rectangular flow guide. At the inlet of the flow guide is a flow straightener, consisting of a 2 in. length of stainless

steel honeycomb, with an opening of 3/16 in. across the flats of the hexagonal flow passages. The effect of the flow guide is to provide a fully developed turbulent flow profile 1 in. in front of the test section. The average velocity in the flow guide is 1.3 ft/sec for the low velocity tests and 4.7 ft/sec for the high velocity tests.

The water in the test vessel is brought up to and maintained at the required test temperature by 12 immersion heaters. Six heaters are threaded into fittings on the bottom head. These are rated at 650 watts each at 230 volts. The six top heaters are rated at 1000 watts each at 230 volts, with all of the resistance heating wire being concentrated in the 3 in. length at the end away from the threaded fitting. The ends of the top heaters are always immersed below the water surface, thus insuring adequate heat removal from the top immersion heaters. Each set of six heaters is wired in three phase, delta connection to the 460 volt supply, with two heaters being in series on each leg of the connection. The immersion heaters have an Inconel sheath. They are supplied by the Watlow Manufacturing Company.

The liquid level in the test vessel is measured by a Minneapolis-Honeywell indicating bellows meter, rated at 2500 psi static pressure with a full scale range of 0-25 in. water. The pressure connections are shown at the left side of the vessel in Fig. 5. The connection immediately below the top head is connected to the high pressure side

of the meter because this leg of the pressure transmitting line is always filled with liquid due to condensation. The connection immediately above the bottom head is connected to the low pressure side of the meter. The meter was calibrated against a U-tube manometer at atmospheric pressure and found to indicate well within the specified accuracy of ±1-1/4% full scale.

A low level shut-down switch is incorporated as a safety feature. A well is inserted in the connection shown in Fig. 5, somewhat below the liquid free surface. Into this well is inserted a 3/8 in. diam heater, rated at 130 watts and 80 volts. Also in the well and adjacent to the heater is a thermocouple which generates an emf in opposition to another thermocouple positioned in the steam space. The differential emf is sensed by a sensitive relay manufactured by Assembly Products, Inc. If the differential emf exceeds 5 millivolts, the relay shuts off all power to the system. Due to the high heat transfer coefficient between a heated surface and boiling water, the temperature of the well remains nearly that of the boiling water and of the steam. If the water level drops and the well is exposed to steam, the temperature rises due to the lower heat transfer coefficient. This in turn actuates the safety shut-down. The low level shut-down has a time lag of approximately 1 min when the liquid level falls below the well.

Figure 6 shows the test vessel in the erected position before

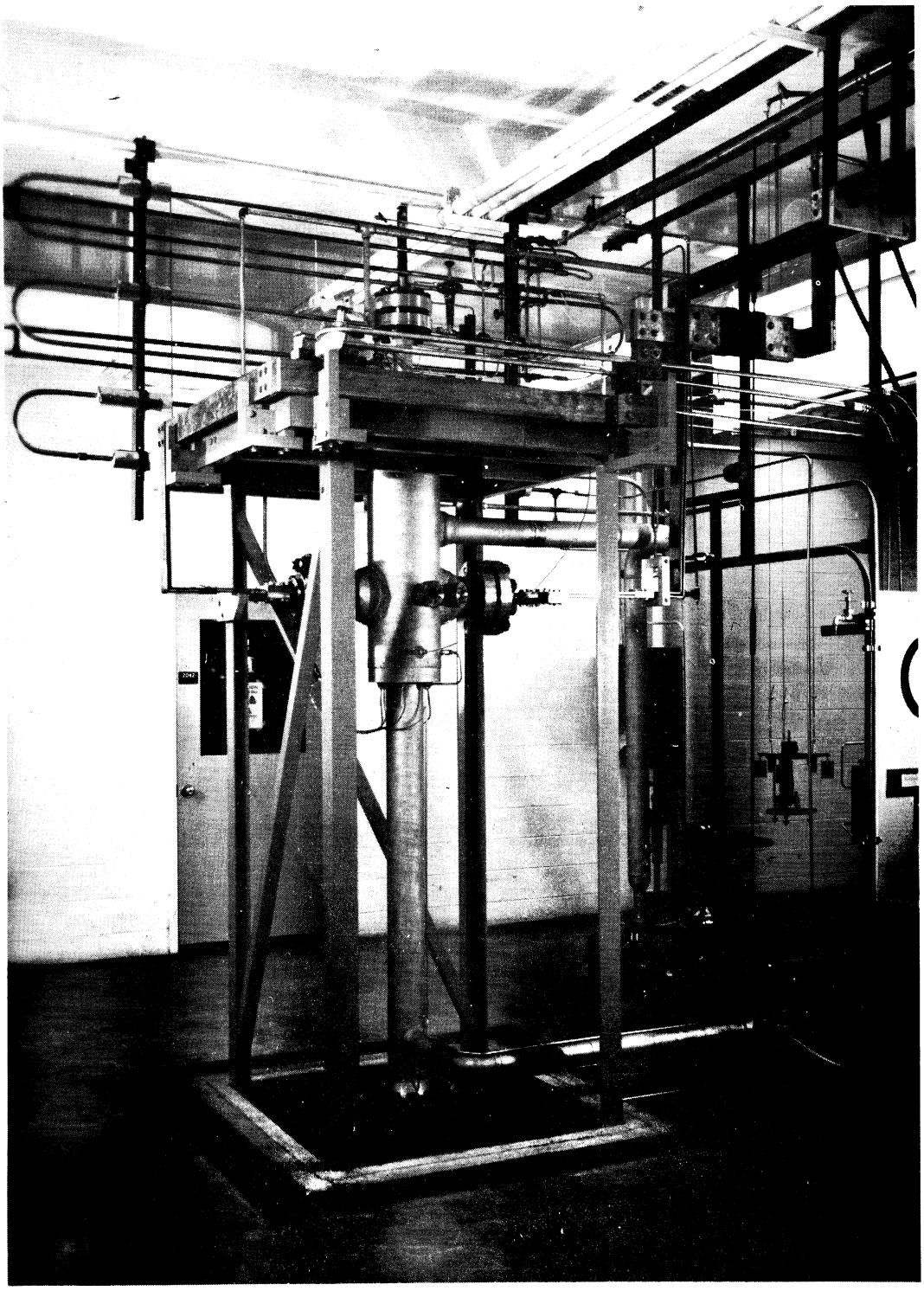

Fig. 6. Test vessel, before insulation is applied.

thermal insulation was applied. The test vessel and the 6 in. inlet section were covered with 4 in. of calcium silicate insulation. The piping loop was covered with a 2 in. layer of the same material. Flanges were covered by 2 in. thick molded Fiberglas sections held by insulation straps. This provides ready access to the flange studs and nuts. The insulated vessel and piping are shown in Fig. 7.

D. SYSTEM FLOW CIRCUITS

The test vessel is connected with three flow circuits which serve the functions of providing the circulation necessary for forced convection studies, of maintaining the water at a specified purity, and of controlling the pressure. The complete flow diagram is shown in Fig. 8. Referring to the figure, the test section (2) is shown in the test vessel (1) on the left. These items have been described in previous sections. The remainder of the system will be described in the following sub-sections:

1. Primary Flow Loop

The primary flow loop (4) consists of a 4 in. schedule 80 stainless steel pipe leading from the upper portion of the test vessel to a circulating pump, whence it flows through the flow metering section, the control valve, heater, and back to the inlet at the bottom of the test vessel. The range of velocities normal to the test section which can be achieved is from 0 to 5 ft/sec.

a. Circulating Pump.—The circulating pump (3) is supplied by

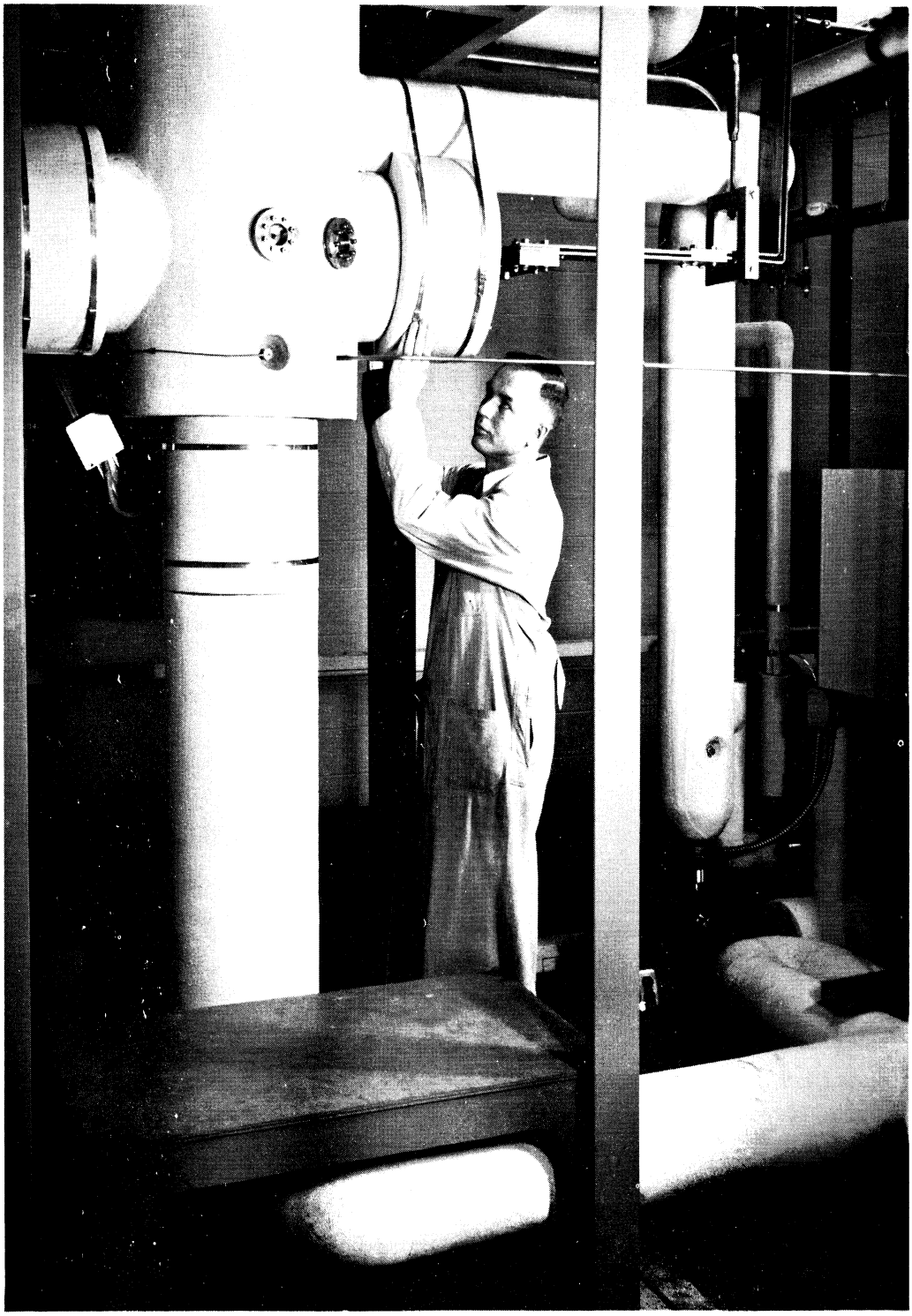

Fig. 7. Insulated vessel and piping.

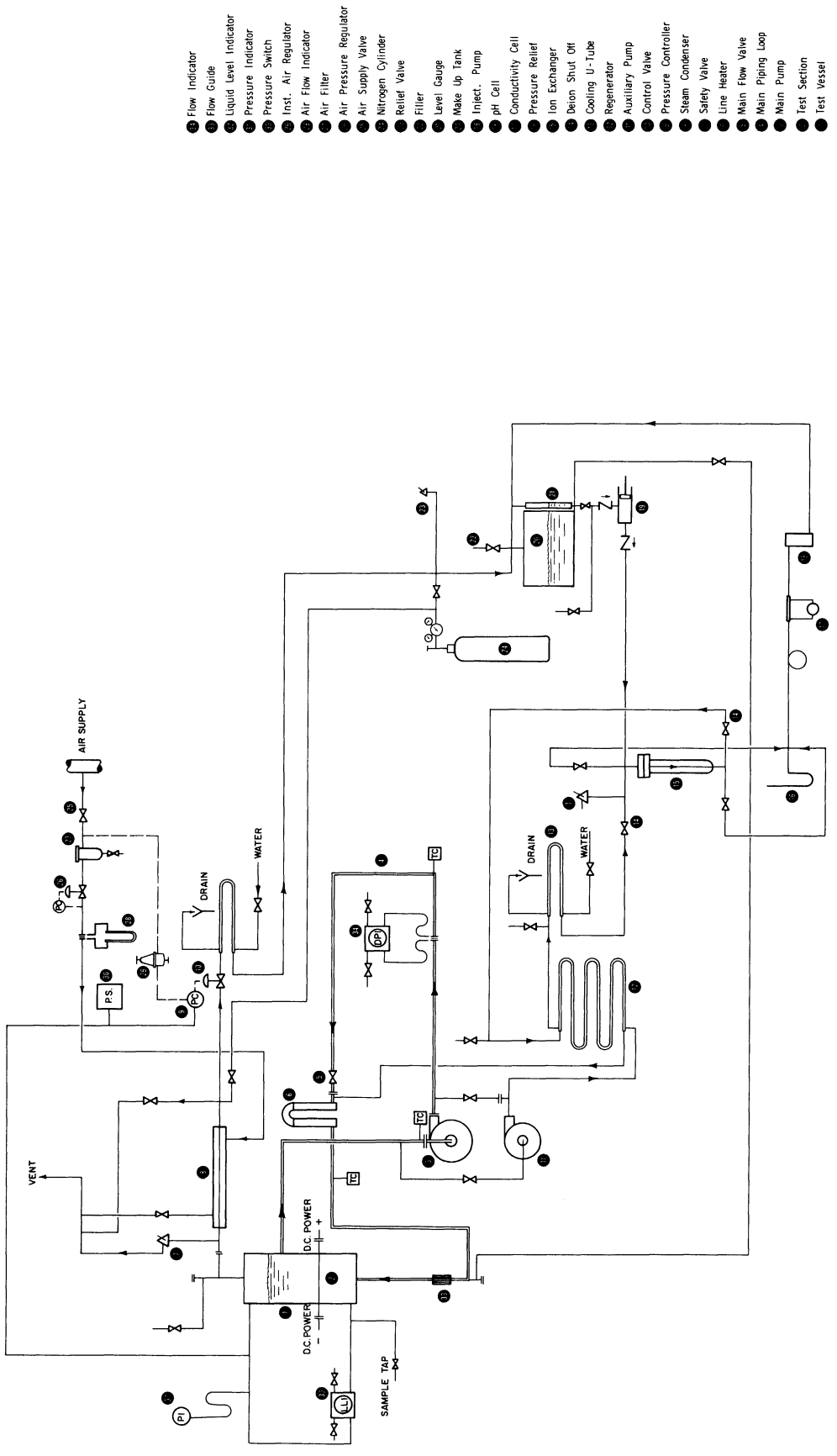

Fig. 8. System flow diagram.

Melrath Canned Pumps, Inc. to the following specifications:

Capacity- 140 gal/min water
Discharge head- 40 ft
Net positive suction head- 4 ft
Static pressure- 2000 psig
Materials- All wetted parts of 300 series stainless steel
Drive- direct connected electric motor
Power- 440 volts, 60-cycle, 3-phase

The most stringent requirements which this pump must meet are the pressure and temperature associated with boiling water at 2000 psig and the very low available net positive suction head (NPSH). The static head on the pump is approximately 7 ft. Due to the flow resistance of the suction piping, the NPSH is less than the 7 ft available due to elevation of the free surface above the pump. Since it is not feasible to increase the available NPSH by cooling the water as it flows to the pump, due to the very large heat exchange requirements, the pump must operate at the low value of 4 ft NPSH. The circulating pump performs this service as specified. During circulation at atmospheric pressure and 211°F (degassing) the pump is quite noisy. This noise, presumably due to cavitation, disappears at higher pressures and lower flow rates.

The pump and totally enclosed motor have no thermal insulation or cooling. The pump, therefore, operates at nearly saturation temperature (467-600°F). The 5 hp induction motor operates at nearly these temperatures, since it is cooled only by natural convection of the ambient air. The pump has operated continuously for periods of

12 hrs at 1550 psia and 600°F.

b. Flow Measurement.—The pump discharges into a 60 in. long section of 3 in. schedule 80 stainless steel pipe. This length of 20 diam preceeds a sharp-edge orifice designed to ASME standards. The orifice diameter is 2.000 ± .001 in. This orifice was installed in its piping system and calibrated by weigh tank measurements.

The pressure differential across the orifice flange taps is indicated by two Minneapolis-Honeywell indicating bellows meters, similar to the test vessel liquid level indicator (32). One of these meters (34) is shown in Fig. 8. It has a range of 0-100 in. of water. A similar meter with a range of 0-25 in. of water is installed in parallel with the first in order to permit more accurate flow measurements for the low velocity runs, when the orifice differential is approximately 4 in. water. The temperature of the water flowing through the orifice is measured by a thermocouple (TC) installed in an elbow downstream of the meter. This temperature is needed to make the density correction to the orifice reading.

c. Flow Control.—The flow through the primary loop is controlled by manually throttling on a 2 in. "Y" valve (5). This valve is similar to a globe valve but has a lower pressure drop when fully open. The valve has a Type 316 stainless steel body and is a Powell No. 1314 A. For 600°F service the Teflon valve packing was removed and replaced with mica impregnated asbestos rings.

d. Temperature Control.—Following the flow control valve the water passes through a line heater (6). This consists of a "U" tube of 3-in. schedule 80 stainless steel pipe with three immersion heaters in each leg. The six heaters are wired in three pairs so that the same amount of heat is put into each leg. The total rating of the immersion heaters is 18.2 kw. One pair of heaters is controlled by a variable voltage transformer which permits power variations of 0-4.6 kw. A second pair of heaters is rated at 4.6 kw and has ON-OFF control. The third pair of heaters is rated at 9.0 kw and has ON-OFF control. This control arrangement permits infinite variation of the power inputs from 0-18.2 kw but uses a small size variable transformer.

The temperature of the water following the line heater is measured by another thermocouple (TC). The flow enters the bottom of the test vessel through the 6 in. pipe in which is inserted a flow straightener and guide (33).

e. Installation.—The entire primary flow loop is fabricated from Type 347 stainless steel pipe and flanges. With the exception of the pump suction line, the loop is in a horizontal plane, 8 in. above the floor. The entire loop and pump baseplate is spring mounted to permit thermal expansion without creating excessive stresses due to restraints of fixed supports. Portions of the loop before and after the calcium silicate insulation was applied may be

seen in Figs. 6 and 7.

2. Water Purification Loop

Provision is made for continuous purification of the water by means of the filtration and deionizing of a small stream which by-passes the primary flow loop. Referring to Fig. 8, the main pump (3) or the auxiliary circulating pump (11) creates the pressure necessary to force approximately 1 gal/min through the purification loop. This hot water (470-600°F) is cooled in a counter-current flow heat exchange or regenerator (12) which reduces the temperature to 150°F. It is further cooled by heat exchange with cooling water in a U-tube type exchanger (13) so that the effluent does not exceed 100°F. The flow rate is controlled by throttling on the shut-off valves (14). The cooled water passes through the ion exchanger (15) which employs Rohm and Haas MB-1 Amberlite resin to give an effluent resistivity of about 4 megohm-cm. The ion exchanger also has a filter to remove solid particles. The deionized and filtered water is returned to the primary flow loop ahead of the line heaters, having been warmed to within 50°F of the saturation temperature by the regenerator (12).

The total quantity of water in the system is approximately 50 gal. If the assumptions are made of perfect mixing, and complete deionizing in the bed, then the purification flow of 1 gal/min would reduce the ion concentration by 1/e every 50 min. In actual service the clean-up is considerably slower, due to the incomplete deionizing

and the creation of new ions from the walls of the system. By circulating through the ion exchanger from 2 to 4 hr, the water resistivity can be increased to above 1 megohm-cm, starting with single distilled water of 500,000 ohm-cm.

a. Auxiliary Circulating Pump.—An auxiliary circulating pump, similar to but smaller than the main pump, permits the deionizing loop to be operated independently of the main loop. The pump is Chempump Model CFT-3/4-3/4-S. It is also a canned rotor pump and has a water cooled stator.

b. Regenerator.—The regenerator consists of 60 ft of 1/2 in. O.D. by .065 in. wall tubing inside of an equal length of 1/2 in. schedule 10 pipe (.840 in. O.D. by .083 in. wall). All material is Type 347 stainless steel. The 60 ft length is formed into a multiple S-shape, consisting of six lengths each 10 ft long. The tubing and pipe size were chosen such that high velocities, and resulting high heat transfer coefficients, would exist on both the tube and shell side at the rated flow of 1 gal/min. The regenerator is hung from the ceiling in a vertical plane and can be seen at the top rear of Fig. 6.

c. U-Tube Exchanger.—The U-tube exchanger consists of 20 ft of Type 304 stainless steel tubing, 1/2 in. O.D. by .065 in. wall, inside of a jacket of 3/4 in. O.D. copper tubing. The high pressure water passes counter-current to a flow of cooling water in the

jacket. This exchanger insures that the water entering the ion exchanger does not exceed the 140°F limit of the resin.

d. Ion Exchanger.—The ion exchanger assembly is shown in Fig. 9. It is a stainless steel pressure vessel containing approximately 7 lbs of Rohm and Haas Amberlite MB-1 resin. This resin is capable of increasing the electrical resistivity from 500,000 ohm-cm to 4 megohm-cm at a flow rate of 1 gal/min. A "Neva-Clog" filter is placed at the inlet to the resin bed. It is made from Type 347 stainless steel and is supplied by Multi-Metal Wire Cloth Co. A Micro Metallic sintered stainless steel filter, with a five micron mean-pore opening, is placed at the outlet of the bed to retain the resin and filter any particulate matter from the stream.

e. Sample Taps.—Sample taps are installed in the lines leading to and from the ion exchanger. A third sample tap is connected directly to the test vessel through the lower liquid level connection. One sample at a time is taken and passed through an electrolytic conductivity flow cell. This cell is connected to an Industrial Instruments Solu Bridge, Type RD-32, which indicates the specific resistance of the water. The range of the bridge is 20,000 to 4,000,000 ohm-cm, with an accuracy of 5% of the indicated reading.

The sample of water which flows through the conductivity cell is also passed through the cell of a Leeds and Northrup Model 7401 pH indicator. Since the measurement of pH introduces a small amount of

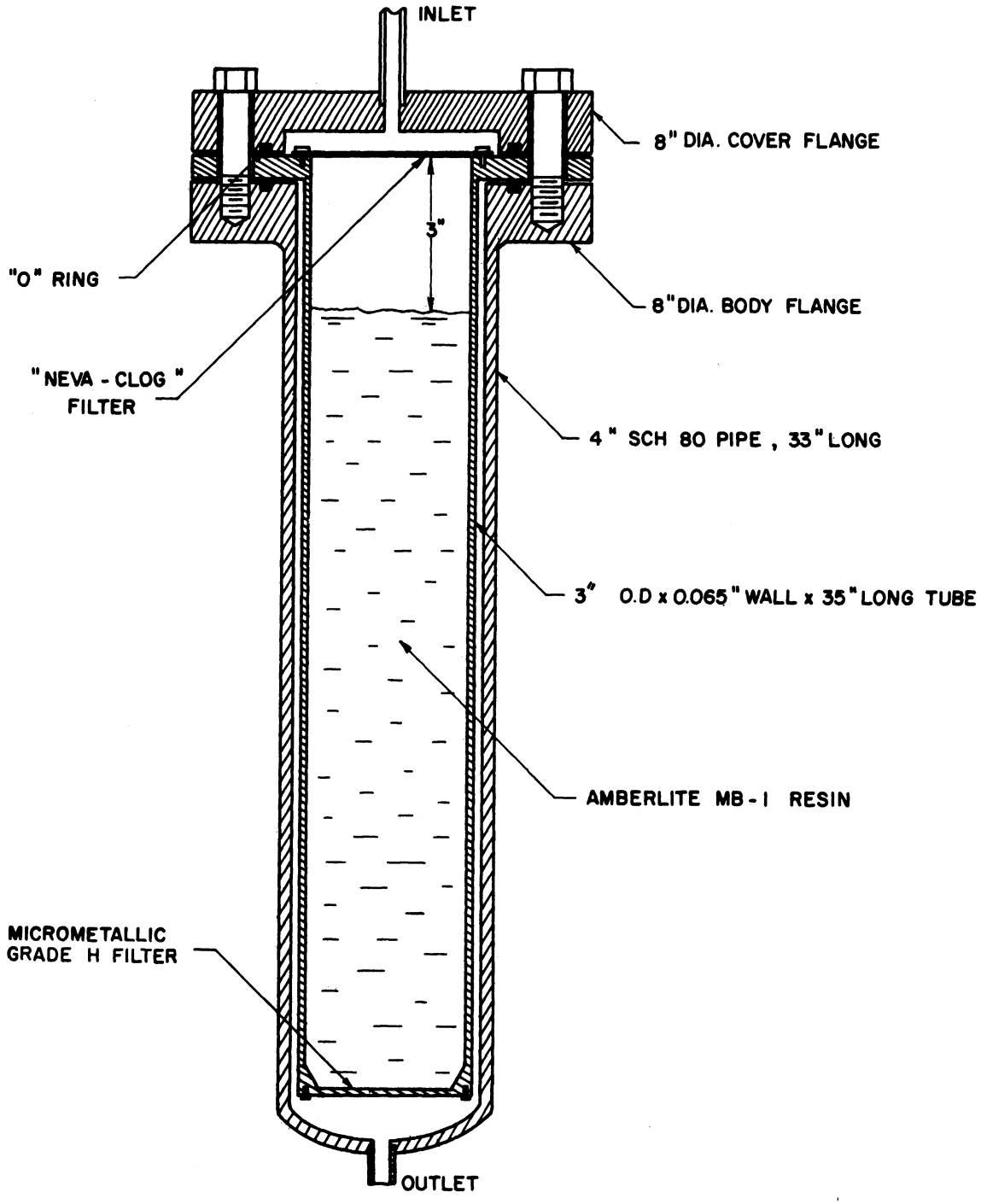

Fig. 9. Ion-exchanger assembly.

potassium chloride into the water, the sample of water is discarded after analysis.

3. Pressure Control Loop

The pressure in the system is generated and maintained by the boiling of water in the test vessel. Initially the water is thoroughly degassed by vigorous boiling, operating the condenser as a reflux condenser, and permitting the noncondensable gases to escape through vents at the highest part of the system. Referring to Fig. 8, steam from the test vessel (1) flows to the condenser (8). Most of the steam is condensed with the heat being removed by the warming of compressed air. Steam may be vented through a manually operated needle valve or through the Research Controls diaphragm operated control valve (10). This valve may be operated manually or automatically by the Fisher pressure controller (9). The pressure on the system is indicated by a Heise precision gage (31), having a range of 0-2500 psig and 2.5 psi scale divisions. It was calibrated to read correctly to within 0.1%.

a. Steam Condenser.—The steam condenser consists of a Type 347 stainless steel tube, 1-1/8 in. O.D. by 0.120 in. wall by 6 ft long, positioned centrally within a copper tube of 1-5/8 in. O.D. by .072 in. wall. The assembly is inclined from the horizontal with a pitch of 1 in./ft. The steam enters the lower end and the condensate drains counter current to the steam flow. The upper vent is con-

nected to the noncondensable gas bleed. The copper jacket has a Crane No. 404 expansion joint to permit differential thermal expansion of the stainless tube and the copper jacket. The jacket is silver soldered to the stainless tube by copper heat exchanger tees. In operation the cooling air flows countercurrent to the steam flow. The condensing capacity of the unit is regulated by adjustment of the cooling air flow rate and pressure. The design rating is 20,000 Btu/hr.

b. Steam Bleed System.—Provision is made to bleed automatically excess steam from the system by a Research Controls needle valve, actuated by a Fisher controller. The minimum band on the controller is 2% of full range, or 60 psi. It was found in operation that manual control of the heat input to the immersion heaters and heat rejection in the air cooled condenser permitted such precise pressure control that flucuations could not be observed on the Heise pressure gage. This control was achieved by semi-continuous observation of the steam space thermocouple emf. Variations of one microvolt could be observed. This corresponds to 0.025°F or approximately 0.25 psi change in saturation pressure at a level of 1,000 psia. During tests the steam temperature was held constant to ± 0.1°F (± 1 psi) for periods of several hours at a time.

4. Water Make-up System

The water make-up system consists of means of storing, injecting and draining the distilled water used in the system. Referring to

Fig. 8, distilled water is supplied to the 55 gal stainless steel make-up drum (20) through the filler connection (22). A vertical Tygon tube serves as the level gage (21). The make-up tank is kept purged with nitrogen from a cylinder (24). Excess pressure on the tank is prevented by a relief valve (23). Water is injected into the system by an injection pump (19). This water is fed to the inlet side of the ion exchanger (15) so that the make-up water is deionized before it reaches the test vessel. The system may be drained back into the make-up drum through a line connected to the low point of the system. Nitrogen from the cylinder is used to break the vacuum and pressurize the test vessel for complete drainage.

a. Make-up Drum.—The make-up drum is a 55 gal drum of Type 304 stainless steel. It is mounted horizontally on a table above the main piping loop at the rear of the control panel. The drum is seen at the left of Fig. 10.

b. Injection Pump.—The injection pump is a Wallace and Tiernan Metering Pump - Series 200. It has a single stainless steel plunger of 1/2 in. diam. The speed is fixed at 83 strokes per min but the stroke is adjustable from 0-100%. The maximum rating is 5.9 gph at 2,000 psi. The pump is driven through a worm gear by a one horsepower electric motor which is controlled manually from the 440 volt control panel. The pump is shown in the foreground of Fig. 11. It is mounted on the same table as the make-up drum.

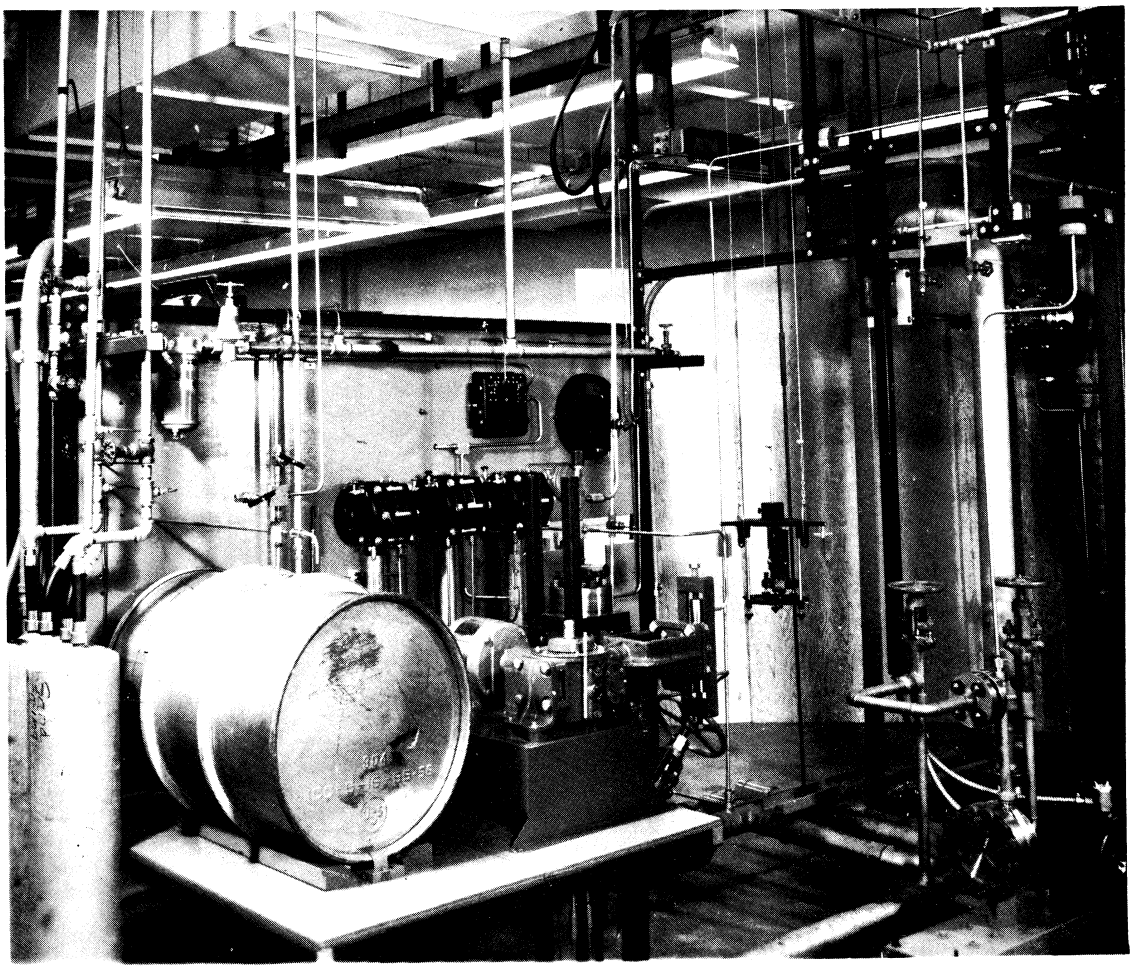

Fig. 10. Rear of panel, showing 55 gal make-up drum.

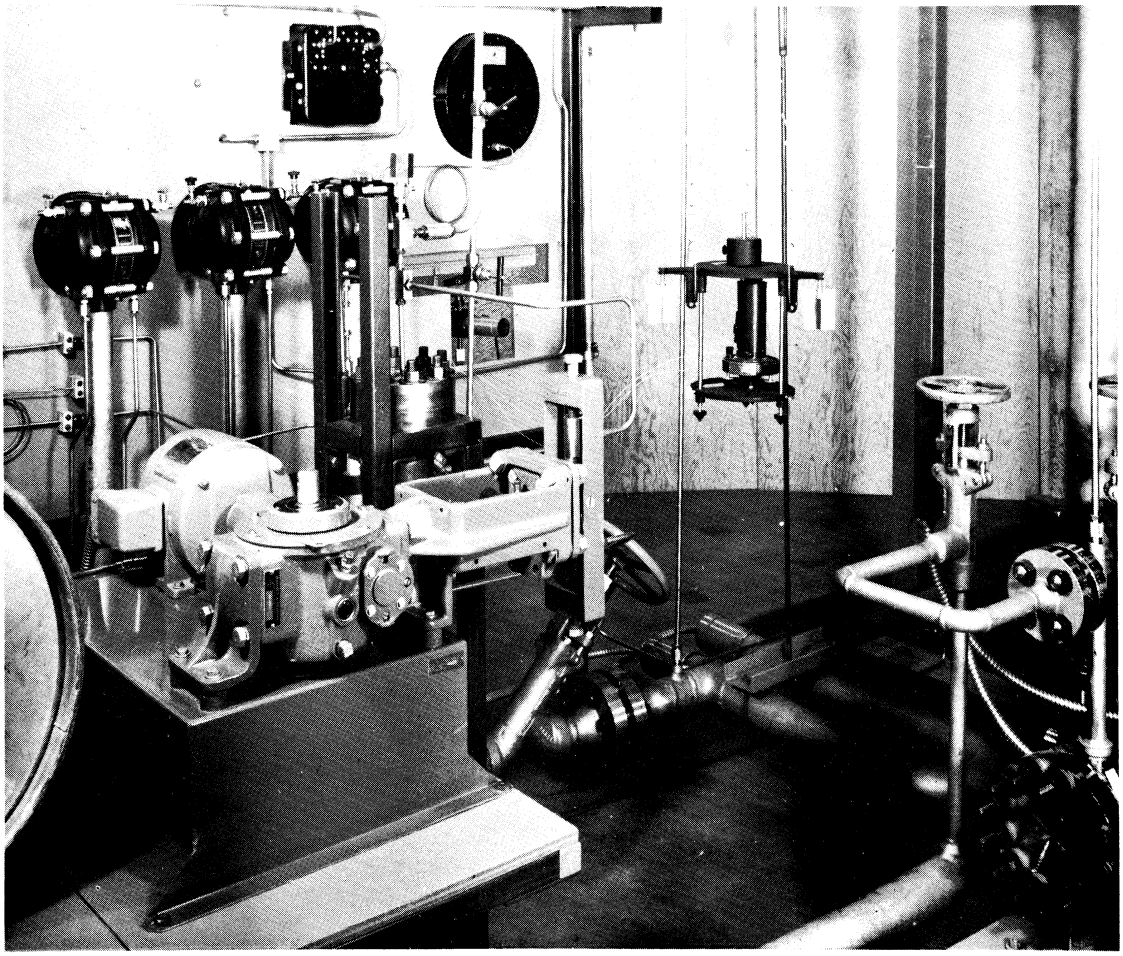

Fig. 11. Rear view, showing injection pump.

5. Safety Devices

The system is protected from excessive pressure by two Farris safety valves, set to relieve at the maximum design pressure of 2000 psig. One valve is connected directly to the steam space of the test vessel and discharges to a vent pipe which exhausts into the suction of a large building roof ventilator. The second valve is on the ion exchanger and is installed to prevent excessive pressure in the exchanger vessel in the event that both ion exchanger shut-off valves are closed when the injection pump is started. Despite every reasonable care in operation, this situation occurred several times during test runs and the safety valve functioned as required.

A pressure switch is also installed on the system. This is a Barksdale Catalog No. B2T-A32SS. It has two independent contacts adjustable between 160 and 3200 psig. One contact is used as a high pressure shut-off and is set at 1700 psig. It shuts off all 440 volt power to the system on excessive pressure. The other contact is set at 420 psig. It shuts off all 440 volt power to the system if the pressure drops below the set point. This serves to protect the pumps and heaters in the event of a line break and sudden loss of water from the system.

E. CONTROL PANELS AND POWER SUPPLIES

The operation of the low heat-flux boiling apparatus is monitored and controlled from a control panel along with the a-c electri-

cal control and power distribution panel and direct current generator control panel. In Fig. 12 the process panel is at the left, the d-c generator control panel in the center, and the a-c panel on the right.

1. Process Control Panel

On the process control panel are mounted the following instruments:

	Name	Details
1.	Differential Pressure Indicator, Minneapolis-Honeywell	0-25 in. water range, 1-1/4% full scale accuracy, to indicate liquid level in test vessel
2.	Differential Pressure Indicator, Minneapolis-Honeywell	0-25 in. water range, 1-1/4% full scale accuracy, to indicate orifice differential, low flow
3.	Differential Pressure Indicator, Minneapolis-Honeywell	0-100 in. water range, 1% full scale accuracy-to indicate orifice differential, high flow
4.	Pressure Gauge, Heise	2500 psi range, 0.1% full scale accuracy, to indicate pressure of system
5.	Pressure Controller, Fisher	0-3000 psi range, to control valve bleeding steam from the system
6.	Pressure Switch, Barksdale	160-3200 psi range, to provide electrical shutdown on high or low pressure

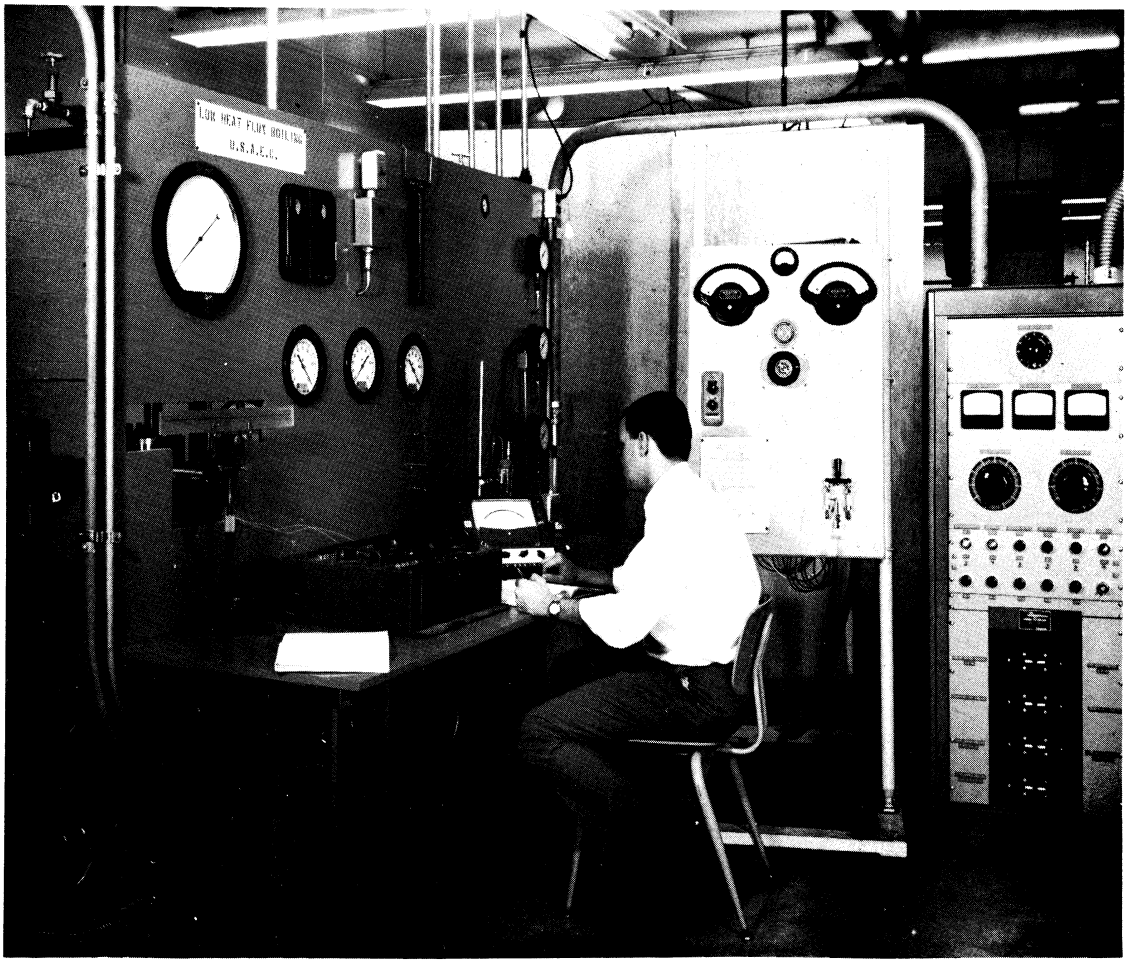

Fig. 12. Process and electrical control panels.

	Name	Details
7.	U-Type Manometer, King	0-10 in. range, to indicate flow of cooling air to condenser
8.	pH Indicator, Leeds and Northrup	Model 7401, to indicate pH of water
9.	Conductivity Cell, Industrial Instruments	Range 20,000 to 4,000,000 ohm-cm, to indicate electrical conductivity of water
10.	Galvanometer, Leeds and Northrup	Type 2285, to indicate thermocouple null balance
11.	Potentiometer, Leeds and Northrup	Type K-3, to measure thermocouple emf
12.	Pressure Gauges	0-100 psig, 3 gauges, to indicate cooling water pressures
13.	Air Regulator, Wilkerson	0-20 psig, to regulate cooling air flow

2. Alternating Current Panel

An alternating current electrical control and power distribution panel was designed and fabricated to supply and control the 440 volt, 60 cycle, 3 phase power required for the immersion heaters and pump motors. The electrical schematic diagram of this panel is seen in Fig. 13. On the left of the figure is a 110 volt control circuit with interlocking safety relays actuated by the low level switch and the pressure switches. On the right is shown the heater and pump circuits. The immersion heaters total 28.1 kw rating. The Chempump,

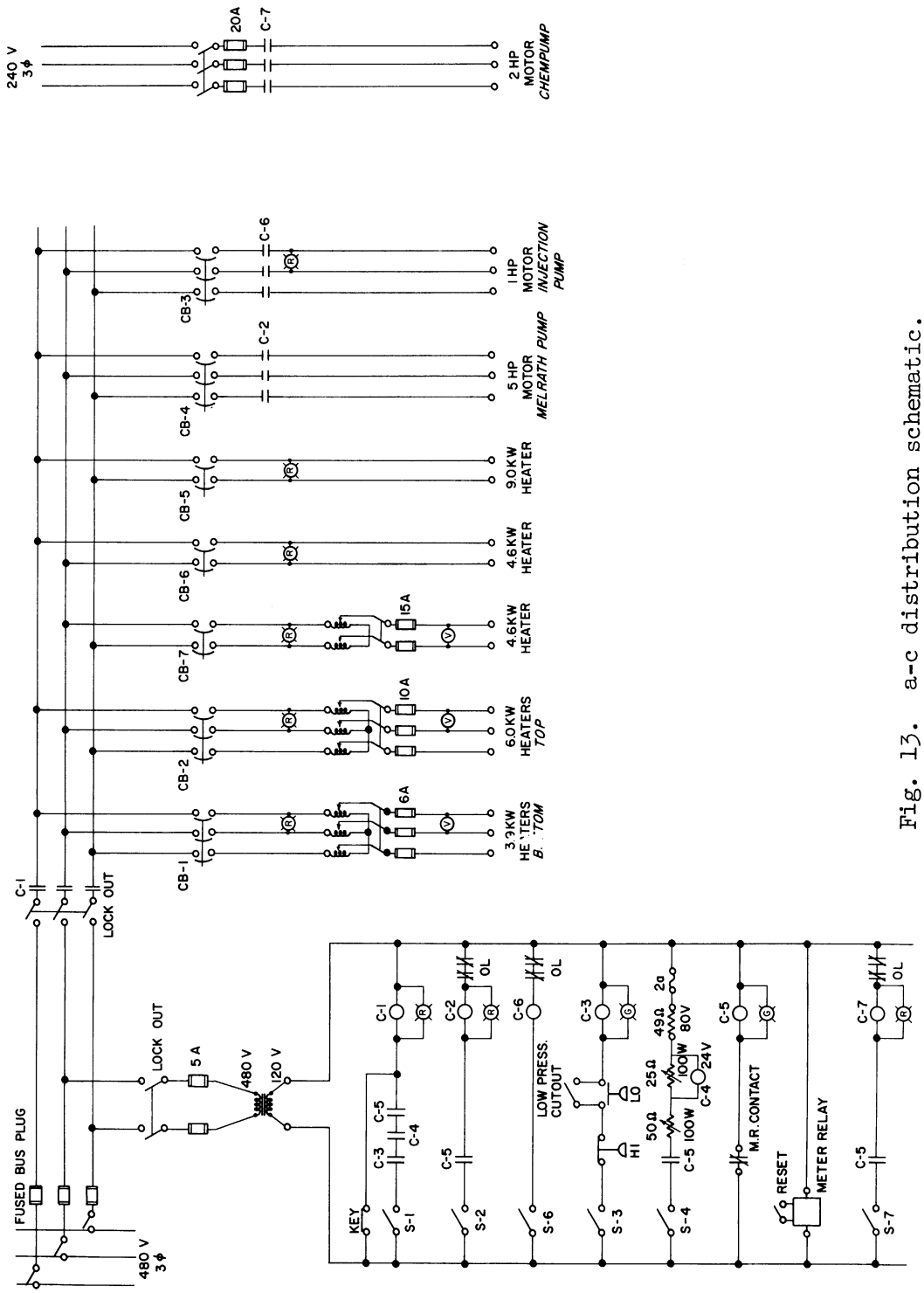

Fig. 13. a-c distribution schematic.

supplied from surplus stock, was wired for 220 volt, 3 phase power and requires a separate circuit. All circuits are protected against overload and equipped with indicating lights and meters.

3. Direct Current Panel

Direct-current resistance heating of the test section is caused by the passage of currents up to 3000 amp at 12 volts, produced by a Hanson-Van Winkle-Munning motor-generator set of 36 kw rating. This current is distributed throughout the laboratory by copper bus bars of 3 sq in. cross-sectional area. The voltage from the generator may be varied from 4 volts minimum to an overload of 15 volts. The control panel for this m-g set is seen in the center of Fig. 12.

An alternate supply of d-c power is supplied by a 50 kw germanium rectifier also manufactured by Hanson-Van Winkle-Munning. Rated maximum continuous output of this unit is 2000 amp at 25 volts. It is equipped with a remote control which controls the voltage from 0 to 25 volts. This power supply was used in some of the very low heat-flux tests.

III. TEST PROCEDURES

A. TEMPERATURE MEASUREMENT

The measurement of temperature is a matter of fundamental importance in any heat transfer research, inasmuch as the temperature gradient is the driving force which causes the flow of heat. In this study all temperatures are measured by the use of chromel-constantan thermocouples, calibrated against a platinum resistance thermometer as described in Appendix A.

All thermocouples have silver soldered or welded hot junctions. The wires are brought directly to distilled water ice reference junctions, without intermediate junctions. The emf from the reference junctions is sensed through shielded copper leads by a Type K-3 Universal Potentiometer (Leeds and Northrup) used with a Model 2284d moving coil galvanometer, mounted in a Julius suspension hung from the roof of the laboratory building.

1. Steam Temperature

The steam temperature thermocouple is encased in and insulated from a stainless steel sheath of 1/8 in. diam. This thermocouple protrudes downward from the top flange with its tip being from 1 to 3 in. above the liquid level. The arrangement is seen in Fig. 5. The immersion depth is approximately 24 in. which insures a vanishingly small conduction error.

The thermocouple used to measure the steam temperature was checked against another thermocouple inside the same sheath and also against a separate 1/16 in. diam sheathed couple. As noted in Appendix A, these three thermocouples yielded very consistent readings. The standard deviation of 42 readings taken by two observers during Run HM-29 is .06°F. Thus the odds are favorable (10 to 1) that any given reading is within ±.1°F, neglecting certain types of systematic errors. It is noted that the depth of immersion for the thermocouples as installed for test runs is always greater than the immersion during calibration. This eliminates a type of error cited by Dahl,[41] due to decreasing the depth of immersion.

2. Test Section Temperatures

As described earlier, the test section has 12 thermocouples pressed against the inside wall. The four thermocouples in the center of the test section are used for all data reported except zero heat flux temperature checks. The thermocouple emf is measured by the same instrumentation as the steam temperatures. Some readings, especially during pool boiling tests at lower pressures, fluctuated with time. A few such readings varied as much as ±12 μv or ±.3°F. In every case the emf was observed over a number of cycles of the fluctuations and a mean value recorded.

The inside wall of the test section is an adiabatic surface. This eliminates a temperature gradient through the .003 in. thick mica

insulator and, hence, the measured temperature is the same as that of the inside surface of the metal test section.

3. Wall Temperature Drop

The temperature at the outside surface of the test section is required in order to determine the temperature gradient between the heat transfer surface and the saturation temperature of the water. The temperature drop across the wall at a heat flux of 100,000 Btu/hr-ft^2 is about 14°F. This small variation in temperature makes valid the assumption of constant physical properties. With this assumption the equation which expresses the wall temperature drop is

$$T_i - T_o = \Delta T_{wall} = \frac{q'''}{2k}\left[\frac{r_o^2 - r_i^2}{2} - r_i^2 \ln(r_o/r_i)\right] \qquad (14)$$

where q''' is the heat generation per unit volume.

The heat generation rate, q''', Btu/hr-ft^3, is found from the product of the resistivity, ρ_e, ohm-ft, and the square of the current density, i, amp/ft^2;

$$q''' = i^2 \rho_e c_1 \qquad (15)$$

where c_1 is a conversion factor equal to 3.413 Btu/watt-hr. Based on the total cross-section of the test section, A_{tube}, ft^2, and the total current, I, amperes this is

$$q''' = \frac{I^2 \rho_e c_1}{(A_{tube})^2} \qquad (16)$$

The tube wall temperature drop, to the nearest 0.1°F, is subtracted from the average value of the four center thermocouples to give an average outside tube surface temperature. The use of average temperatures and total tube cross-sectional area renders unnecessary a consideration of slight variations in tube wall thickness around the circumference in computing the tube wall temperature drop. In Appendix D individual thermocouple readings are presented which show that there is no significant variation in temperature along the test section axis.

B. POWER MEASUREMENT

The total current which passes through the test section is determined by measuring the voltage drop across a shunt of 10^{-5} ohm resistance. An L & N, Type 8662, potentiometer is used to measure the voltage drop across the shunt and indicate the current to the nearest ampere.

C. ELECTRICAL RESISTIVITY MEASUREMENT

As noted above, the electrical resistivity, ρ_e, is required to calculate the heat generation term, q'''. This property was measured as a function of temperature by passing a small known electrical current through a sample of the Monel tube and measuring the voltage drop across a known length. This gives the resistivity of the tube in the "as fabricated" condition. Values obtained are given in Table I.

TABLE I

ELECTRICAL RESISTIVITY OF MONEL TUBE

Temperature, °F	Resistivity, μohm-cm, ±1%
100	49.4
200	50.6
300	51.6
400	52.5
500	53.2
600	53.8

D. THERMAL CONDUCTIVITY MEASUREMENT

The thermal conductivity, k, used to calculate the wall temperature drop was measured by using plates of Monel machined from the thick wall tube, or shell, from which the tubes were drawn. The shell size was 2-1/2 in. O.D. by .312 in. wall. This was split, flattened, annealed at 1800°F, and machined into a flat plate, .2973 in. thick by 2-1/2 in. square. The thermal conductivity of this plate was measured with a comparison technique by the Dynatech Corp., Cambridge, Mass. Results are presented in Table II.

TABLE II

THERMAL CONDUCTIVITY OF MONEL

Temperature, °F	Thermal Conductivity, Btu/hr-ft-°F, ±5%
450	16.4
550	17.4
650	18.5

E. PRELIMINARY PREPARATIONS

The system was washed with methylene chloride solvent after fabrication. Prior to making test runs, it was rinsed with distilled water several times. Finally, it was filled with approximately 43 gal of single distilled water.

Before each run, or series of runs made in a group, the water in the system was heated to 211°F or slightly higher and held under a pressure of less than 30 psig. For a period of 2 hr the water was boiled vigorously with most of the steam being condensed and returned to the system. A small bleed of steam and noncondensable gases was permitted from the two high points from the system. The main circulating pump was run during this period, circulating about 50 gal/min, to insure that all water in the system is subjected to the degassing action. In previous work, Clark and Rohsenow,[43] found that a period of 3/4 hr was sufficient to reduce the oxygen content to approximately 1.5 ml air/l. After the degassing the vents were closed, the cooling air to the condenser shut off, and the pressure allowed to increase to the desired operating pressure.

During heating the water was circulated by the pump and a flow through the ion exchanger was maintained to increase the resistivity of the water from the initial value of 500,000 ohm-cm to a value greater than 10^6 ohm-cm (1 megohm-cm) for test runs. Frequently values as high as 2 megohm-cm were attained. A heating period 3 to 4 hr was required to raise the pressure to 1000 psig.

F. ATTAINMENT OF STEADY STATE CONDITIONS

At the beginning of a run, or after making a change of a controlled variable during a run, sufficient time was allowed for the attainment of steady state conditions before data were taken. This ranged from 20 min to 1 hr, depending on the steadiness of steam space temperature. The heat balance of the system was manually adjusted so that the temperature did not vary by more than ±0.1°F over any series of readings. Usually an entire run, lasting from 3 to 6 hr, was made without the temperature varying more than ±0.2°F. At 1000 psig this is equivalent to a change in saturation pressure of ±2 psi, or less than the least scale division on the Heise pressure gauge.

At a specified test condition, readings were made of the various thermocouple emfs, pressure, flow rate, power input, etc. During each test, data were recorded in the same sequence. The steam space thermocouple was read just prior and after the reading of the test section thermocouples. If there were a difference in steam space readings, an average was taken. Several measurements were made of the electrical current through the test section, and an average value reported. The readings had a maximum variation of 1% while reading the test section thermocouples.

All data were taken by two observers, one reading the K-3 potentiometer, and the other taking and recording the remaining data. The two observers frequently switched roles to minimize the effect of personal bias in reading.

IV. TEST RESULTS

A. SUMMARY

The experimental results are summarized in a series of curves showing the relationship between the heat flux and the temperature difference between the outer surface of the tube wall and the saturation temperature of the liquid. It was found in this study, and has been reported by others,[7,44] that there is a difference in the wall superheat at a given heat flux, dependent upon whether the point had been approached from a higher or lower heat flux. All data used in the summary curves were taken when approached from a higher flux, since this results in more reproducible data. Hereafter this will be termed "decreasing" flux, although each data point represents an equilibrium reached after at least 20 min of constant heat flux. The "increasing" flux data are presented on more detailed curves in a subsequent section. A tabulation of all data is included in Appendix C.

Figure 14 shows the effect of pressure on pool boiling of saturated distilled water on the outside of a horizontal Monel tube of 3/4 in. O.D. The principal effect of increasing pressure is the decrease in the wall superheat at a given flux. The slopes of the curves vary slightly with pressure, decreasing from 2.09 to 1.77 as the pressure is increased from 535 psia to 1550 psia. An empirical equation which fits the data for pool boiling in the region plotted to within

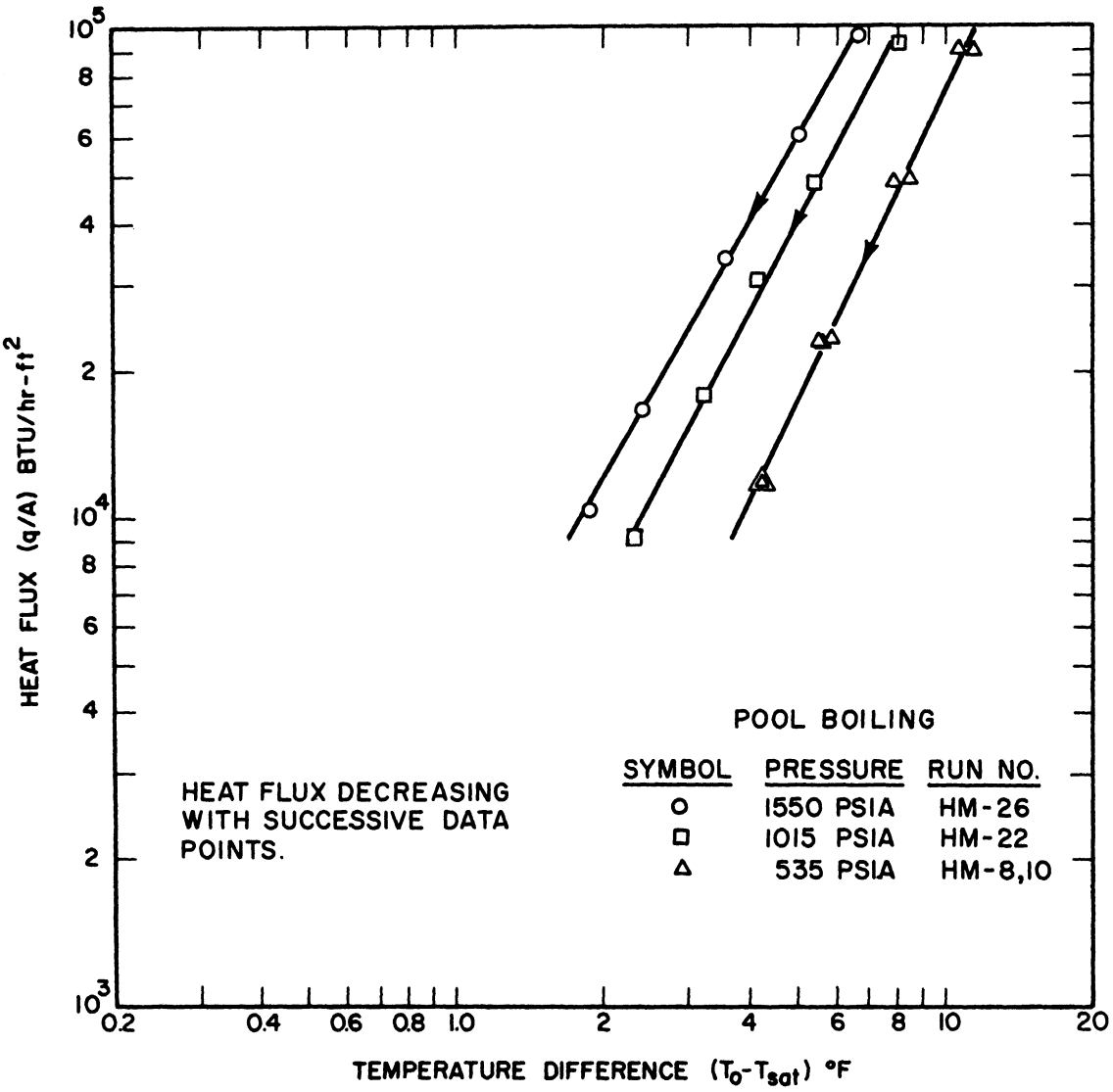

Fig. 14. Pool boiling of saturated distilled water on the outside of a horizontal Monel tube, 3/4 in. O.D., showing effect of pressure.

10% is

$$(q/A) = 13{,}700(p^*)^{1.72}(T_w - T_{sat})^{f(p^*)} \qquad (17)$$

where $f(p^*) = 1.56(p^*)^{-1/6}$ and heat flux, q/A, is expressed in Btu/hr-ft^2, p^* is the reduced pressure, p/p_{crit}, and $(T_w - T_{sat})$ is the wall superheat, °F.

The summarized results for boiling with a flow normal to the tube and upward at 1.3 ft/sec are shown on Fig. 15. The general characteristics are the same as in pool boiling, with the slopes of the curves decreasing from 2.03 for a pressure of 535 psia to a slope of 1.82 at 1550 psia. The curves are displaced to the left showing that a smaller wall superheat is required at a given flux. This decrease in wall superheat is small, ranging from about 0.2°F at a flux of 10,000 Btu/hr-ft^2 to about 0.6°F at a flux of 100,000 Btu/hr-ft.^{2}

Figure 16 presents data for nucleate boiling with a normal velocity of 4.7 ft/sec. The slopes of the three curves are quite similar, being 1.83 at 535 psia, 1.87 at 1015 psia, and 1.85 at 1550 psia. It is within the accuracy of the data to consider that the three curves have a common slope of 1.85. The curves are displaced to the left of those on Fig. 15, indicating an even smaller wall superheat for a given heat flux.

B. EFFECT OF VELOCITY

A plot showing the effect of approach velocity at a given pres-

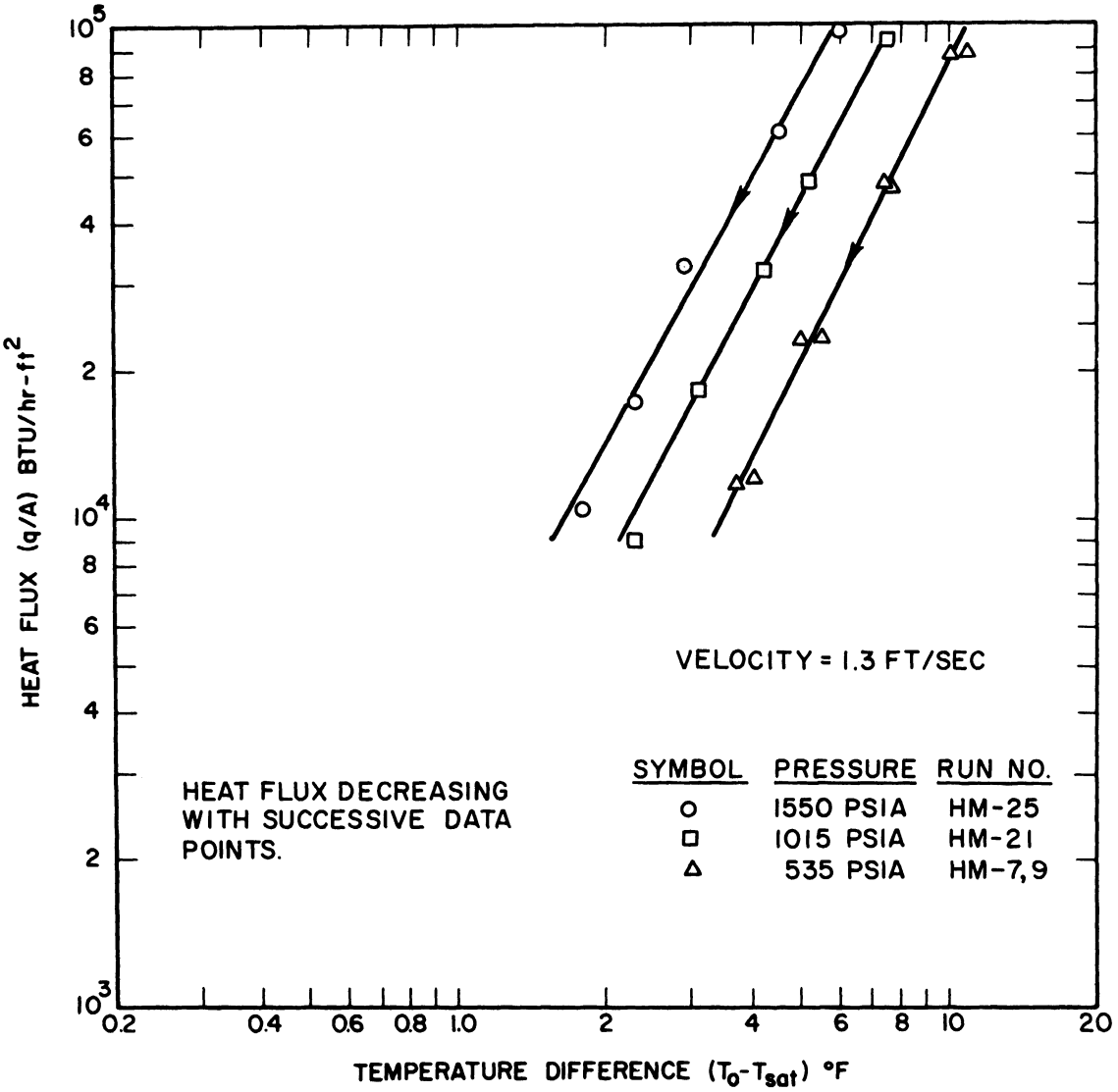

Fig. 15. Boiling of saturated distilled water flowing at 1.3 ft/sec normal to 3/4 in. O.D. Monel tube.

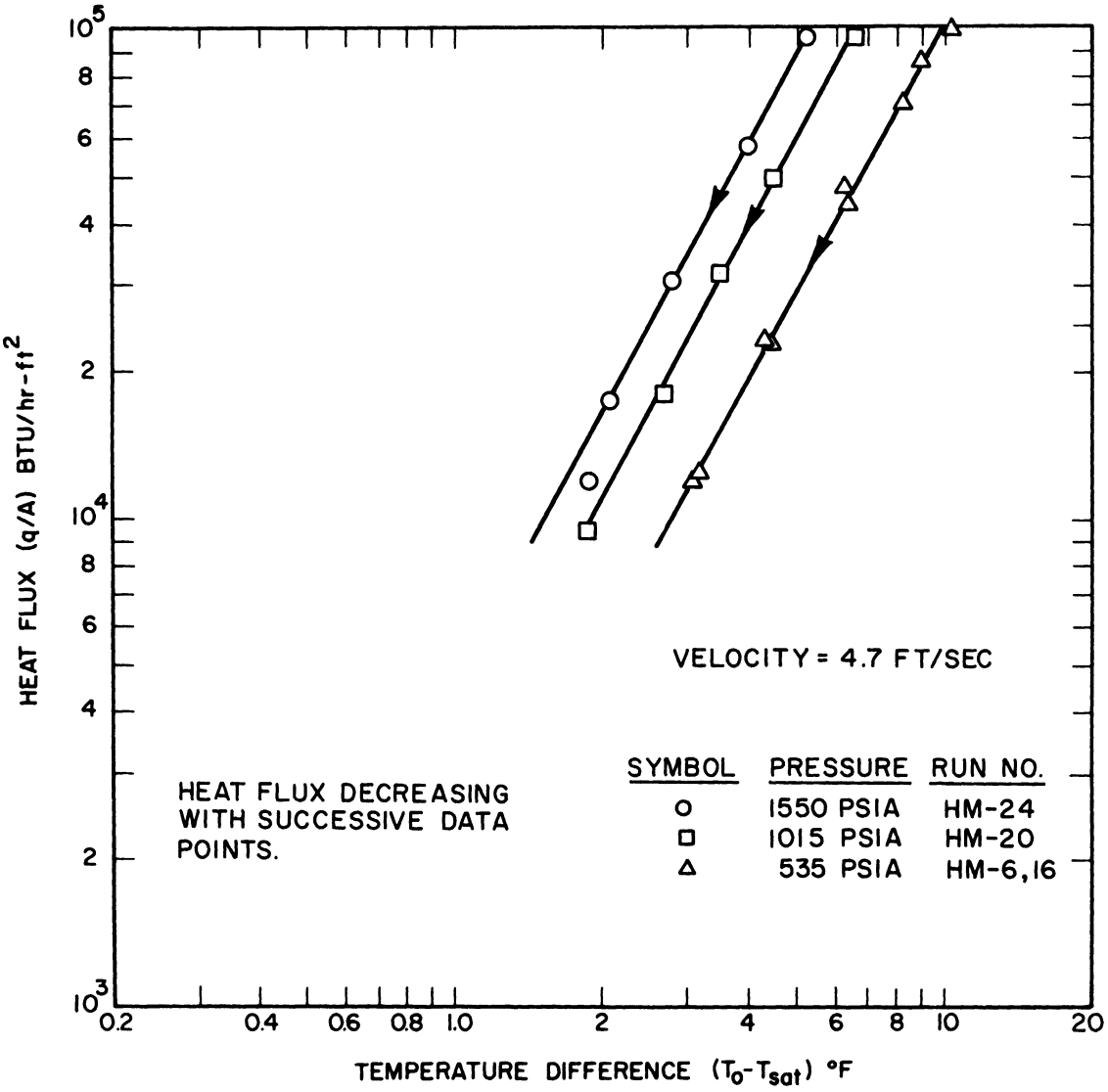

Fig. 16. Boiling of saturated distilled water flowing at 4.7 ft/sec normal to 3/4 in. O.D. Monel tube.

sure is presented in Fig. 17. The data on this figure are taken from the same runs as in the previous three figures. At pressures of 535 and 1550 psia the results are similar although Fig. 17 employs only data taken at 1015 psia. The slopes of the three curves are nearly identical, with 1.90 being a mean value.

C. POOL BOILING AT 535 PSIA

Data taken during three runs of pool boiling at 535 psia are shown in Fig. 18. The range of heat flux is from 2,000 to 100,000 Btu/hr-ft^2. It is evident that more scatter exists in the data taken for increasing heat flux.

The three points of Run No. HM-12, decreasing heat flux, which are shown at 9420, 5350, and 3550 Btu/hr-ft^2 are significantly displaced from the remainder of the decreasing curve. The operation at decreasing heat flux on Run HM-12 was interrupted at a flux of 23,100 Btu/hr-ft^2 and a period of zero flux existed for 5 min. The direct current was again passed through the test section for the remaining three points of Run HM-12. Therefore the heat flux history of these three points does not include the higher heat flux of 100,000 Btu/hr-ft^2.

D. BOILING WITH FORCED CONVECTION AT 535 PSIA

Data from four runs made with constant conditions of 535 psia and a normal velocity of 1.3 ft/sec are plotted in Fig. 19. The relatively wide scatter of the data taken with increasing heat flux is evident. The curve for increasing heat flux is drawn through the points of Runs

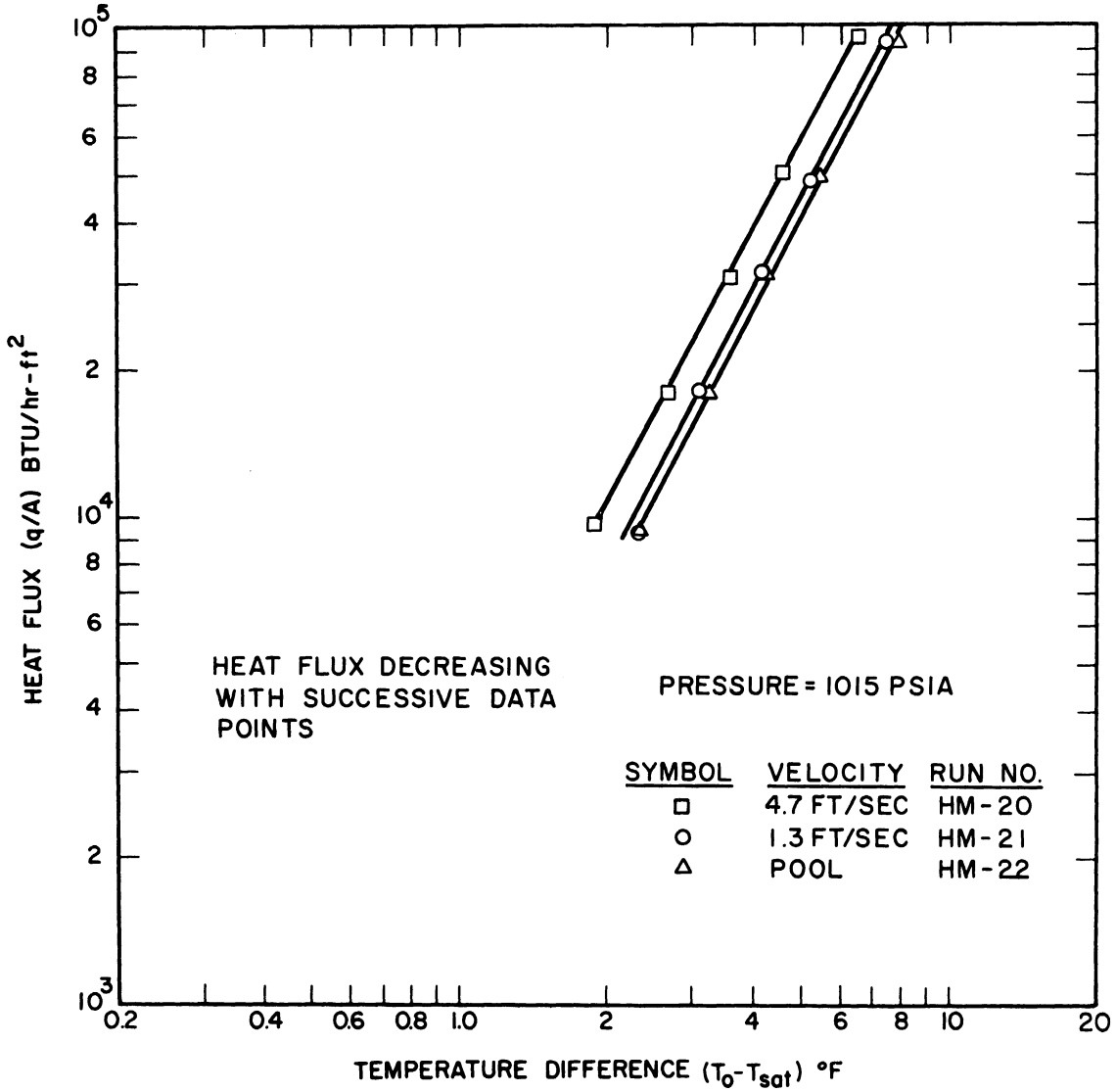

Fig. 17. Effect of velocity normal to a 3/4 in. tube on heat transfer to saturated distilled water at 1015 psia.

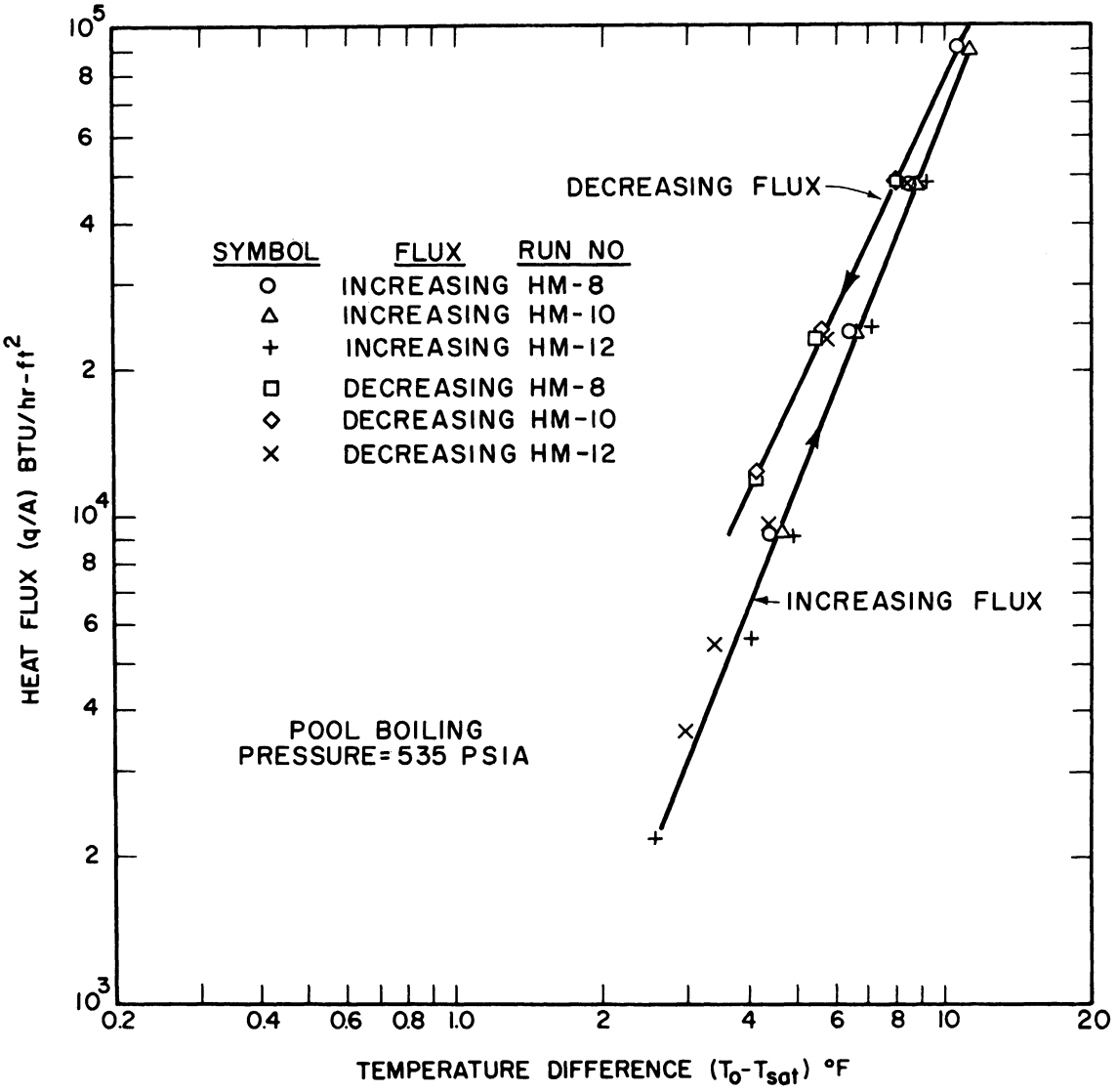

Fig. 18. Pool boiling of saturated distilled water at 535 psia.

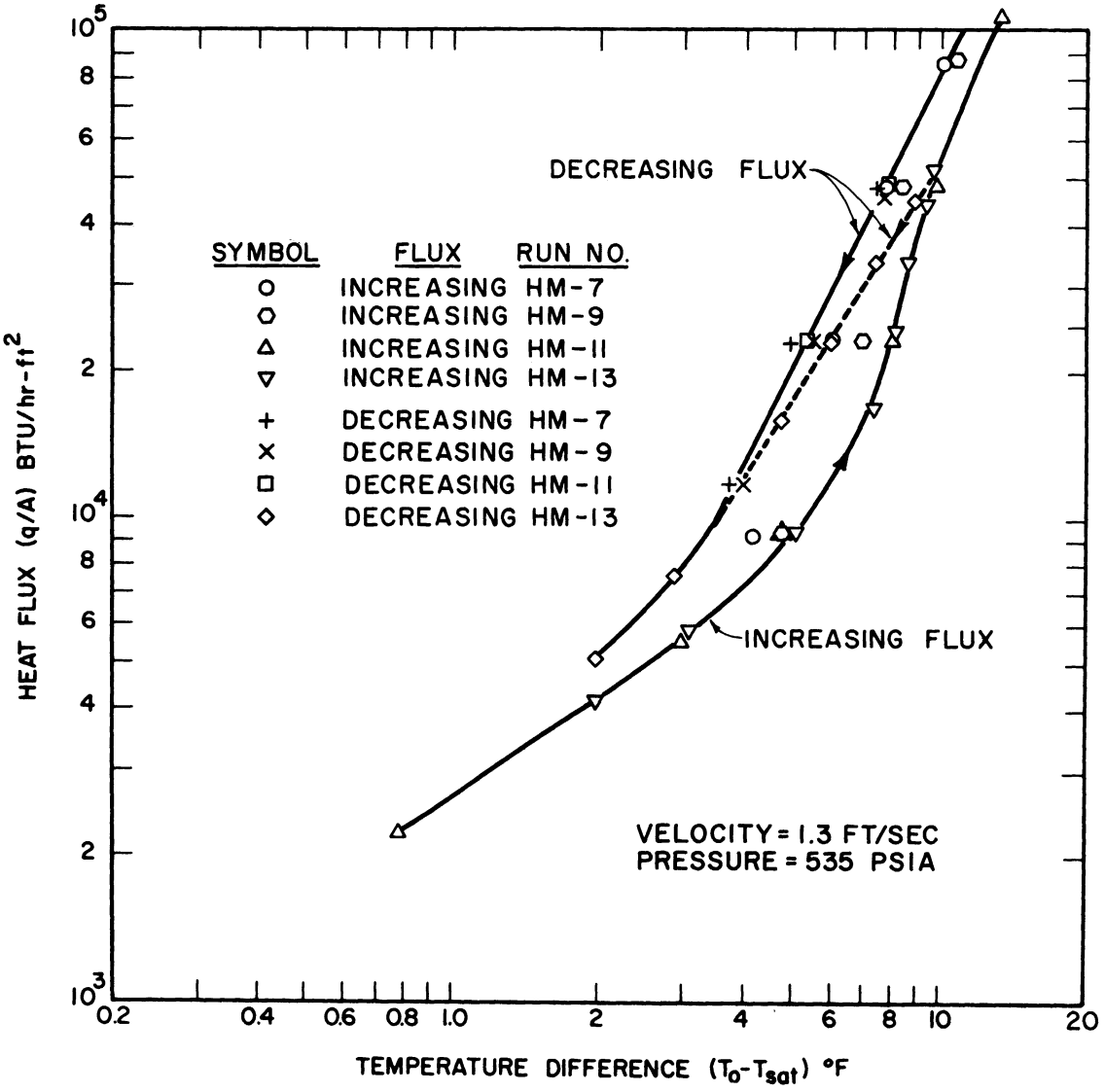

Fig. 19. Heat transfer to saturated distilled water flowing at 1.3 ft/sec and 535 psia.

HM-11 and HM-13.

The data exhibit less scatter on decreasing flux and a single curve is representative of the three runs which had a peak flux during the run of about 100,000 Btu/hr-ft^2. Of considerable interest is the behavior of the decreasing heat flux curve for Run HM-13, shown by a broken line. In this case the peak flux during the run was 51,800 Btu/hr-ft^2.

At very low heat fluxes the curves exhibit less steep slopes, indicating nonboiling heat transfer.

The data for higher velocity forced convection heat transfer at 535 psia are presented in Fig. 20. Only a few points were observed for increasing heat flux but the results are consistent with those of pool boiling and low velocity flow. The decreasing flux data show two distinct, almost parallel, curves. The solid curve is based on points which have a prior history of about 100,000 Btu/hr-ft^2. The broken curve is based on points which have a history of 43,500 Btu/hr-ft^2 as a maximum.

E. POOL BOILING AT 1015 PSIA

Data which show the effect of heat flux history on pool boiling at 1015 psia are shown in Fig. 21. The maximum heat flux during the run was 96,000 Btu/hr-ft^2. This was held more than 1 hr to permit the temperature difference to decrease to a reasonably steady value. The decrease noted in 1 hr was 0.5°F. All runs at 1015 and 1550 psia were

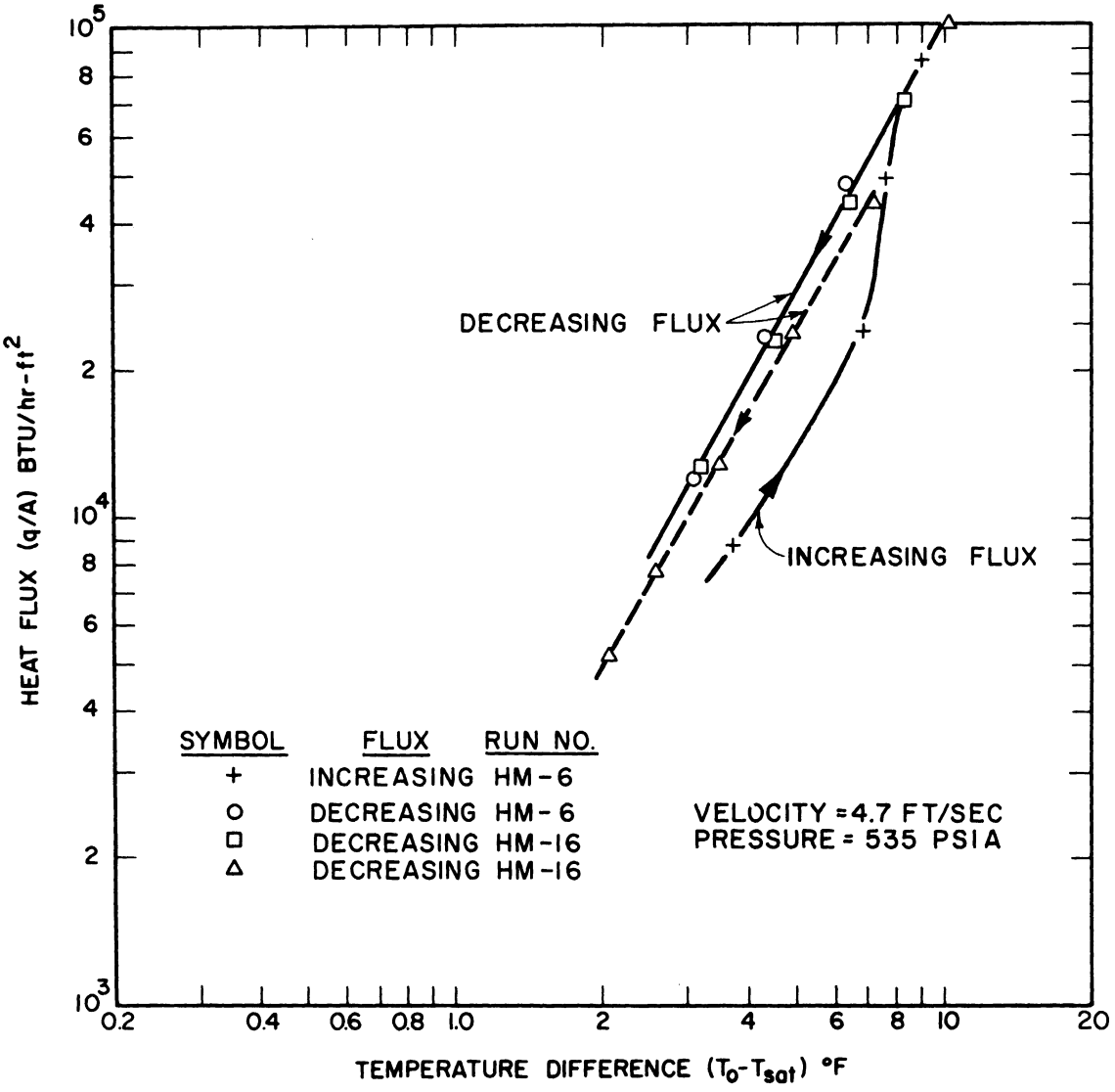

Fig. 20. Heat transfer to saturated distilled water flowing at 4.7 ft/sec and 535 psia.

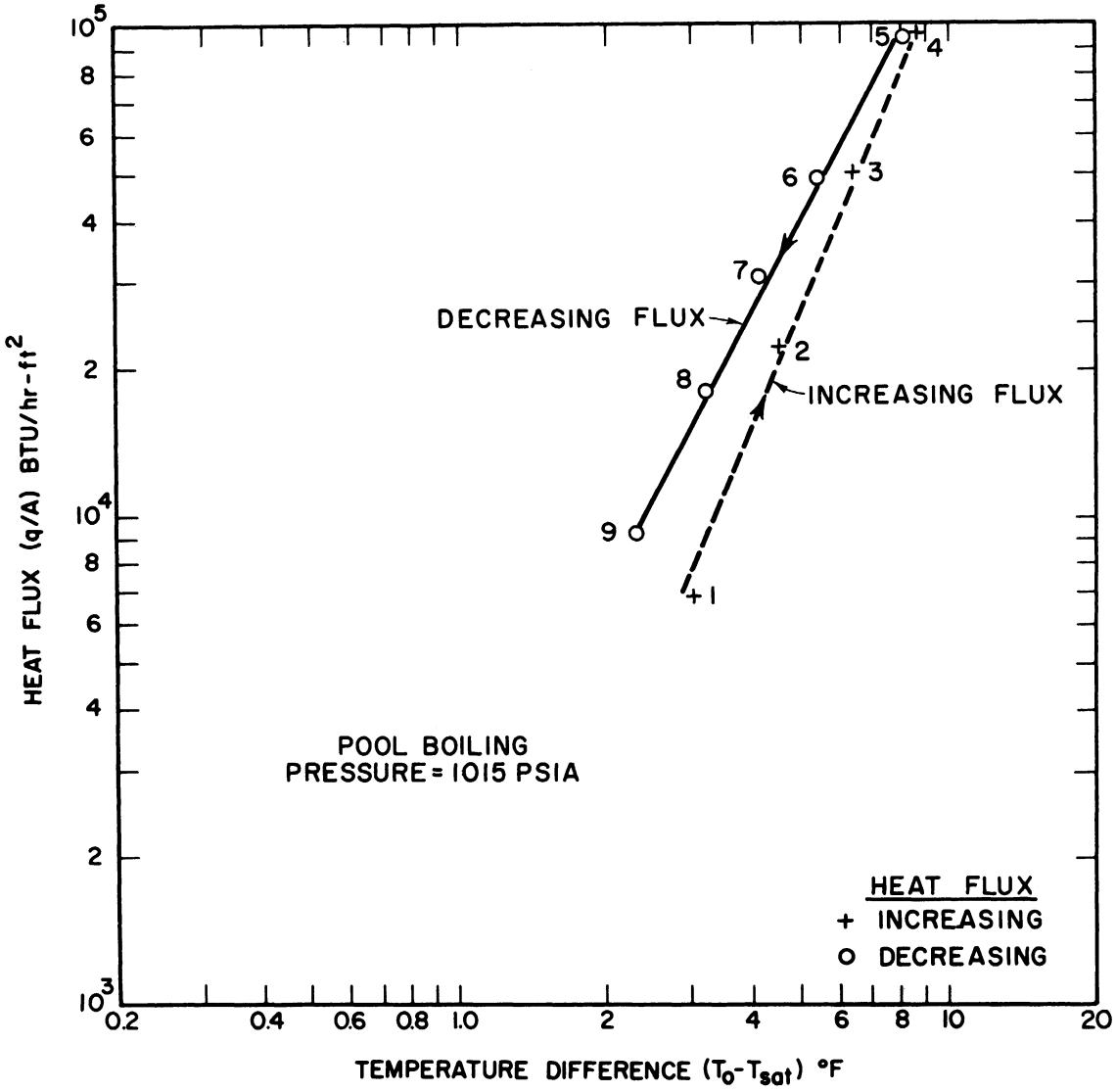

Fig. 21. Pool boiling of saturated distilled water at 1015 psia (Run HM-22).

made with the peak heat flux held constant for at least 1 hr. The points are numbered in the sequence in which they were taken. This sequence is typical for all figures.

F. BOILING WITH FORCED CONVECTION AT 1015 PSIA

The complete sets of data taken for tests with forced convection at 1015 psia are presented in Figs. 22 and 23.

G. BOILING AT 1550 PSIA

The data showing increasing and decreasing heat flux sequences for boiling of saturated distilled water at 1550 psia are presented in Figs. 24-26. These curves are similar to those at lower pressures.

It was noted during the various runs that the emf fluctuations of the thermocouples inside the test section decreased in amplitude as the system pressure increased and were less with decreasing heat flux than with increasing heat flux.

H. EFFECT OF CONSTANT HEAT FLUX

In order to determine the long term effect of boiling at constant heat flux, two similar tests were conducted using saturated distilled water at 535 psia flowing normal to the horizontal tube at a velocity of 1.3 ft/sec. The first test involved aging the surface for 10 min at a flux of 48,000 Btu/hr-ft^2, then decreasing the current to hold the flux constant at about 33,500 Btu/hr-ft^2. The results are tabulated in Table III.

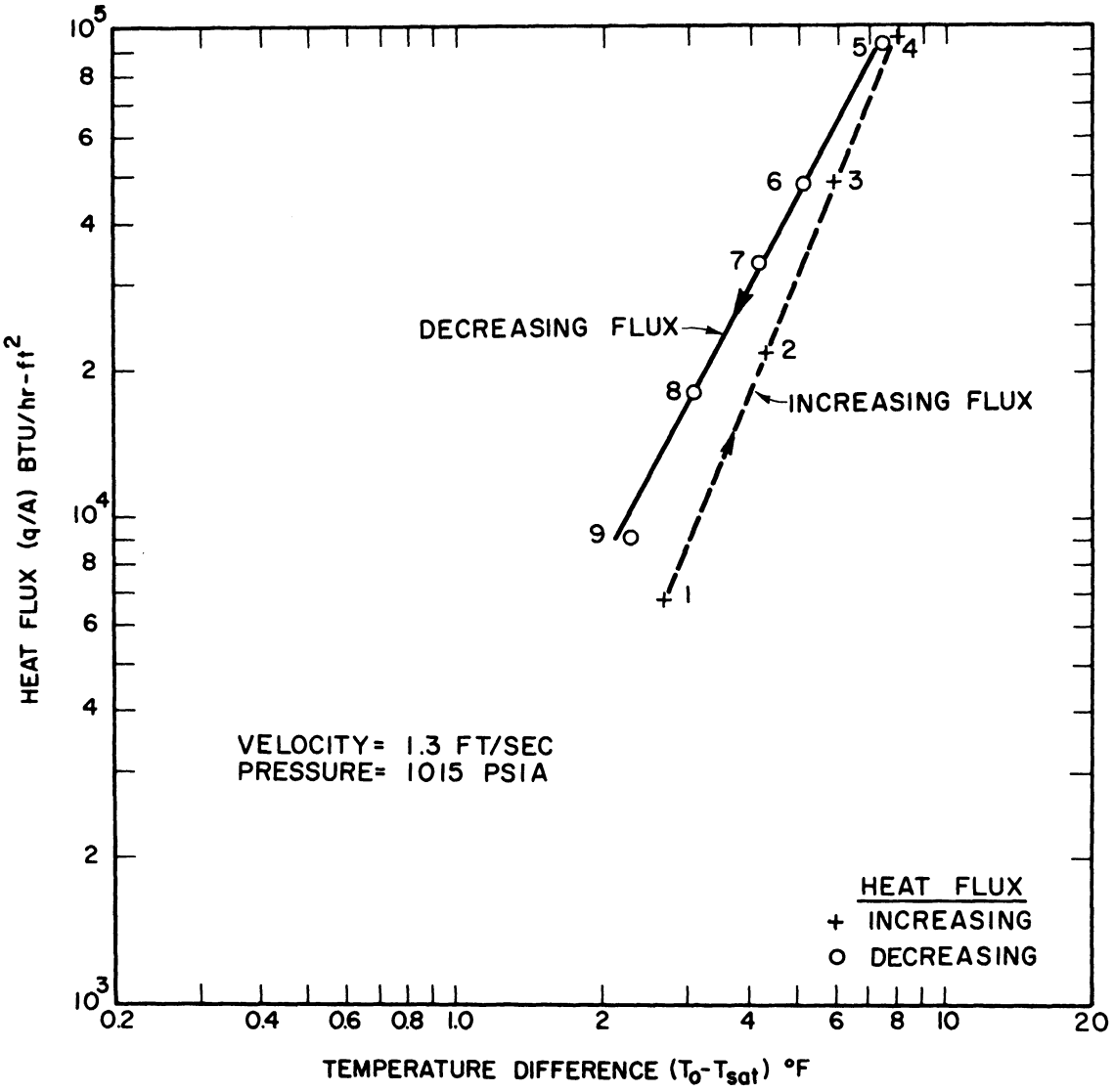

Fig. 22. Boiling of saturated distilled water flowing at 1.3 ft/sec and 1015 psia (Run HM-21).

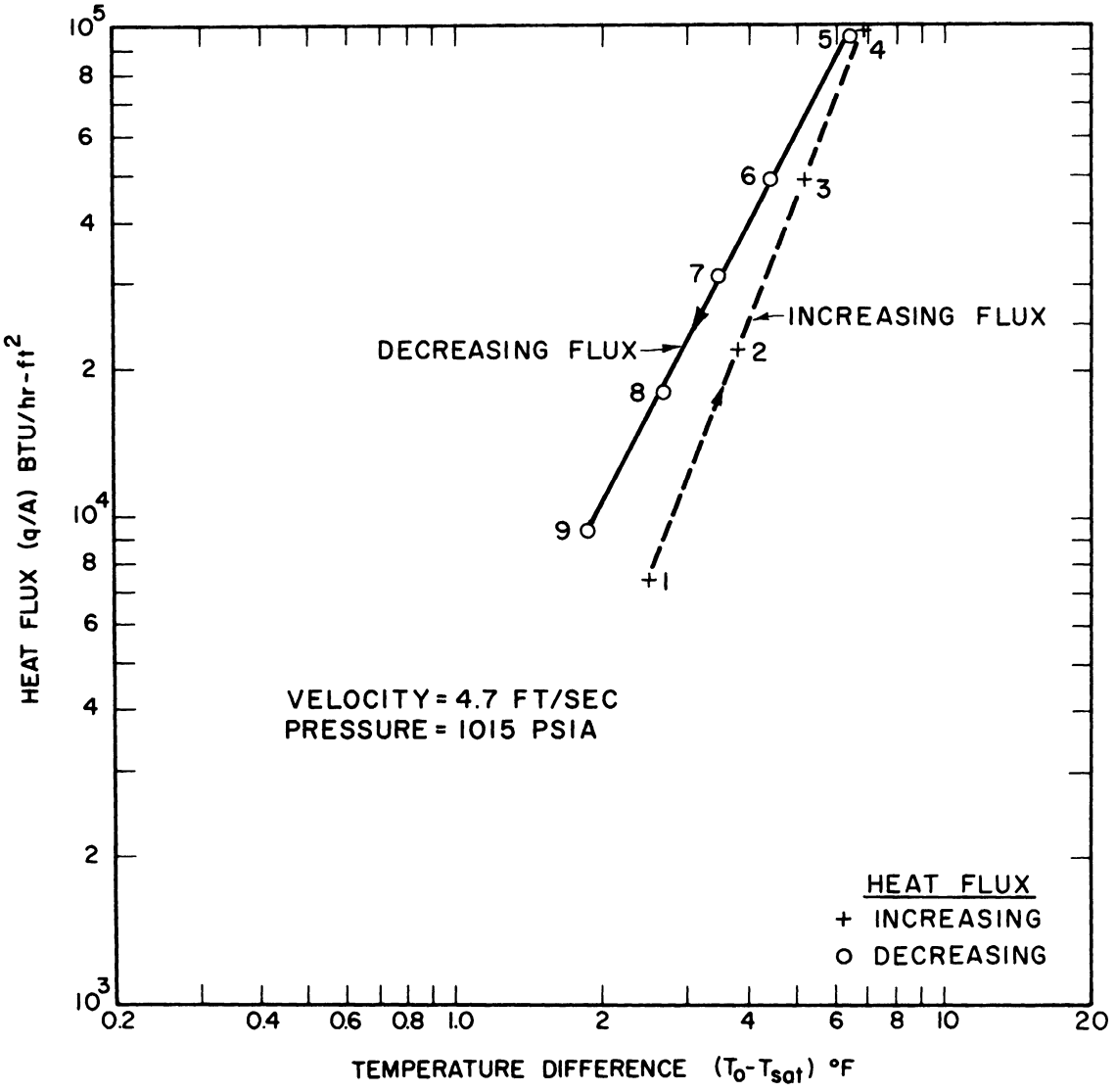

Fig. 23. Boiling of saturated distilled water flowing at 4.7 ft/sec and 1015 psia (Run HM-20).

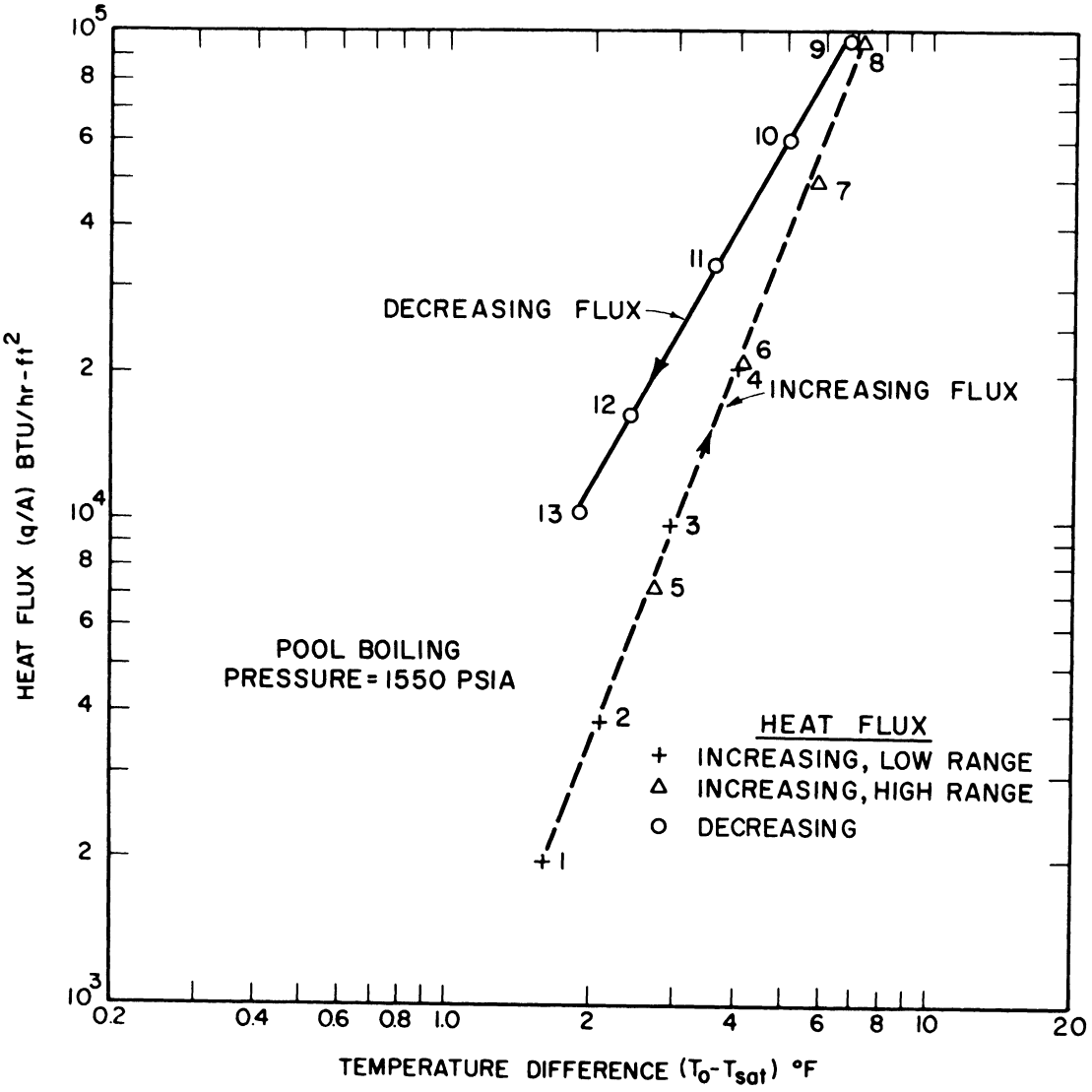

Fig. 24. Pool boiling of saturated distilled water at 1550 psia (Run HM-26).

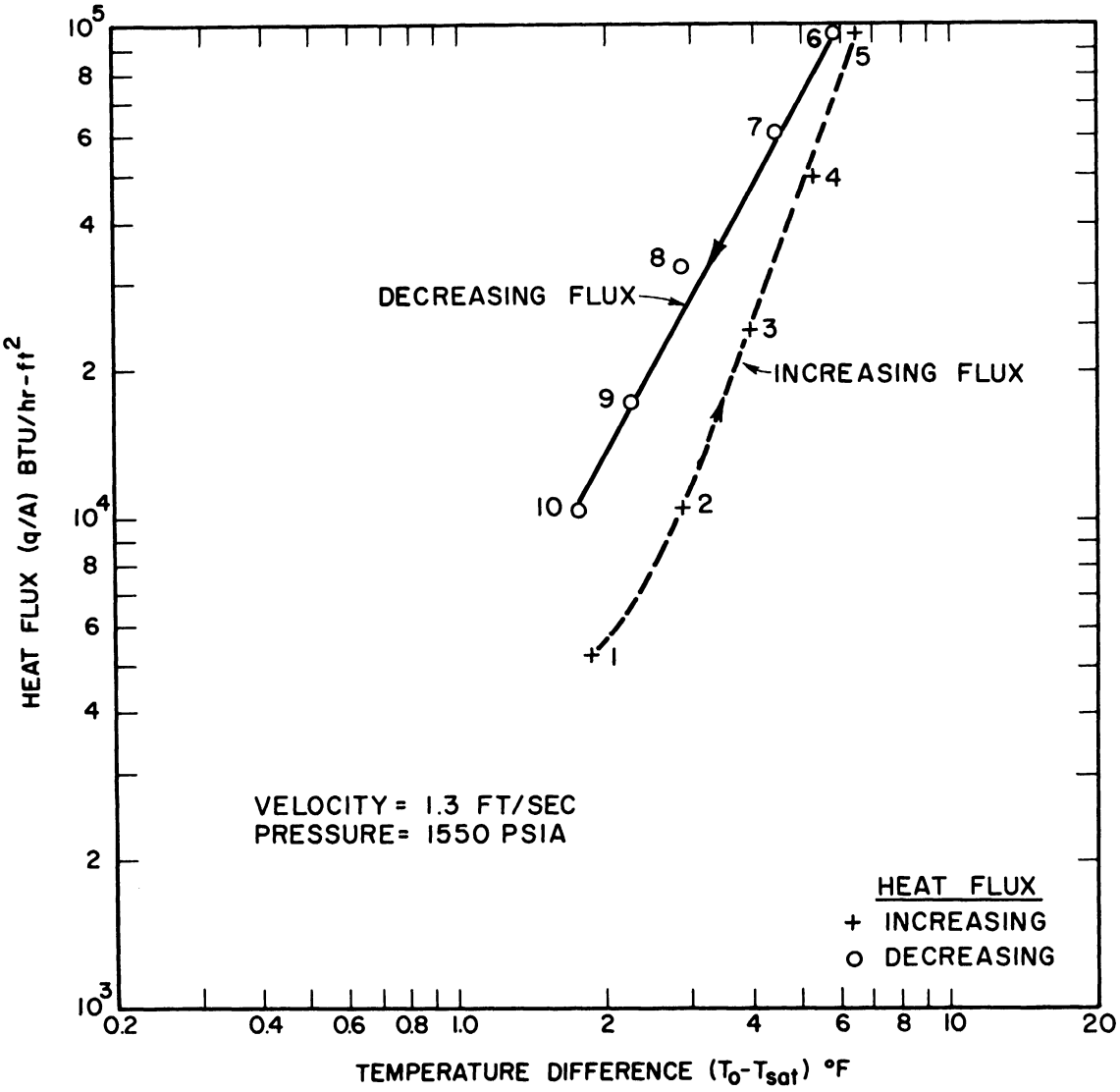

Fig. 25. Boiling of saturated distilled water flowing at 1.3 ft/sec and 1550 psia (Run HM-25).

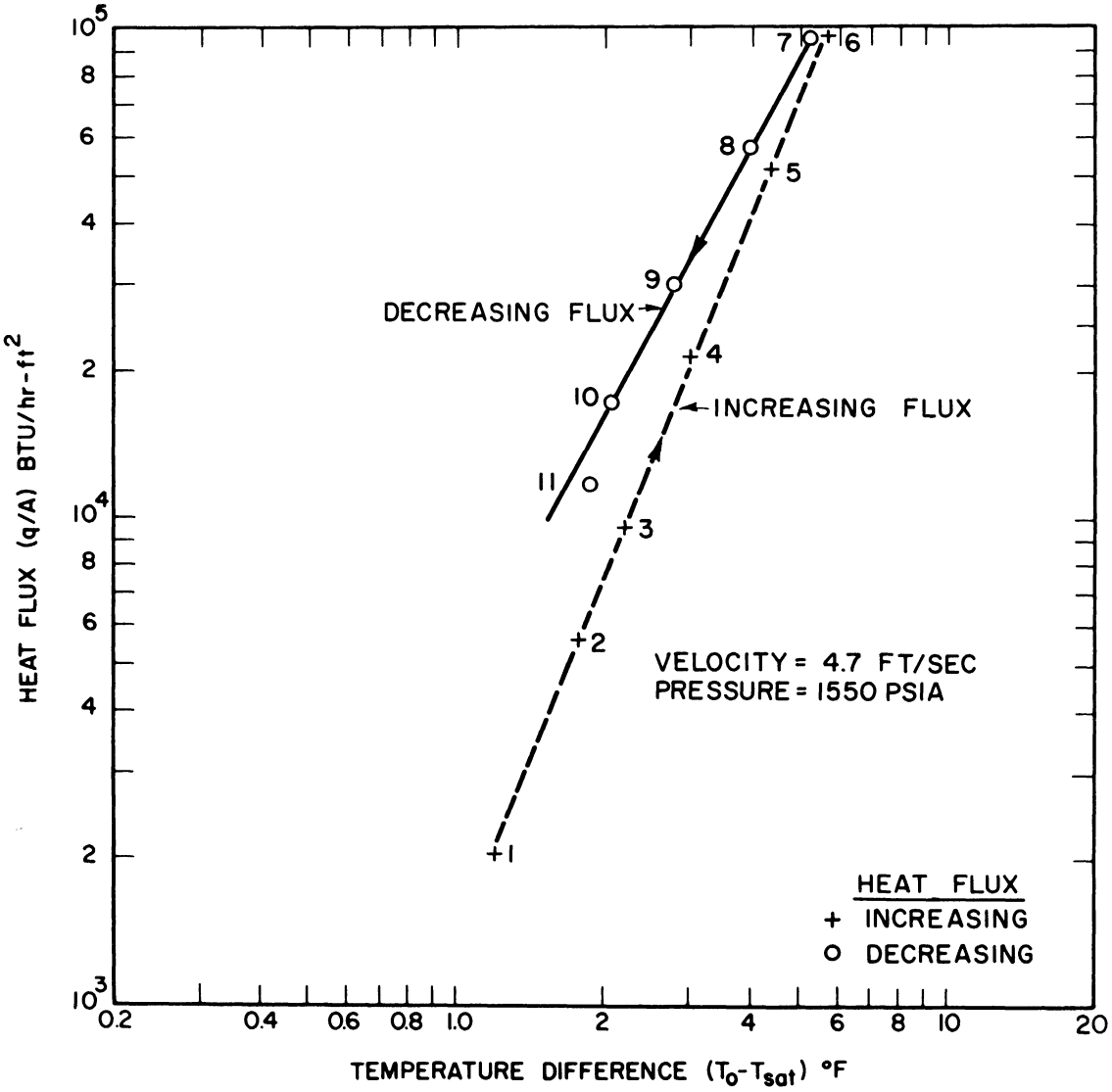

Fig. 26. Boiling of saturated distilled water flowing at 4.7 ft/sec and 1550 psia (Run HM-24).

TABLE III

CONSTANT HEAT FLUX BOILING SUBSEQUENT TO AGING AT HIGHER FLUX

(Run HM-14)

Time Duration, hr	(T_o-T_{sat}), °F	Heat Flux, Btu/hr-ft^2
0	7.4	33,100
0.5	7.2	33,000
1.0	7.2	32,600
1.5	7.2	33,500
2.0	7.2	33,800
2.5	7.1	33,800
3.0	7.1	33,800
3.5	7.1	33,900
4.0	7.0	33,800
4.5	7.0	33,800
5.0	7.2 (?)	33,500

The temperature difference showed a sudden decrease of 0.2°F and gradually dropped another 0.2°F over the next 4 hr. The last point may be inaccurate due to small changes which occurred in the steady state conditions of the system.

In the second test of constant heat flux boiling the heat flux was increased in three steps to the steady value of 32,500 Btu/hr-ft^2. Thus there was no history of a higher heat flux for the run. All other conditions remained the same as the first constant flux test. Table IV lists the data of this test. In this case the temperature difference had a higher value at the start, being on the increasing flux curve. The temperature difference became smaller and approached that of Table III after 6 hr.

TABLE IV

CONSTANT HEAT FLUX BOILING WITHOUT PRIOR AGING AT HIGHER FLUX

(Run HM-15)

Time Duration, hr	(T_o-T_{sat}), °F	Heat Flux, Btu/hr-ft^2
	2.0	4,280
	4.4	9,170
0	7.7	32,500
0.5	7.7	32,400
1.0	7.6	32,800
1.5	7.4	32,400
2.0	7.3	32,200
2.5	7.4	33,300
3.0	7.4	33,300
3.5	7.4	33,400
4.0	7.2	32,700
4.5	7.1	32,700
5.0	7.1	32,200
5.5	7.1	32,500
6.0	7.1	32,500

I. EFFECT OF PEAK HEAT FLUX HISTORY

In Fig. 19 it was noted that the slope and position of the decreasing heat flux curve was a function of the peak heat flux history, as well as a function of pressure and velocity. A test was conducted with a peak heat flux of 210,000 Btu/hr-ft^2 under conditions similar to those of Fig. 19. (Velocity of 1.3 ft/sec and pressure of 535 psia.) The result is shown on Fig. 27. Special attention should be paid to the change of scale compared to the other figures. The consequence of the higher peak heat flux history is a slightly smaller wall superheat for a given heat flux.

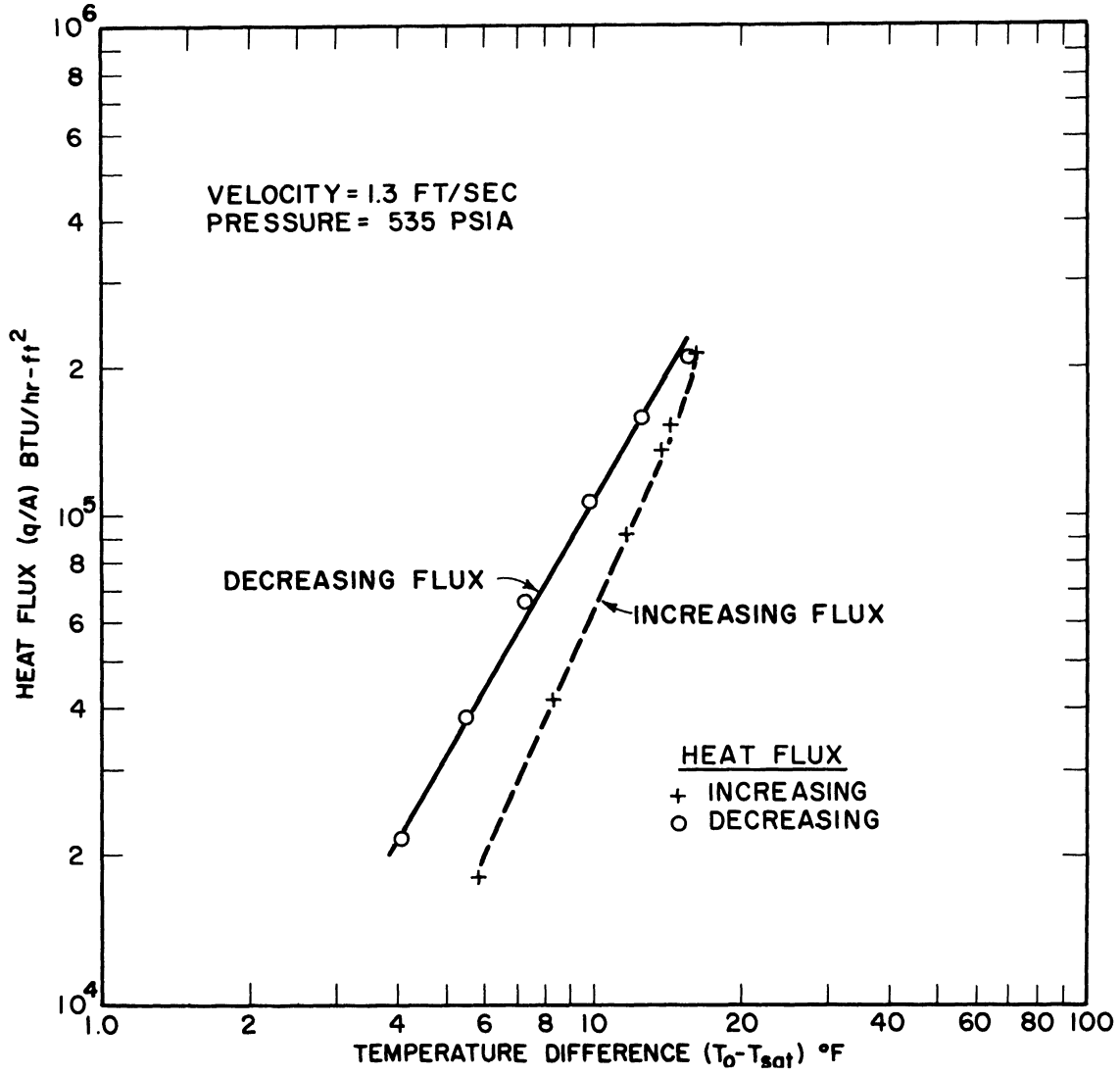

Fig. 27. Boiling of saturated distilled water flowing at 1.3 ft/sec and 535 psia. Peak heat flux of 210,000 Btu/hr-ft^2 held for 1 hr (Run HM-23).

J. EFFECT OF CYCLING OF HEAT FLUX

The effect of increasing and decreasing the heat flux without intervening periods of zero heat flux was studied to determine if the increasing flux curve would be similar to the curve of increasing flux which begins with zero flux. Conditions of 535 psia and 1.3 ft/sec approach velocity were selected. After aging the heating surface for 1 hr at 93,000 Btu/hr-ft^2, the flux was decreased in three steps to 9,000 Btu/hr-ft^2. It was then increased in three steps to the previous peak, held for 1 hr and the cycle repeated. The decreasing flux data all fall on a single curve slightly to the left of the increasing flux data. The shift is about 0.1°F at 10,000 Btu/hr-ft^2 flux and about 0.5°F at 100,000 Btu/hr-ft^2. Figure 28 shows these two curves which are almost coincident. The data are tabulated in Table V.

TABLE V

CYCLING HEAT FLUX DATA

(Run HM-19)

Time	(T_o-T_{sat}), °F	Heat Flux, Btu/hr-ft^2
1150	11.8	94,700
1240	11.1	92,600
1300	7.5	49,400
1320	4.9	22,000
1340	3.2	9,130
1400	5.1	22,100
1420	8.0	48,200
1440	11.3	91,500
1520	10.8	89,200
1540	7.6	49,200
1600	4.8	21,300
1620	3.1	8,940
1640	5.2	22,500
1700	8.0	48,600
1720	11.3	95,100
1800	10.9	92,800
1820	7.5	48,600
1840	4.7	21,100
1900	3.1	8,980

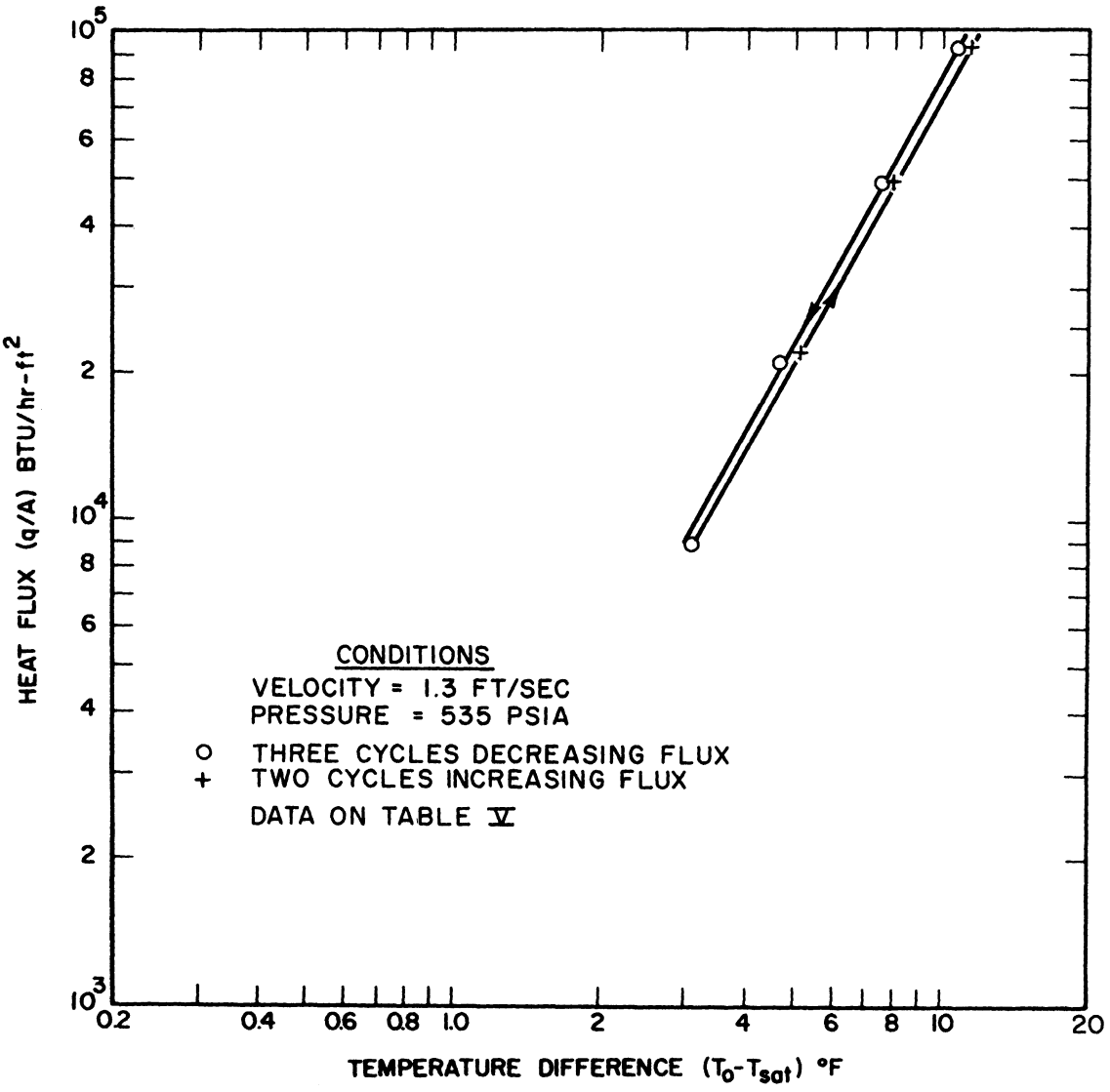

Fig. 28. Effect of cycling of heat flux.

K. EFFECT OF SURFACE CONTAMINATION ON BOILING CHARACTERISTICS

If the outer wall of the tube is covered by a layer of thermally insulating material, such as an oxide film, the heat transfer characteristics are changed. During the various tests this occurred twice and the results were similar. The first occurrence was caused by the breakage of an electrical immersion heater, and the dispersal of its magnesium oxide internal insulation. The second occurrence was the build-up of a layer of black iron oxide, estimated by microscopic inspection to be approximately .0002 in. thick. All particles of the black oxide were found to be magnetic by subjecting them to a magnetic field while settling in a water slurry. The effect of the iron oxide film is to cause a greater wall superheat at a given flux and also to change the characteristic slope of the curve. In Fig. 29 are plotted two curves for 4.7 ft/sec flow at 1015 psia. The curve labeled HM-20 was taken from Fig. 23. The curve labeled HM-28 shows the effect of the surface layer of contamination. The slopes of the curves are 1.87 for Run HM-20 and 1.58 for Run HM-28.

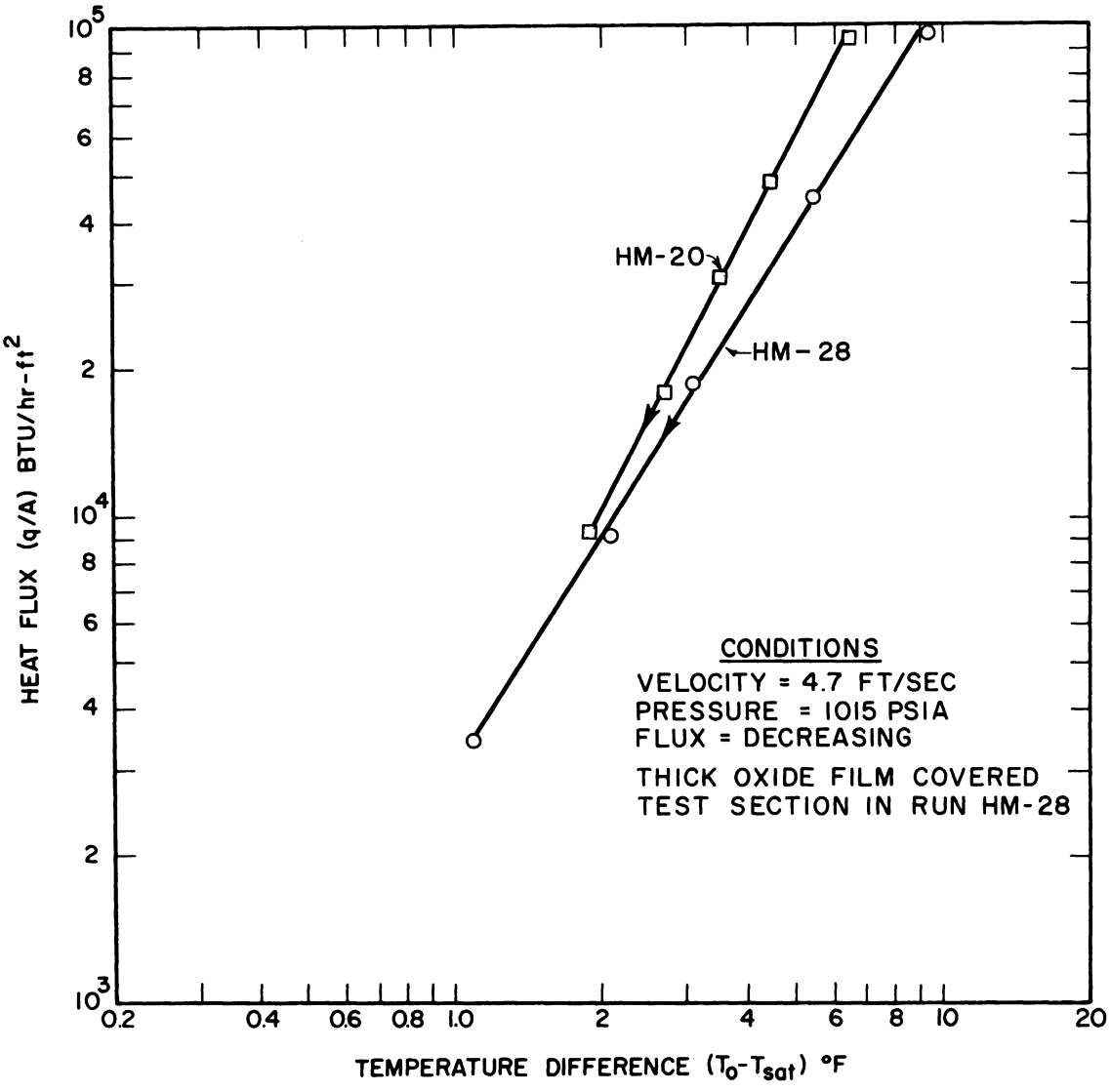

Fig. 29. Effect of surface contamination on boiling characteristics.

V. DISCUSSION AND CONCLUSIONS

A. EFFECT OF WALL SUPERHEAT

The heat flux in nucleate boiling is a function of wall superheat more than any other single factor. Usually this is expressed by an equation in which the heat flux is proportional to the wall superheat raised to a power n

$$(q/A) \sim (T_w - T_{sat})^n \qquad (18)$$

In this study, the exponent n was found to vary slightly, from 1.77 to 2.09. All data could be correlated by a single equation whose exponent is 1.9 but it is believed that such a correlation, restricted to the range of experimental variables covered, is of less value than the more exact empirical Eq. (17) or the actual points shown on the several figures.

An exponent of 2 was found to describe the data of Forster and Greif[32] and Vliet and Leppert.[35] The results of the present work could be correlated with an equation whose temperature superheat exponent is 2, at some loss of precision. However, it is clear that the higher exponent of 3 used by Rohsenow[30] and Levy[47] is not warranted over the range of conditions tested.

B. PRESSURE EFFECT

The effect of increasing the system pressure is to decrease the

wall superheat necessary to cause a given heat flux. This effect is most clearly seen in Figs. 14-16 and is in general agreement with the pool boiling results of Addoms.[29] Ellion[8] presents an analysis by which the excess pressure required at a nucleus to form a growing bubble may be calculated. Assuming a spherical cavity, neglecting the specific volume of the liquid relative to the vapor, and assuming the vapor follows the perfect gas law, he shows that the excess temperature of the vapor in the bubble is a function of the system pressure in the following relation

$$T_v - T_{sat} = \frac{2\sigma R T_{sat}^2}{p h_{fg} r} \qquad (19)$$

where R is the gas constant and r is the bubble radius. Comparing the $(T_v - T_{sat})$ values at pressures of 1550 and 535 psia, Eq. (19) predicts that at 535 psia the temperature difference should be 1.62 times that of 1550 psia. From Fig. 14 it can be seen that the value is 2.1 at a flux of 10,000 Btu/hr-ft^2 and 1.9 at a flux of 100,000 Btu/hr-ft^2.

The effect of pressure on a bubble of given size is to require less wall superheat to overcome the surface tension. In addition to this factor, the amount of heat transferred by each bubble is a function of pressure due to vapor density and latent heat dependence on saturation pressure. Therefore, it is expected that pressure would have a significant effect on the characteristics of nucleate boiling.

C. EFFECT OF VELOCITY

The effect of the velocity of the bulk liquid normal to the axis of the test section is to decrease the wall superheat at a given flux. The decrease is proportional to the velocity as might be expected from considerations of forced convection heat transfer. The effect was the same at all levels of pressure.

As described in an earlier section, the test section is immersed in a pool of water, 10-3/4 in. diam. In forced convection tests, a stream of water issues upward and normal to the test section at a distance of 1 in. below it. The test section is subjected to a constant pressure environment, with the bulk stream impinging on the lower side and eddy currents forming on the upper side.

In a study of a tube confined in a channel, Vliet and Leppert[35] used photographic means to observe the boiling pattern. They found the forward side of the tube has small bubbles which are dragged to about the 90° position where they separate from the wall. The bubbles on the back of the cylinder become considerably larger and tend to blanket this side of the heating surface as the flux increases. The same general pattern may be expected to occur in these tests.

For boiling of saturated water at atmospheric pressure, the effect of velocities up to 10 ft/sec was found to be negligible by previous workers.[35] This may be due to the fact that the much larger wall superheats required at low pressure (20-30°F) mask the relatively small decrease in wall superheat due to bulk velocity. This decrease

varies from about 0.5°F to 2.0°F, depending on the heat flux and pressure.

D. EFFECT OF HEAT FLUX HISTORY

The effect of heat flux history is seen in Figs. 18-26. These show that, at all pressures and velocities observed, the temperature difference between the wall and the liquid saturation temperature is smaller if there is a history of higher heat flux during the same run.

It is postulated that as higher heat fluxes are imposed on the tube surface, additional nucleation sites are activated by becoming filled with vapor. Once activated, these sites trap residual vapor as long as the tube is hotter than the bulk liquid. Therefore, on the initial heating curve sites can be activated only by an excess superheat. Once a site is active, a smaller wall superheat is required to maintain bubble formation. The site activation is a function of geometry of the pits on the surface and the increasing curve may have an S shape, or be straight, as discussed by Westwater.[48] The curve which fits the decreasing heat flux data is more nearly a straight line, as seen on Fig. 19.

The magnitude of the previous heat flux is a factor in determining the number of subsequent active sites and consequent wall superheat. This is indicated by the dashed curve on Fig. 19, the shift in the curves on Fig. 20, and the displacement of the curve on Fig. 27 relative to the decreasing curves of Fig. 19.

The data are more reproducible on the decreasing curve and the temperature fluctuations are less. Some researchers[7,36,44] have noted this effect and "aged" their surface at a high heat flux before reducing the flux to the desired value for data collection. The heat flux history is not reported for all data.

It is postulated that nucleation sites may be activated by the small fluctuations in wall temperature which occur at a given heat flux. Moore and Mesler[50] measured local surface temperature fluctuations of the same order as the temperature difference between the average wall temperature and the liquid saturation temperature. Thus inactive sites on a surface may be subjected to a severe local temperature excursion which activates them, even though the macroscopic heat flux remained constant.

The data tabulated in Tables III and IV show that the wall superheat decrease at constant heat flux is a very long term effect. Presumably additional sites are being activated even after a period of 5 hr at constant heat flux. It seems reasonable to suppose that there is a single, characteristic curve which would represent the boiling conditions, for a given surface-fluid combination regardless of aging or lack of it. If such exists it probably represents a condition corresponding to the maximum possible number of active nucleating sites present on the surface. The wall superheat is decreasing in both cases (Tables III and IV) and appears to be approaching an asymptotic value of about 6.5°F to 7.0°F. The decreasing curve on Fig. 19 gives

a value of 6.5°F at a flux of 33,500 Btu/hr-ft^2.

The decrease in wall superheat for prolonged boiling at a constant heat flux certainly rules out the gradual accumulation of an insulating film of oxide or other contamination. The decrease is in contradiction with the experimental results of Bankoff, et al.,[49] in the pool boiling of organic liquids from a platinum wire at atmospheric pressure. It is possible that what Bankoff observed was a continuous degassing of the surface, similar to that found by Jakob.[1]

E. EFFECT OF SURFACE CONTAMINATION

The results shown in Fig. 29 need little discussion since they represent a nonreproducible condition as indicated by the loose surface film which was visually inspected. A calculation of the insulating effect of a layer shows that a thickness of .00015 in. will cause a wall superheat increase of 3°F at a flux of 100,000 Btu/hr-ft^2. The thermal conductivity of the oxide layer is assumed to be 0.4 Btu/hr-ft-°F. In addition to insulating the surface, a thick oxide film changes the nucleation characteristics of the surface. This may cause a change in the shape of the curve, as well as an increase in wall superheat at a given flux.

F. GENERAL CONCLUSIONS

The data obtained during this investigation are of a higher order of precision than most previous work under these conditions. Appendixes A and B give details of the precision of measurements. This greater

precision has resulted in defining the effects of velocity and heat flux history on the low heat flux boiling of water at elevated pressures.

In order to draw more general conclusions regarding the less significant variables of nucleate boiling, different tube materials and geometries should be investigated. Another area of interest is the effect of water chemistry. Most of the industrial pressurized water systems operate with a pH of about 9 in order to reduce corrosion. Data are needed for the boiling of water under this condition.

APPENDIX A

THERMOCOUPLE CALIBRATION APPARATUS

Thermocouples are widely used for the measurement of temperature. A thermocouple consists of an electrical circuit created by two dissimilar metals whose junctions are maintained at different temperatures. Under these conditions an electromotive force is generated. This emf is a function of the two metals used, the relative temperature difference between the junctions, and the absolute temperature level. The basic laws of thermoelectric circuits are given by Roeser.[38]

Although the approximate relation between the emf generated and the temperature is well established for the various suitable thermocouple metal combinations, to achieve accurate results, thermocouples must be calibrated to yield temperatures that are in agreement with the International Temperature Scale. This scale is defined by the standard platinum-resistance thermometer in the range of -182.970 to 630.5°C. The platinum-resistance thermometer is calibrated at the primary fixed points (1948 ITS) which, in our range of temperature, are:

1. Temperature of equilibrium between ice and air-saturated water (ice point)—0.000°C.

2. Temperature of equilibrium between liquid water and its vapor (steam point)—100.000°C.

3. Temperature of equilibrium between sulfur and its vapor (sulfur point)—444.600°C.

The Callendar formula is used to express the temperature as a function of resistance of the platinum thermometer.

There are several methods of calibrating thermocouples to yield accurate indications of temperature, as discussed by Roeser and Lonberger.[39] The most direct procedure is to compare the thermocouples directly with the standard platinum-resistance thermometer. To make a comparison, a reservoir is needed whose temperature can be regulated at a steady value and yet periodically varied to cover the desired range. Because it is desired to cover a wide range of temperatures in a single apparatus, a thermostated liquid bath is not suitable. Therefore a solid copper cylinder, 6 in. in diameter by 18 in. long, was selected to be the controlled isothermal medium.

Direct-temperature regulation of the copper cylinder to ±0.1°F would be difficult and direct regulation to ±0.001°F virtually impossible. Constancy of temperature is necessary to eliminate uncertainties in the calibration. To achieve the desired result, the cylinder is surrounded by, but thermally insulated from, another system having a large thermal inertia. This second system is a copper pipe, capped at both ends except for access holes to the inner block. The size is approximately 11 in. O.D., with a 3/8 in. wall thickness.

The outer copper cylinder, or pipe, is thermally insulated from the ambient air by a 5 in. layer of insulation. This whole assembly is positioned in an extended 55-gal steel drum. The temperature of the outer pipe is controlled by the action of an electronic controller,

using a thermocouple emf signal, which energizes electrical heaters clamped to the outer surface of the pipe. This controller has a ±1°F band and the power control is either on or off. In an analysis made by Clark, et al.,[40] it is shown that for the physical system used, a temperature amplitude of 1°F on the pipe will be damped to approximately ±0.001°F in the inner cylinder. In operation no measurable temperature cycling could be observed. A picture of the complete apparatus is seen in Fig. 30.

The temperature of the inner block is accurately measured by a Leeds and Northrup Cat. No. 8163-B platinum resistance thermomenter. This thermometer was calibrated by comparison to a National Bureau of Standards calibrated thermometer. The coefficients provided yield an accuracy of ±0.01°C. The resistance of the thermometer was measured by a Type G-2 Mueller Bridge and a Model 2284d moving coil galvanometer, manufactured by L & N. The resistors of the bridge are held at a constant temperature by a thermostat. The precision of the bridge is ±.0003 ohm. This corresponds to a temperature precision of ±.003°C, or, better than the thermometer calibration. The resistance of the thermometer is converted into a value of temperature by use of the Callendar equation. In order to minimize the effort of solving the quadratic equation directly for temperature and to reduce the probability of error, having measured the resistance, a computer program was written and executed on the IBM 7090 computer. This yielded a table giving the thermometer resistance, to the nearest 0.001 ohm,

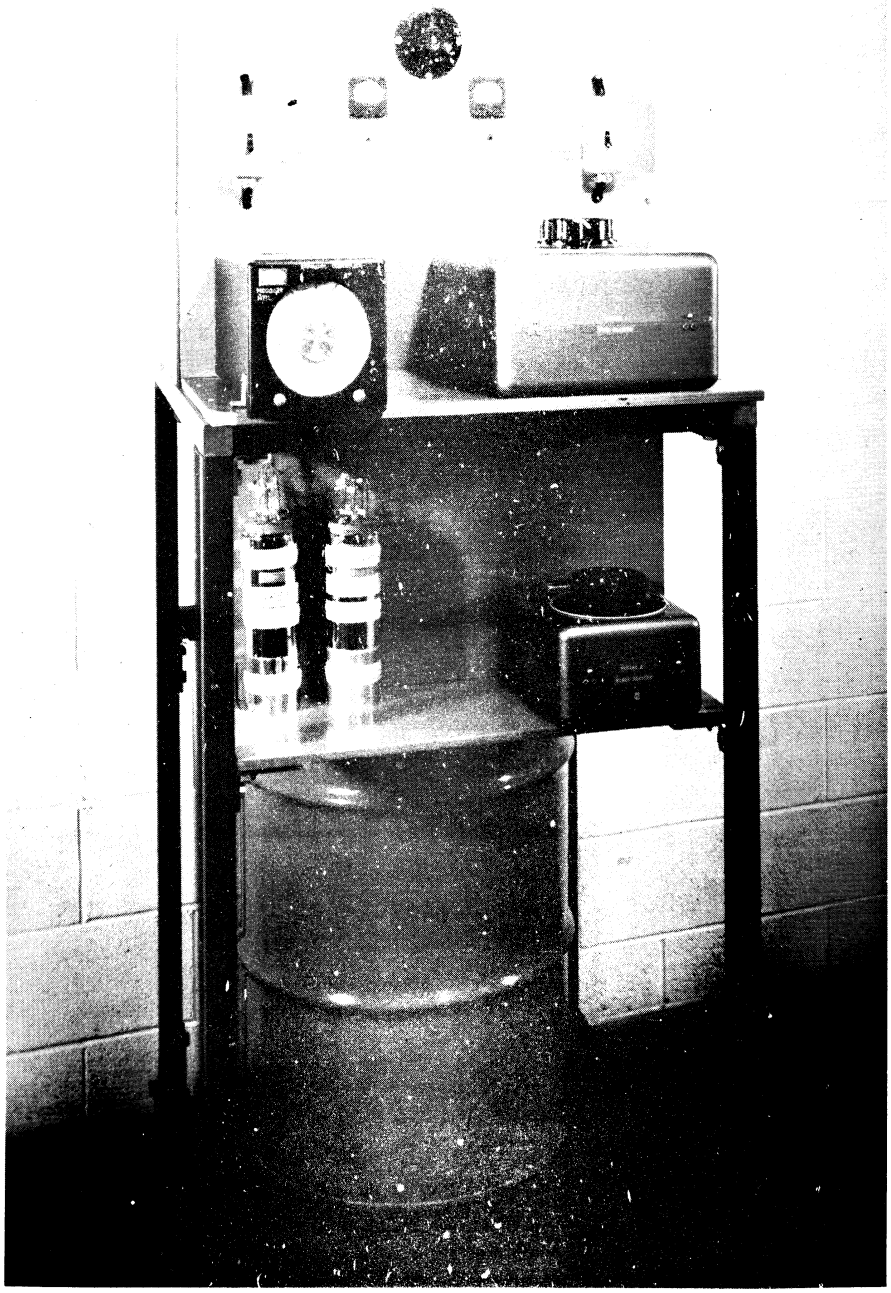

Fig. 30. Thermcouple calibration apparatus.

for every temperature between 0 and 510°C, in increments of 0.1°C. With a measured value of resistance, this table yields the temperature, accurate to .01°C, by simple interpolation.

The test section of the low heat flux boiling apparatus consists of a 3/4 in. O.D. Monel tube in which are installed 12 thermocouples made from 30 ga chromel-constantan wire. The tube is 7 in. long and is silver soldered to short sections of the copper electrode. Each thermocouple in the test section was calibrated by measurement of its emf when the whole test section subassembly was inserted into a well in the inner cylinder of the constant temperature apparatus and held at a temperature accurately measured by the platinum resistance thermometer, located in an adjacent well.

Sheathed thermocouples, used to measure the steam and water temperatures, were inserted into other wells in the cylinder and calibrated simultaneously. The copper cylinder was heated to 660°F, which is in excess of the maximum service temperature of 600°F. An aging effect caused a change in the emf generated, probably due to metallurgical changes which take place at the high temperature. After reheating to 660°F, a recheck of all calibration points was made. The aging effect, due to the second heating, diminished markedly and was in the same direction for all thermocouples. This led to the conclusion that the thermocouples would be satisfactory for the intended use.

Although all 12 thermocouples in the test section were made in similar fashion and from the same spool of wire, the emf-temperature

relation differed slightly among them. A Type K-3 Universal Potentiometer (L & N) was used with a Model 2284d moving coil galvanometer to measure the thermocouple emf. The reference junction was held in a distilled water ice bath. According to the manufacturer, the potentiometer-galvanometer combination is accurate to within ± (0.015% of reading plus 2 μv) in the range used. This corresponds to a maximum deviation of ±5 μv at a level of 550°F, or about ±0.125°F. Although the absolute accuracy of the instrumentation is as stated, the readings of one thermocouple relative to another are believed to be within ±2 μv, or ±.05°F. The emf of the 12 thermocouples had a spread of 24 μv at 549.7°F. The four thermocouples in the center of the test section, which are used during the test runs, had a spread of 6 μv, or equivalent to 0.15°F. This indicates the necessity of individual thermocouple calibration for precise work.

From the calibration of a thermocouple at various known temperatures, a curve of emf versus temperature may be constructed to provide a means of interpolating between the calibration points. It is customary to make use of a standard curve and to plot the deviation from the standard curve. A table giving standard, or average, values for chromel-constantan is provided by Shenker, et al.[42] The table is limited to temperatures in 10°F increments and emf values to 0.1 mv. Thus, if readings are made to .001 mv (1 μv), there may be a significant error caused by the round-off of the table. By making use of graphical techniques to insure smooth first and second derivatives,

a table of emf versus temperature was generated by the IBM 7090 computer. This table, which, if rounded off, yields the two place table of Shenker, tabulates temperature in increments of 0.1°F from 30 to 1200°F and electromotive force to three places (1 μv). Since 0.1°F represents about 4 μv change in emf, an emf reading accurate to ±2 μv may be easily converted to temperature to the nearest 0.1°F.

In summary, the thermocouples used in these tests were individually calibrated against a platinum resistance standard thermometer. The accuracy error which is obtained from the instruments (K-3 potentiometer-galvanometer) is ±.13°F at the calibration points, and probably greater between calibration points. The sensitivity of the instruments is better than this, however, and it is believed that systematic errors will be cancelled when a sequence of temperatures, measured over a short period of time, are used to determine temperature differentials. Thus, a temperature difference should be correct to ±0.1°F. To support this claim, the temperatures indicated by three steam space thermocouples were examined for Run HM-29. There are 14 sets of three readings rounded off to the nearest 0.1°F. In one set, all three thermocouples yield the reading of 545.5°F. In 11 sets, two thermocouples yield identical readings and the third thermocouple a temperature 0.1°F different. In two sets, the thermocouples yield different temperatures, each 0.1°F from the nearest other one, e.g., 545.4, 545.5, 545.6°F. The standard deviation of the 42 points is .06°F.

Further evidence of the thermocouple performance is obtained from the readings of the 12 test section couples immersed in boiling water but no heat flux from the test section. Although such a pool of boiling water has small temperature variations, due to local superheating or subcooling, the readings were as follows:

Number of Couples Having Same Reading	Reading
1	545.3°F
4	545.4°F
6	545.5°F
1	545.6°F

The standard deviation of this sample is .09°F.

Another set of readings from Run HM-28, under forced convection but without heat flux from the test section, were as follows:

Number of Couples Having Same Reading	Reading
1	545.8°F
9	545.9°F
2	546.0°F

The standard deviation of this sample is .05°F.

Run HM-27, also forced convection but no heat flux, gives similar results:

Number of Couples Having Same Reading	Reading
1	544.5°F
8	544.6°F
2	544.7°F
1	544.8°F

The standard deviation of this sample is .08°F.

APPENDIX B

ESTIMATION OF ERRORS

1. TEMPERATURE MEASUREMENT

As discussed in Appendix A, temperatures are measured by thermocouples, carefully calibrated to yield readings of highest possible accuracy. Rather than analyze the uncertainty interval in the result on the basis of a single reading and the estimated uncertainty in the instrument components as discussed by Kline and McClintock,[51] a preferable approach is the use of the results of statistical treatment of several cases where large samples are available.

In Appendix A there is cited a case of 42 readings of the steam space temperature, with a standard deviation of .06°F. The standard deviation is not based on the equation for the whole population

$$\sigma = \sqrt{\sum x^2/n} \tag{20}$$

but on the modified form which yields a more exact value for a sample when the true value of the steam temperature is not independently known.[52] Thus,

$$s' = \sqrt{\sum x^2/(n-1)} \tag{21}$$

where x is the deviation of each point from the sample average and n is number of sample points and s' is the standard deviation of the sample.

Three sets of readings of the test section thermocouples were shown to have standard deviations of .09, .05 and .08°F. The average of these three standard deviations is .07°F, or almost identical to the standard deviation of the steam space couples. The reader is reminded that 68.2% of all readings will fall within plus-or-minus one standard deviation for a Gaussian distribution.

The steam space temperature is based on the average of two readings for all data points. Since the error of an average is inversely proportional to the square root of the number of readings making up the average, this averaging of two readings reduces the probable error by a factor of $1/\sqrt{2}$. Even though we neglect this possible improvement (due to the fact that the actual steam temperature may have changed during the interval between two readings), we may claim that the odds are 10 to 1 that any given steam space temperature is precise to within ±0.1°F.

The test section has four thermocouples pressed against the inner wall. Due to temperature fluctuations, it is assumed that the standard deviation of these readings is 0.1°F instead of the 0.07°F measured under zero heat flux conditions. Because four temperatures are averaged to obtain the value used, the error is only half the probable error of a single reading. Thus, at 10 to 1 odds, the ratio of the deviation to the standard deviation is 1.7, from a table of probability of occurrence of deviations.[53] If this ratio is multiplied by the square root of the number of readings averaged (4), the result is

$$(1.7)(0.1°F)/\sqrt{4} = .085°F \qquad (22)$$

This indicates that the odds are better than 10 to 1 that the inside average wall temperature is precise to within ±0.1°F.

2. CURRENT MEASUREMENT

A L & N 8662 potentiometer can be read to within ±.005 mv on the low range scale. When used to measure the current passing through a shunt of 10^{-5} ohm, the readings varied from 2 to 16 mv. The shunt calibration with current and temperature was not determined. Therefore, a typical error in this measurement may be greater than the error in the potentiometer reading, but probably does not exceed 0.5%.

3. RESISTIVITY MEASUREMENT

The resistivity of the Monel test section was measured as a function of temperature to within ±1%. This was verified by analysis of the measurement errors and reproducibility of the data in several tests.

4. THERMAL CONDUCTIVITY MEASUREMENT

As discussed earlier, the thermal conductivity of the Monel was determined to within ±5% by an outside laboratory. This may result in a fairly large systematic error but will not invalidate any conclusions based on data at a single average temperature.

5. WALL TEMPERATURE DROP

As described in Eqs. (14)-(16), the wall temperature drop is a

function of the resistivity, thermal conductivity, square of the current density, and geometric values which were kept constant throughout all tests. At any given level of temperature, the only variable is the square of the current. Therefore, wall temperature drops computed by these equations are precise, relative to one another, to within ±1%.

When the wall temperature drop is compared in two cases where the pressure and corresponding temperature is different, uncertainties in the thermal conductivity and resistivity affect the uncertainty of the result. Thus, the wall temperature drop has an uncertainty of 5.2%. In comparing data obtained in this investigation at different conditions, the relative wall temperature drops are more precise than ±5.2% because the thermal conductivities were taken from a smooth curve and it is unlikely that the relative error of the conductivity from 475 to 600°F exceeds ±2%.

In summary, the wall temperature drops are precise to one another to ±2.5%, but on an absolute basis have an uncertainty of the order of ±6%. The calculated wall temperature drops were rounded off to the nearest 0.1°F.

6. OUTSIDE WALL TEMPERATURE

The average outside wall temperature is obtained by subtracting the wall temperature drop from the average inside wall temperature. This value, therefore, is less precise than the average inside wall temperature and its precision a direct result of that of the wall

temperature drop. At low heat fluxes (and low wall temperature drops), the odds are 10 to 1 that the outside wall temperature is precise to within $\pm 0.2°F$. At high heat fluxes, the wall temperature drop is of the order of 13°F. In this case the outside wall temperature is precise, in an absolute sense, to within $\pm 0.9°F$. In comparison to other data of this investigation, the precision is $\pm 0.4°F$.

7. TEMPERATURE DIFFERENCE BETWEEN WALL AND SATURATION ($T_o - T_{sat}$)

From the preceding sections, the odds are 10 to 1 that the values of the temperature difference between the average outside wall temperature and the liquid saturation temperature are precise, relative to one another to within ±0.3°F at a heat flux of 10,000 Btu/hr-ft^2 and to within ±0.5°F at a heat flux of 100,000 Btu/hr-ft^2. On an absolute basis, the temperature difference is precise within ±.5°F at the low flux and ±1.0°F at the higher flux.

8. HEAT FLUX

The uncertainty in the heat flux values computed from the current, resistivity, and tube dimensions is approximately ±2.0%.

9. FLOW VELOCITY

The velocity was found by dividing the volumetric flow rate, obtained from the orifice pressure drop, by the cross-sectional area of the flow guide. Fluctuations in the orifice differential increase the uncertainty of the measurement, but it is believed to be accurate to

within ±6% at the low velocity of 1.3 ft/sec and ±4% at the high velocity of 4.7 ft/sec.

10. PRESSURE

The system pressure was read from a precision bourdon tube gauge, calibrated to within 0.1% of full scale, or 2.5 psi. A systematic discrepancy existed between the indicated pressure and the observed steam saturation temperature. This amounted to approximately 0.8°F, with the thermocouple indicating a temperature lower than saturation temperature which corresponds to the observed pressure. It is believed that this systematic error has no effect on the temperature differences reported and a negligible bearing on the pressure dependence of heat flux versus temperature difference in nucleate boiling of water at low heat flux.

APPENDIX C

DATA

Date	Run No.	Press psia	Vel. Ft/sec	Time	q/A Btu/hr-ft^2	Temperatures - ^oF Avg T_i	ΔT Wall	Avg T_o	T_{sat}	(T_o-T_{sat})
5/20/63	HM-6	535	4.7	1335	8,670	478.2	1.2	477.0	473.3	3.7
				1420	23,900	483.2	3.4	479.8	473.0	6.8
				1450	49,000	487.6	6.9	480.7	473.1	7.6
				1525	85,600	494.0	12.1	481.9	472.9	9.0
				1545	47,700	486.1	6.7	479.4	473.1	6.3
				1610	23,100	480.8	3.3	477.5	473.2	4.3
				1630	11,800	478.0	1.7	476.3	473.2	3.1
5/20/63	HM-7	535	1.3	1845	9,160	478.4	1.3	477.1	472.9	4.2
				1915	23,600	482.2	3.3	478.9	472.8	6.1
				1945	48,000	487.5	6.8	480.7	472.9	7.8
				2015	86,500	495.5	12.2	483.3	473.1	10.2
				2040	47,600	487.2	6.7	480.5	473.1	7.4
				2115	22,800	481.5	3.2	478.3	473.3	5.0
				2135	11,700	478.6	1.7	476.9	473.2	3.7
5/21/63	HM-8	535	Pool	0015	9,200	478.8	1.3	477.5	473.1	4.4
				0045	24,100	482.9	3.4	479.5	473.1	6.4
				0115	47,200	488.2	6.6	481.6	473.1	8.5
				0145	90,200	496.4	12.7	483.7	473.0	10.7
				0215	48,000	487.5	6.8	480.7	472.8	7.9
				0245	23,000	481.8	3.2	478.6	473.1	5.5
				0310	11,800	479.0	1.7	477.3	473.1	4.2
5/22/63	HM-9	535	1.3	1500	9,350	479.2	1.3	477.9	473.1	4.8
				1520	23,100	483.4	3.3	480.1	473.1	7.0
				1545	48,000	488.4	6.8	481.6	473.1	8.5
				1610	87,700	496.4	12.4	484.0	473.2	10.8
				1645	46,900	487.3	6.6	480.7	473.1	7.6
				1715	23,200	482.0	3.3	478.7	473.2	5.5
				1750	11,900	478.8	1.7	477.1	473.1	4.0
5/22/63	HM-10	535	Pool	2100	9,350	479.1	1.3	477.8	473.1	4.7
				2130	23,800	483.2	3.4	479.8	473.1	6.7
				2200	47,000	488.6	6.6	482.0	473.1	8.9
				2230	89,400	497.0	12.6	484.4	473.0	11.4
				2300	47,700	487.7	6.7	481.0	473.1	7.9
				2325	22,900	481.9	3.2	478.7	473.1	5.6
				2345	11,900	479.0	1.7	477.3	473.1	4.2
5/24/63	HM-11	535	1.3	1230	2,220	474.2	0.3	473.9	473.1	0.8
				1255	5,590	476.9	0.8	476.1	473.1	3.0
				1330	9,390	479.2	1.3	477.9	473.1	4.8
				1400	23,200	484.5	3.3	481.2	473.1	8.1
				1430	48,000	489.8	6.8	483.0	473.1	9.9
				1500	106,700	501.4	15.0	486.4	473.0	13.4
				1515	48,100	487.8	6.8	481.0	473.1	7.9
				1530	23,400	481.8	3.3	478.5	473.1	5.4
5/24/63	HM-12	535	Pool	2030	2,180	476.0	0.3	475.7	473.1	2.6
				2045	5,580	478.0	0.8	477.2	473.1	4.1
				2100	9,050	479.3	1.3	478.0	473.1	4.9
				2110	24,400	483.7	3.4	480.3	473.1	7.2
				2130	47,400	488.9	6.7	482.2	473.1	9.1
				2200	108,000	502.1	15.2	486.9	473.2	13.7
				2210	48,000	488.4	6.8	481.6	473.1	8.5
				2220	23,100	482.3	3.3	479.0	473.2	5.8
				2240	9,420	478.9	1.3	477.6	473.2	4.4
				2250	5,350	477.3	0.7	476.6	473.1	3.5
				2300	3,550	476.6	0.5	476.1	473.1	3.0

Date	Run No.	Press psia	Vel. Ft/sec	Time	q/A Btu/hr-ft^2	Temperatures - °F: Avg T_i	ΔT Wall	Avg T_o	T_{sat}	$(T_o - T_{sat})$
5/28/63	HM-13	535	1.3	1425	4,160	475.7	0.6	475.1	473.1	2.0
				1440	5,830	477.1	0.8	476.3	473.2	3.1
				1455	9,400	479.6	1.3	478.3	473.1	5.2
				1505	16,900	482.9	2.4	480.5	473.1	7.4
				1525	24,200	484.8	3.4	481.4	473.2	8.2
				1545	33,600	486.4	4.7	481.7	473.0	8.7
				1605	43,900	488.7	6.2	482.5	473.0	9.5
				1620	51,800	490.2	7.3	482.9	473.0	9.9
				1635	44,600	488.4	6.3	482.1	473.1	9.0
				1655	33,500	485.2	4.7	480.5	473.0	7.5
				1710	23,200	482.6	3.3	479.3	473.2	6.1
				1730	15,900	480.1	2.2	477.9	473.1	4.8
				1745	7,660	477.1	1.1	476.0	473.1	2.9
				1820	5,140	475.9	0.7	475.2	473.2	2.0
6/4/63	HM-16	535	4.7	1310	98,000	498.5	13.8	484.7	473.2	11.5
				1330	98,400	497.8	13.9	483.9	473.3	10.6
				1400	99,300	497.5	14.0	483.5	473.1	10.4
				1415	70,100	491.4	9.9	481.5	473.2	8.3
				1430	43,600	485.6	6.1	479.5	473.1	6.4
				1445	22,700	480.8	3.2	477.6	473.1	4.5
				1500	12,500	478.2	1.8	476.4	473.2	3.2
				Shut down and restart						
				1530	43,500	486.4	6.1	480.3	473.1	7.2
				1545	23,500	481.3	3.3	478.0	473.1	4.9
				1605	12,600	478.3	1.8	476.5	473.0	3.5
				1625	7,600	476.8	1.1	475.7	473.1	2.6
				1640	5,160	476.0	0.7	475.3	473.2	2.1
6/12/63	HM-20	1015	4.7	1045	7,490	548.9	1.0	547.9	545.4	2.5
				1105	22,200	552.3	3.0	549.3	545.5	3.8
				1125	49,200	557.4	6.7	550.7	545.4	5.3
				1145	99,800	565.9	13.5	552.4	545.4	7.0
				1215	97,500	565.3	13.2	552.1	545.4	6.7
				1245	96,500	565.1	13.1	552.0	545.4	6.6
				1305	49,700	556.7	6.7	550.0	545.5	4.5
				1325	31,500	553.2	4.3	548.9	545.4	3.5
				1345	18,000	550.5	2.4	548.1	545.4	2.7
				1405	9,500	548.7	1.3	547.4	545.5	1.9
6/12/63	HM-21	1015	1.3	1515	6,800	549.0	0.9	548.1	545.4	2.7
				1535	21,800	552.6	3.0	549.6	545.3	4.3
				1555	48,900	557.9	6.6	551.3	545.4	5.9
				1615	96,200	566.4	13.0	553.4	545.5	7.9
				1645	93,600	565.8	12.7	553.1	545.4	7.7
				1715	92,900	565.6	12.6	553.0	545.5	7.5
				1735	48,300	557.1	6.5	550.6	545.4	5.2
				1755	31,700	553.9	4.3	549.6	545.4	4.2
				1815	18,100	551.0	2.5	548.5	545.4	3.1
				1835	9,080	548.9	1.2	547.7	545.4	2.3
6/12/63	HM-22	1015	Pool	2025	6,930	549.3	0.9	548.4	545.4	3.0
				2045	22,100	552.9	3.0	549.9	545.4	4.5
				2105	50,100	558.6	6.8	551.8	545.4	6.4
				2125	96,000	567.0	13.0	554.0	545.4	8.6
				2155	94,600	566.5	12.8	553.7	545.4	8.3
				2225	93,800	566.2	12.7	553.5	545.4	8.1
				2245	48,800	557.4	6.6	550.8	545.4	5.4
				2305	30,700	553.7	4.2	549.5	545.4	4.1
				2325	18,000	551.1	2.4	548.7	545.5	3.2
				2345	9,200	549.0	1.2	547.8	545.5	2.3

Date	Run No.	Press psia	Vel. Ft/sec	Time	q/A Btu/hr-ft^2	Temperatures - °F: Avg T_i	ΔT Wall	Avg T_o	T_{sat}	(T_o-T_{sat})
6/14/63	HM-23	535	1.3	1210	18,200	481.5	2.6	478.9	473.1	5.8
				1230	42,300	487.3	6.0	481.3	473.0	8.3
				1250	91,600	497.8	12.9	484.9	473.1	11.8
				1310	136,500	506.2	19.2	487.0	473.1	13.9
				1340	153,800	509.2	21.7	487.5	473.2	14.3
				1400	216,600	519.9	30.5	489.4	473.1	16.3
				1500	210,700	518.3	29.7	488.6	473.1	15.5
				1520	156,800	507.7	22.1	485.6	473.1	12.5
				1540	107,300	498.2	15.1	483.1	473.2	9.9
				1600	66,300	489.7	9.3	480.4	473.1	7.3
				1620	38,500	484.0	5.4	478.6	473.1	5.5
				1640	21,800	480.3	3.1	477.2	473.1	4.1
6/18/63	HM-24	1550	4.7	0910	2,090	601.1	0.3	600.8	599.6	1.2
				0925	5,720	602.1	0.7	601.4	599.6	1.8
				0945	9,630	603.0	1.2	601.8	599.6	2.2
				1000	21,800	605.5	2.9	602.6	599.6	3.0
				1020	52,600	610.9	6.9	604.0	599.6	4.4
				1040	97,300	618.1	12.8	605.3	599.6	5.7
				1110	97,700	618.0	12.8	605.2	599.6	5.6
				1140	97,000	617.6	12.8	604.8	599.5	5.3
				1200	57,700	611.2	7.6	603.6	599.6	4.0
				1220	30,200	606.4	4.0	602.4	599.6	2.8
				1240	17,500	604.0	2.3	601.7	599.6	2.1
				1300	11,800	602.9	1.5	601.4	599.5	1.9
6/18/63	HM-25	1550	1.3	1425	5,200	602.2	0.7	601.5	599.6	1.9
				1450	10,500	603.9	1.4	602.5	599.6	2.9
				1505	24,000	606.7	3.1	603.6	599.6	4.0
				1520	49,100	611.4	6.5	604.9	599.6	5.3
				1535	96,600	618.9	12.7	606.2	599.6	6.6
				1605	96,200	618.4	12.7	605.7	599.5	6.2
				1635	97,100	618.4	12.8	605.6	599.6	6.0
				1655	60,500	612.1	8.0	604.1	599.6	4.5
				1712	32,500	606.7	4.3	602.4	599.5	2.9
				1732	17,200	604.1	2.3	601.8	599.5	2.3
				1752	10,400	602.8	1.4	601.4	599.6	1.8
6/18/63	HM-26	1550	Pool	1945	1,990	601.5	0.3	601.2	599.6	1.6
				2005	3,890	602.2	0.5	601.7	599.6	2.1
				2020	9,820	603.8	1.3	602.5	599.6	2.9
				2035	20,750	606.3	2.7	603.6	599.6	4.0
				Shut down and restart						
				2055	7,230	603.2	0.9	602.3	599.6	2.7
				2110	21,200	606.5	2.8	603.7	599.6	4.1
				2130	49,500	611.9	6.5	605.4	599.6	5.8
				2150	96,800	619.5	12.7	606.8	599.6	7.2
				2220	97,200	619.2	12.8	606.4	599.6	6.8
				2240	60,200	612.6	7.9	604.7	599.6	5.1
				2300	33,600	607.6	4.4	603.2	599.6	3.6
				2320	16,600	604.2	2.2	602.0	599.6	2.4
				2340	10,450	602.9	1.4	601.5	599.6	1.9
7/2/63	HM-28	1015	4.7	1200	97,500	568.1	13.2	554.9	545.5	9.4
				1225	45,380	557.1	6.1	551.0	545.5	5.5
				1245	18,720	551.1	2.5	548.6	545.5	3.1
				1305	9,045	548.8	1.2	547.6	545.5	2.1
				1325	3,465	547.1	0.5	546.6	545.5	1.1

WATER RESISTIVITY

Run No.	Average Resistivity (megohm-cm ±5%)	pH
HM-6	0.6	8.8
HM-7	0.95	8.6
HM-8	0.6	8.6
HM-9	1.1	8.6
HM-10	0.7	8.6
HM-11	1.4	8.1
HM-12	0.8	8.3
HM-13	1.5	8.0
HM-14	1.9	7.9
HM-15	1.9	7.7
HM-16	1.3	7.8
HM-19	1.9	8.0
HM-20	2.0	7.7
HM-21	2.0	7.6
HM-22	1.7	7.6
HM-23	1.9	7.9
HM-24	1.6	7.6
HM-25	1.4	7.8
HM-26	1.3	7.6
HM-28	2.0	7.6

APPENDIX D

TEST SECTION TEMPERATURE PROFILES

The data presented in Figs. 14-29 and Appendix C are based on the average inside wall temperatures of the test section at the mid-point of its length. As previously discussed, the use of average wall temperatures and total tube cross-sectional area, Eq. (16), renders unnecessary a consideration of slight variations in tube wall thickness around the circumference in computing the tube wall temperature drop.

Measurements made during runs HM-6, 7, and 8 indicated that there was no significant variation in temperature along the axis of the test section. This may be observed by inspection of the individual thermocouple readings presented in this section. In all cases of decreasing heat flux (the more stable and reproducible condition), the average of all the thermocouple readings was the same or within 0.1°F of the average of the four thermocouples at the mid-point of the test section. In order to reduce the length of time required to take a set of readings, and thereby minimize long time trends in the temperature drift of the system, the only test section temperatures recorded in runs subsequent to HM-10 were those at the mid-point.

The temperature variation around the circumference of the mid-point of the test section is due to the variation in wall thickness of the test section and the differences in heat transfer rate from the surface to the boiling water due to the geometry of the system. As noted

in Section II-B, the tube wall thickness varied from .0510 in. to .0540 in. The tube wall thickness was not constant along the length of the tube and the exact thickness at each thermocouple location was not determined.

The thermocouples are located in the test section as shown on Fig. 4 and according to the following tabulation:

Thermocouple No.	Axial Position	Orientation
TC-1	Right end	0°
TC-2	Right end	90°
TC-3	Right end	180°
TC-4	Right end	270°
TC-5	Mid-point	0°
TC-6	Mid-point	90°
TC-7	Mid-point	180°
TC-8	Mid-point	270°
TC-9	Left end	0°
TC-10	Left end	90°
TC-11	Left end	180°
TC-12	Left end	270°

Referring to Fig. 4, the thermocouples along the top are TC-9, 5, and 1, reading from left to right. Those along the bottom are TC-11,7, and 3, also reading from left to right.

Following are individual thermocouple readings for the complete run HM-6 and the decreasing heat flux portions of runs HM-7 and 8. Mid-point temperatures are given for runs HM-24, 25, and 26. Thermocouple TC-10 is not reported because of a poor hot junction which caused completely erratic readings.

Run No.	Time	q/A Btu/hr-ft^2	Temperatures - ^oF												
			TC-1	TC-2	TC-3	TC-4	TC-5	TC-6	TC-7	TC-8	TC-9	TC-11	TC-12	Avg of TC 1-12	Avg of TC 5-8
HM-6	1335	8,670	477.9	477.6	477.8	477.6	478.0	477.6	478.4	478.8	478.0	477.9	477.9	478.0	478.2
P = 535 psia	1420	23,900	483.5	482.4	482.8	482.8	483.8	482.9	483.0	483.0	483.5	482.9	483.0	483.1	483.2
V = 4.7 ft/sec	1450	49,000	486.9	488.8	488.0	487.9	486.9	487.8	487.8	487.9	487.5	487.9	487.9	487.8	487.6
	1525	85,600	493.2	494.6	494.6	494.7	493.3	494.1	494.2	494.5	493.6	494.3	494.5	494.1	494.0
	1545	47,700	485.5	486.7	486.4	486.5	485.5	486.1	486.2	486.5	485.9	486.3	486.5	486.2	486.1
	1610	23,100	480.4	481.1	480.8	480.9	480.3	480.8	480.9	481.3	480.6	480.8	481.1	480.8	480.8
	1630	11,800	477.8	478.1	477.9	477.9	477.7	477.9	478.0	478.3	477.7	477.7	477.9	477.9	478.0
HM-7	2015	86,500	495.7	497.0	495.5	495.8	495.7	496.5	494.8	495.2	495.7	495.0	495.1	495.6	495.5
P = 535 psia	2040	47,600	487.1	488.0	487.0	487.4	487.1	487.6	486.8	487.2	487.5	486.9	487.2	487.2	487.2
V = 1.3 ft/sec	2115	22,800	481.5	482.1	481.4	481.8	481.3	481.5	481.3	481.8	481.4	481.1	481.6	481.5	481.5
	2135	11,700	478.5	478.8	478.4	478.7	478.4	478.5	478.5	478.9	478.6	478.3	478.8	478.6	478.6
HM-8	0145	90,200	496.4	497.0	496.2	496.8	496.7	497.4	495.5	495.9	496.7	495.6	496.1	496.4	496.4
P = 535 psia	0215	48,000	487.6	487.7	487.0	487.7	487.9	488.3	486.8	487.1	488.0	486.6	487.0	487.4	487.5
V = Pool	0245	23,000	482.3	482.2	481.4	482.2	482.2	482.2	481.2	481.6	482.2	481.0	481.6	481.8	481.8
	0310	11,800	479.4	479.4	478.6	479.4	479.1	479.1	478.5	479.1	479.3	478.4	479.1	479.0	479.0
HM-24	1140	97,000					617.5	618.5	617.2	617.2					617.6
P = 1550 psia	1200	57,700					611.0	611.8	610.9	611.2					611.2
V = 4.7 ft/sec	1220	30,200					606.1	606.8	606.2	606.3					606.4
	1240	17,500					603.9	604.3	604.0	604.0					604.0
	1300	11,800					602.7	603.1	602.9	602.8					602.9
HM-25	1635	97,100					618.5	619.5	617.9	617.9					618.4
P = 1550 psia	1655	60,500					612.0	612.8	611.7	611.7					612.1
V = 1.3 ft/sec	1712	32,500					605.8	607.5	606.8	606.9					606.7
	1732	17,200					604.1	604.4	604.0	604.1					604.1
	1752	10,400					602.7	602.9	602.7	602.8					602.8
HM-26	2220	97,200					619.5	620.5	618.4	618.5					619.2
P = 1550 psia	2240	60,200					612.7	613.6	612.0	612.1					612.6
V = Pool	2300	33,600					607.6	608.2	607.3	607.4					607.6
	2320	16,600					604.1	604.5	604.0	604.1					604.2
	2340	10,450					602.8	603.0	602.8	603.0					602.9

BIBLIOGRAPHY

1. Jakob, M., Heat Transfer, Vol. I, John Wiley and Sons, New York, 1949.

2. McAdams, W. H., Heat Transmission, 3rd ed., McGraw-Hill Book Co., New York, 1954.

3. Kreith, F., Principles of Heat Transfer, International Textbook Co., Scranton, 1958.

4. Rohsenow, W. M. and Choi, H. Y., Heat, Mass, and Momentum Transfer, Prentice-Hall, Englewood Cliffs, N. J., 1961.

5. Clark, J. A., Merte, H., Lady, E. R., Vander Veen, J., and Yang, W. J., Low Heat-Flux Boiling, Univ. of Mich. ORA Report 04653-1-P, Ann Arbor, 1962.

6. Clark, J. A., Merte, H., Lady, E. R., Vander Veen, J., and Yang, W. J., Low Heat-Flux Boiling, Univ. of Mich. ORA Report 04653-2-P, Ann Arbor, April, 1962.

7. Corty, C. and Foust, A. S., "Surface Variable in Nucleate Boiling," Chem. Eng. Prog., Sym. Series, 51 (1955).

8. Ellion, M. E., A Study of the Mechanism of Boiling Heat Transfer, JPL-Memo-20-88 (1954).

9. Bankoff, S. G., Ebullition from Solid Surfaces in the Absence of a Pre-Existing Gaseous Phase, Heat Transfer and Fluid Mechanics Institute, Stanford Univ. Press, 1956.

10. Jakob, M., "Local Temperature Differences as Occurring in Evaporation, Condensation and Catalytic Reaction," Temperature, Its Measurement and Control in Science and Industry, Reinhold Publishing Corp., New York, 1941.

11. Nishikawa, K., et al., Heat Transfer in Nucleate Boiling, Mem. Fac. Eng., Kyushu Univ., 15 (1955) and 16 (1956).

12. Kurihara, H. M. and Myers, J. E., "Fundamental Factors Affecting Boiling Coefficients," AIChE. Journal, 6, No. 1, 83 (1960).

BIBLIOGRAPHY (Continued)

13. Gaertner, R. F. and Westwater, J. W., "Population of Active Sites in Nucleate Boiling Heat Transfer," Chem. Eng. Prog., Sym. Series, 56 (1960).

14. Gaertner, R. F., "Distribution of Active Sites in the Nucleate Boiling of Liquids," Chem. Eng. Prog., Sym. Series, 59 (1963).

15. Clark, H. B., Strenge, P. S., and Westwater, J. W., "Active Sites for Nucleate Boiling," Chem. Eng. Prog., Sym. Series, 55 (1959).

16. Hsu, Y. Y., "On the Size Range of Active Nucleation Cavities on a Heating Surface," ASME Trans., Series C, J. of Heat Transfer, 84 (1962).

17. Yamagata, K., et al., Trans. Jap. Soc. Mech. Eng., 17, 163 (1951).

18. Westwater, J. W., et al., Univ. of Ill., Urbana, 1958.

19. Clark, J. A. "Thermodynamics of Bubbles," M.I.T., Cambridge, Mass. D.I.C., Tech. Report No. 7, ONR Contract N5 or i-07827 (NR-035-267), Jan. 1, 1956.

20. Plesset, M. S. and Zwick, S. A., "The Growth of Vapor Bubbles in Superheated Liquids," J. App. Phys., 25, No. 4 (1954).

21. Forster, H. K. and Zuber, N., "Growth of a Vapor Bubble in a Superheated Liquid," J. App. Phys., 25, No. 4 (1954).

22. Forster, H. K. and Zuber, N., "Dynamics of Vapor Bubbles and Boiling Heat Transfer," AIChE. Journal, 1, No. 4 (1954).

23. Rohsenow, W. M. and Clark, J. A., "A Study of the Mechanism of Boiling Heat Transfer," Trans. ASME, 73 (1951).

24. Gunther, F. C. and Kreith, F., Photographic Study of Bubble Formation in Heat Transfer to Subcooled Water, Heat Transfer and Fluid Mechanics Inst., Stanford Univ. Press., 1949.

25. Zuber, N., Hydrodynamic Aspects of Nucleate Pool Boiling, Part I. The Region of Isolated Bubbles, RW-RL-164, RAMO Woolridge, Div. of Thompson-Ramo-Woolridge, Inc., Jan. 27, 1960.

26. Chang, Y. P., Heat Transfer and Critical Conditions in Nucleate Boiling of Subcooled and Flowing Liquids, TID-6045, 1960.

BIBLIOGRAPHY (Continued)

27. Chang, Y. P. and Snyder, N. W., "Heat Transfer in Saturated Boiling," Chem. Eng. Prog., Sym. Series, 56 (1960).

28. Chang, Y. P., "Some Possible Critical Conditions in Nucleate Boiling," ASME Trans., Series C, J. of Heat Transfer, 85 (1963).

29. Addoms, J. N., "Heat Transfer at High Rates to Water Boiling Outside Cylinders," D. Sc. Thesis, Chem. Engr. Dept., M.I.T., June, 1948.

30. Rohsenow, W., "A Method of Correlating Heat Transfer Data for Surface Boiling of Liquids," ASME Trans., 74 (1952).

31. Gilmour, C. H., "Nucleate Boiling—A Correlation," Chem. Eng. Prog., 54:10 (1958).

32. Forster, K. E. and Greif, R., "Heat Transfer to a Boiling Liquid; Mechanism and Correlations," Trans. ASME, J. of Heat Transfer, 81 (1959).

33. Rohsenow, W. M., "Heat Transfer, A Symposium 1952," Eng. Res. Inst., Univ. of Mich.

34. De Bortoli, R. A., et al., Forced-Convection Heat Transfer Studies for Water in Rectangular Channels and Round Tubes at Pressures Above 500 psia, WAPD-188, June, 1958.

35. Vliet, G. C. and Leppert, G., "Critical Heat Flux for Nearly Saturated Water Flowing Normal to a Cylinder," ASME Paper No. 62-WA-173 (1962).

36. Vliet, G. C. and Leppert, G., "Critical Heat Flux for Subcooled Water Flowing Normal to a Cylinder," ASME Paper No. 62-WA-174 (1962).

37. Kazakova, E. A., "Maximum Heat Transfer to Boiling Water at High Pressure," Eng. Digest, 12 (1951).

38. Roeser, W. F., "Thermoelectric Thermometry," National Bureau of Standards Handbook 77 - Vol. II (1961).

39. Roeser, W. F. and Lonberger, S. T., "Methods of Testing Thermocouples and Thermoelectric Materials," NBS Circular 590 (1958).

BIBLIOGRAPHY (Concluded)

40. Clark, J. A., Merte, H., and Lady, E. R., Low Heat-Flux Boiling, Univ. of Mich. ORA Report 04653-3-P, Ann Arbor, July, 1962.

41. Dahl, A. I., "Stability of Base-Metal Thermocouples in Air From 800° to 2,200°F," N.B.S. J. Research, 24 (1940), RP 1278.

42. Shenker, H., et al., "Reference Tables for Thermocouples," NBS Circular 561 (1955).

43. Clark, J. A. and Rohsenow, W. M., "Local Boiling Heat Transfer to Water at Low Reynolds Numbers and High Pressures," Trans. ASME, 76 (1954).

44. Griffith, P. and Wallis, J. D., "The Role of Surface Conditions in Nucleate Boiling," Chem. Eng. Prog., Sym. Series, 56 (1960).

45. Bankoff, S. G., "A Note on Latent Heat Transport in Nucleate Boiling," AIChE. Journal, 8, No. 1, 63 (1962).

46. Bankoff, S. G. and Mason, J. P., "Heat Transfer from the Surface of a Steam Bubble in Turbulent Subcooled Liquid Stream," AIChE. Journal, 8, No. 1, 30 (1962).

47. Levy, S., "Generalized Correlation of Boiling Heat Transfer," ASME Paper No. 58-HT-8 (1958).

48. Westwater, J. W., "Things We Don't Know About Boiling Heat Transfer," Theory and Fundamental Research in Heat Transfer, J. A. Clark, editor, Sym. Pub. Div., Pergamon Press, New York, 1963.

49. Bankoff, S. G., Hajjar, A. J., and McGlothin, B. B., "On the Nature and Location of Bubble Nuclei in Boiling from Surfaces," J. App. Phys., 29, No. 12 (1958).

50. Moore, F. D. and Mesler, R. B., "The Measurement of Rapid Surface Temperature Fluctuations During Nucleate Boiling of Water," AIChE. Journal, 7, 620 (1961).

51. Kline, S. J. and McClintock, F. A., "Description and Analysis of Uncertainties in Single Sample Experiments," Mech. Eng. (Jan. 1953).

52. Schenck, H., Theories of Engineering Experimentation, McGraw-Hill Book Co., New York, 1961.

53. Handbook of Chemistry and Physics, 40th ed., Chemical Rubber Publishing Co., Cleveland, Ohio, 1959.